

**UNSTEADY NATURAL CONVECTIVE HEAT TRANSFER OF  
NANOFLUIDS INSIDE A SEMI-CIRCULAR CAVITY UNDER  
THE INFLUENCE OF PERIODIC MAGNETIC FIELD**

by

**Tarikul Islam**

**Student ID: 1017093005**

**Registration No.: 1017093005, Session: October, 2017**


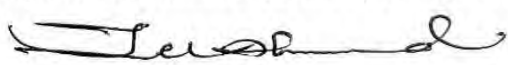



**MASTER OF PHILOSOPHY  
IN  
MATHEMATICS**



**Department of Mathematics  
Bangladesh University of Engineering and Technology (BUET)  
Dhaka-1000, Bangladesh.  
July, 2021**

The thesis entitled “UNSTEADY NATURAL CONVECTIVE HEAT TRANSFER OF NANOFLUIDS INSIDE A SEMI-CIRCULAR CAVITY UNDER THE INFLUENCE OF PERIODIC MAGNETIC FIELD” submitted by Tarikul Islam, Student ID: 1017093005, Registration No.: 1017093005, Session: October-2017, a full-time student of the Master of Philosophy (M.Phil) in the Department of Mathematics has been accepted as satisfactory in partial fulfillment for the degree of Master of Philosophy (M.Phil) in Mathematics on 5<sup>th</sup> July, 2021.

## BOARD OF EXAMINERS

1.   
\_\_\_\_\_  
Dr. Nazma Parveen  
Professor  
Dept. of Mathematics, BUET, Dhaka-1000. Bangladesh. Chairman  
(Supervisor)
2.   
\_\_\_\_\_  
Dr. Khandker Farid Uddin Ahmed  
Professor and Head  
Dept. of Mathematics, BUET, Dhaka-1000. Bangladesh. Member  
(Ex Officio)
3.   
\_\_\_\_\_  
Dr. Md. Mustafizur Rahman  
Professor  
Dept. of Mathematics, BUET, Dhaka-1000. Bangladesh. Member
4.   
\_\_\_\_\_  
Dr. Rehena Nasrin  
Professor  
Dept. of Mathematics, BUET, Dhaka-1000. Bangladesh. Member
5.   
\_\_\_\_\_  
Dr. Md. Shariful Alam  
Professor  
Dept. of Mathematics, Jagannath University, Dhaka-1100. Bangladesh. Member  
(External)

## **AUTHOR'S DECLARATION**

I hereby declare that the work which is being presented in this thesis entitled

**“UNSTEADY NATURAL CONVECTIVE HEAT TRANSFER OF  
NANOFLUIDS INSIDE A SEMI-CIRCULAR CAVITY UNDER  
THE INFLUENCE OF PERIODIC MAGNETIC FIELD”**

submitted in partial fulfillment of the requirements of the degree of Master of Philosophy, Department of Mathematics, Bangladesh University of Engineering and Technology (BUET), Dhaka-1000, Bangladesh, is an authentic record of my own work.

The work is also original except where indicated by and attached with special reference in the context, and no part of it has been submitted for any attempt to get other degrees or diplomas.

All views expressed in the dissertation are those of the author and in no way or by no means represent those of Bangladesh University of Engineering and Technology (BUET), Dhaka-1000, Bangladesh. This dissertation has not been submitted to any other University for examination either in the home or abroad.



---

**Tarikul Islam**

M.Phil Student

Student ID: 1017093005

Registration No.: 1017093005

Session: October, 2017

Department of Mathematics, BUET, Dhaka-1000, Bangladesh.

Date: 5<sup>th</sup> July, 2021.

## CERTIFICATE OF RESEARCH

This is to certify that the work presented in this thesis entitled “**UNSTEADY NATURAL CONVECTIVE HEAT TRANSFER OF NANOFLUIDS INSIDE A SEMI-CIRCULAR CAVITY UNDER THE INFLUENCE OF PERIODIC MAGNETIC FIELD**” is carried out by the author Tarikul Islam, M.Phil student, Department of Mathematics, Student ID: 1017093005, Registration No.: 1017093005, Session: October, 2017, under the supervision of Dr. Nazma Parveen, Professor, Department of Mathematics, Bangladesh University of Engineering and Technology (BUET), Dhaka-1000, Bangladesh.



---

Dr. Nazma Parveen  
Professor  
Department of Mathematics  
Bangladesh University of  
Engineering and Technology  
(BUET), Dhaka, Bangladesh.



---

Tarikul Islam  
Student ID: 1017093005  
Registration No.: 1017093005  
Session: October, 2017  
Department of Mathematics  
BUET, Dhaka, Bangladesh.

## ACKNOWLEDGEMENTS

First of all, I would like to affirm the notable recognizance of Almighty's continual mercy. With great pleasure, the author has the privilege to express her most profound respect, gratitude, and sincere appreciation to my supervisor Dr. Nazma Parveen, Professor, Department of Mathematics, Bangladesh University of Engineering and Technology (BUET), Dhaka, Bangladesh, who initiated me into the realm of this mathematical M.Phil research. Her valuable guidance, continuous inspiration, constant support, intuitive suggestions, relentless encouragement, and generosity help me to complete this thesis work. Furthermore, I am grateful to her for giving me the opportunity to research work with her as an M.Phil student.

I am also grateful to Professor and Head, Dr. Khandker Farid Uddin Ahmed, Department of Mathematics, BUET, Bangladesh, for his support in allowing me to use the departmental facilities in various stages of my work. I am also intensively grateful to the member of the board of examiners, Professor Dr. Md. Mustafizur Rahman and Professor Dr. Rehana Nasrin, Department of Mathematics, BUET, Bangladesh, for their wise and liberal co-operation in providing me all necessary help during my courses of M. Phil degree. I am also grateful to all of my honorable teachers and staff of the Department of Mathematics of BUET, Dhaka.

I am also grateful to the external member of the board of examiners, Professor Dr. Md. Shariful Alam, Department of Mathematics, Jagannath University, Dhaka, Bangladesh, for his valuable suggestions for improving the quality of the work. My sincere thanks to the Department of Mathematics and colleagues of the Department of Mathematics, BSMRSTU, Gopalganj-8100, Bangladesh, for providing me necessary supports and facilities during my research work. My sincere thanks to all my well-wishers for their valuable suggestions for improving the quality of the research work.

Finally, I express my heartiest respect to my parents and all of my family members for their sacrifice, assistance, motivation, and creating a delightful atmosphere to complete the courses, research, and final production of the thesis work.

Author

## ABSTRACT

In this thesis, the fundamental concepts of nanofluids and literature survey have been discussed, and two-dimensional time-dependent natural convection flow and heat transfer inside the semi-circular enclosure charged by nanofluid with the presence of the vertically periodic magnetic field has been investigated numerically. Copper-water nanofluid has been taken as default nanofluid. Different types of nanoparticles and base fluids have been considered to examine the better performance of heat transfer. The top circular wall is heated at low-temperature  $T_c$  while the bottom diameter is heated at high-temperature  $T_h$  ( $T_c < T_h$ ). Moreover, different types of thermal boundary conditions are employed along the bottom diameter. The non-linear governing equations with boundary conditions have been transformed into dimensionless forms using a set of non-dimensional variables. The highly powerful partial differential equations solver finite element technique (FEM) of Galerkin weighted residual type has been employed for the numerical simulations in the present problem. The outcomes illustrate an excellent agreement with previously published research. The different physical model parameters such as Hartmann number, Rayleigh number, nanoparticles diameter, nanoparticles volume, size and shape, and Brownian motion of nano-sized particles have been investigated using streamline contours, isothermal lines, and heat transfer rate in terms of average Nusselt number.

The outcomes show that the parameters mentioned above strongly affect the heat transport and flow field within the cavity. It is seen that heat transport rate enhances with the increase of the buoyancy driven parameter Rayleigh number and volume fraction of nanoparticles, decreasing with the higher magnetic effect. The different types of nanofluids have an influential role in heat transport and fluid flow. The heat transport rate increases 22.1% in water-based whereas 5.4% in engine oil-based nanofluid for 1% copper nanoparticles volume. The different thermal boundary conditions have an important impact in heat transport and fluid flow. The uniform thermal condition (case I) gives a better heat transfer rate than others (case II, III, IV, and V). The blade shape nanoparticles provide a higher heat transport rate than spherical, cylindrical, bricks, and platelets. The small size of nanoparticles conforms better heat transfer rate in the resent analysis. The non-uniform magnetic field and its period have a vital role in fluid flow and heat transport. The non-uniform periodic magnetic field provides a higher temperature transport rate than the uniform magnetic field. It is also seen that the average Nusselt number for kerosene-based

nanofluid is higher than water-based, ethylene glycol-based, and engine oil-based nanofluids. The heat transport rate is observed at 67.86% for Cobalt (Co)-kerosene whereas 23.78% for Co-water, and 5.68% for Co-engine oil nanofluid with 1% nano-particles volume. In addition, The Brownian motion of nano-sized particles has a significant contribution on heat transfer. The rate of heat transfer increases 28.88% with the Brownian effect, whereas it increases only 3.01% without the Brownian effect. Therefore, the small size of nanoparticles with blade shape and Brownian motion at low Rayleigh number ( $Ra = 10^4$ ) provides the best heat transport rate in the case of uniform thermal boundary conditions.

# CONTENTS

<b>BOARD OF EXAMINATIONS</b>	II
<b>AUTHOR'S DECLARATION</b>	III
<b>PERMIT OF RESEARCH</b>	IV
<b>ACKNOWLEDGEMENT</b>	V
<b>ABSTRACT</b>	VI
<b>CONTENTS</b>	VIII
<b>NOMENCLATURE</b>	X
<b>LIST OF TABLES</b>	XII
<b>LIST FIGURES</b>	XIV
<b>CHAPTER ONE</b>	<b>1-19</b>
<b>Fundamental of Nanofluids and Literature Review</b>	
1.1 Introduction	1
1.2 Natural convection heat transfer	2
1.3 Magnetohydrodynamics	3
1.4 Steady and unsteady Flow	4
1.5 Prandtl number	5
1.6 Hartmann number	5
1.7 Rayleigh number	6
1.8 Nusselt number	6
1.9 Definition of nanofluids	7
1.10 Nanoparticles	8
1.11 Nanoparticles size	9
1.12 Base fluids	10
1.13 Solid volume fraction of nanoparticles	10
1.14 Background of the study	10
1.15 Motivation of research	17
1.16 Main objectives of the study	18
1.17 Outline of this thesis	19
<b>CHAPTER TWO</b>	<b>20-24</b>
<b>Computational Procedure</b>	
2.1 Computational Fluid Dynamics	20
2.2 Discretization Approaches	20
2.3 Finite Element Method	21



2.4 Mesh Generation	23
2.5 Algorithm	23
<b>CHAPTER THREE</b>	<b>25-39</b>
<b>Mathematical Model of the Problem</b>	
3.1 Introduction	25
3.2 Physical modeling	26
3.3 Mathematical modeling	28
3.4 Initial and boundary conditions	28
3.5 Physical and thermal properties nanofluids	29
3.6 Dimensional analysis	32
3.7 Calculation of Nusselt number	33
3.8 Finite element formulation	34
<b>CHAPTER FOUR</b>	<b>40-44</b>
<b>Numerical Procedure and Comparisons</b>	
4.1 Computational procedure	40
4.2 Grid independency test	41
4.3 Code validation through streamlines and isotherms	42
4.4 Code validation through data	43
<b>CHAPTER FIVE</b>	<b>45-93</b>
<b>Results and Discussion</b>	
5.1 Time evolution of solution	46
5.2 Effects of magnetic field and it's period	56
5.3 Effects of Rayleigh number	77
5.4 Effects of nanoparticles volume fraction	83
5.5 Effects of different thermal boundary conditions	85
5.6 Average heat transfer rate for different nanofluids	88
5.7 Effects of nanoparticles diameter	90
5.8 Effects of nanoparticles shape factor	91
5.9 Effects of Brownian motion	92
<b>CHAPTER SIX</b>	<b>94-97</b>
<b>Conclusions and Recommendations</b>	
6.1 Summary of the major outcomes	94
6.2 Future work	97
<b>REFERENCES</b>	<b>98-102</b>

## NOMENCLATURE

$a$	:	Amplitude of the wave [m]
$B_0$	:	Magnitude of magnetic field [ $\text{kgs}^{-2}\text{A}^{-1}$ ]
$c_p$	:	Specific heat at constant pressure [ $\text{Jkg}^{-1}\text{K}^{-1}$ ]
$g$	:	Gravitational acceleration [ $\text{ms}^{-2}$ ]
$Ha$	:	Hartmann number
$H$	:	Height of the cavity
$k$	:	Thermal conductivity [ $\text{Wm}^{-1}\text{K}^{-1}$ ]
$K$	:	Wave number
$L$	:	Length of bottom diameter of the enclosure
$Nu_L$	:	Local Nusselt number
$Nu_{av}$	:	Average Nusselt number
$p$	:	Dimensional pressure [ $\text{kgm}^{-1}\text{s}^{-2}$ ]
$P$	:	Dimensionless pressure
$Pr$	:	Prandtl number
$Ra$	:	Rayleigh number
$T$	:	Fluid temperature [K]
$t$	:	Dimensional time [s]
$u$	:	Dimensional horizontal velocity component [ $\text{ms}^{-1}$ ]
$v$	:	Dimensional vertical velocity component [ $\text{ms}^{-1}$ ]
$U$	:	Dimensionless horizontal velocity component
$V$	:	Dimensionless vertical velocity component
$x$	:	Dimensional horizontal coordinate [m]
$y$	:	Dimensional vertical coordinate [m]
$X$	:	Dimensionless horizontal coordinate
$Y$	:	Dimensionless vertical coordinate

### Greek symbols

$\alpha$	:	Thermal diffusivity [ $\text{m}^2\text{s}^{-1}$ ]
$\beta$	:	Thermal expansion coefficient [ $\text{K}^{-1}$ ]

$\delta$	:	Dependent dimensionless variable
$\phi$	:	Solid volume fraction of nanoparticles
$\mu$	:	Dynamic viscosity [ $\text{kgm}^{-1}\text{s}^{-1}$ ]
$\nu$	:	Kinematic viscosity [ $\text{m}^2\text{s}^{-1}$ ]
$\tau$	:	Dimensionless time
$\theta$	:	Non-dimensional temperature
$\rho$	:	Density [ $\text{kgm}^{-3}$ ]
$\sigma$	:	Electric conductivity
$\psi$	:	Stream function
$\lambda_0$	:	Dimensional period of the magnetic field
$\lambda$	:	Dimensionless period of the magnetic field

### **Subscript**

$h$	:	Hot surface
$c$	:	Cold surface
$nf$	:	Nanofluid
$bf$	:	Base fluid
$sp$	:	Solid particle
$L$	:	Local

## LIST OF TABLE

Table No.	Physical Properties	Page No.
3.1	Thermo-physical properties of the different base fluid and solid nanoparticles.	27
3.2	Different shapes of the nanoparticles with geometry.	31
4.1	Grid sensitivity using average Nusselt number for Cu-H <sub>2</sub> O nanofluid for uniform thermal boundary condition (case I) when $Ra = 10^5$ , $Ha = 20$ , $\lambda = 0.5$ , $Pr = 6.8377$ , $n = 3$ , $\phi = 0.04$ , $d = 10\text{nm}$ , and $\tau = 1$ .	42
4.2	Comparison of the present data regarding average Nusselt number ( $Nu_{av}$ ) with previously published paper of Ghasemi <i>et al.</i> [54] for different values of Rayleigh number ( $Ra$ ), and nanoparticles volume fraction ( $\phi$ ) when $Ha = 30$ .	43
4.3	Comparison of the present data of average Nusselt number ( $Nu_{av}$ ) with previously published paper of Ghasemi <i>et al.</i> [54] for different values of Hartmann number ( $Ha$ ) and nanoparticles volume fraction ( $\phi$ ) when $Ra = 10^5$ .	44
4.4	Comparison of the present data of average Nusselt number ( $Nu_{av}$ ) with previously published paper of Weheibi <i>et al.</i> [36] for different Rayleigh number ( $Ra$ ) and nanoparticles volume fraction ( $\phi$ ) when $n = 3$ , and $\tau = 2$ .	44
4.5	Comparison of the present data of average Nusselt number ( $Nu_{av}$ ) with previously published paper of Akgün <i>et al.</i> [55] for various Hartmann numbers ( $Ha$ ) and volume fraction of nanoparticles ( $\phi$ ) when $Ra = 10^5$ .	44
5.1	Variation of average Nusselt number ( $Nu_{av}$ ) along the bottom heated wall for Cu-H <sub>2</sub> O nanofluid for different Hartmann number ( $Ha$ ), nanoparticles diameter ( $d$ ), Rayleigh number ( $Ra$ ) and various thermal boundary conditions (TBC) when $Pr = 6.8377$ , $n = 3$ , $\phi = 0.04$ , $\lambda = 0.5$ , $\tau = 1$ .	73
5.2	Variation of average Nusselt number ( $Nu_{av}$ ) along bottom heated wall with uniform thermal boundary condition (case I) for different types of nanofluids and various nanoparticles volume fractions ( $\phi$ ) when $Ra = 10^5$ , $Ha = 20$ , $d = 10\text{nm}$ , $n = 3$ , $Pr = 6.8377$ , $\lambda = 0.5$ , and $\tau = 1$ .	74

- 5.3 Variation of average Nusselt number ( $Nu_{av}$ ) along heated bottom wall with uniform thermal boundary condition (case I) for different types of nanofluids and different Rayleigh numbers ( $Ra$ ) when  $\phi = 0.04$ ,  $Ha = 20$ ,  $d = 10\text{nm}$ ,  $n = 3$ ,  $\lambda = 0.5$ ,  $Pr = 6.8377$ , and  $\tau = 1$ . 75
- 5.4 Variation of average Nusselt number ( $Nu_{av}$ ) along heated bottom wall with uniform thermal boundary condition (case I) for different types of nanofluids and different Hartmann number ( $Ha$ ) when  $Ra = 10^5$ ,  $\phi = 0.04$ ,  $d = 10\text{nm}$ ,  $\lambda = 0.5$ ,  $n = 3$ ,  $Pr = 6.8377$ , and  $\tau = 1$ . 76
- 5.5 Variation of average Nusselt number ( $Nu_{av}$ ) along bottom heated diameter for uniform thermal boundary condition (case I) for different types of nanofluids and different diameter of the nanoparticles ( $d$ ) when  $Ra = 10^5$ ,  $Ha = 20$ ,  $\phi = 0.04$ ,  $n = 3$ ,  $\lambda = 0.5$ , and  $\tau = 1$ . 78
- 5.6 Variation of average Nusselt number ( $Nu_{av}$ ) along bottom heated wall with uniform thermal boundary condition (case I) for different types of nanofluids and the different shape of the nanoparticles ( $n$ ) when  $Ra = 10^5$ ,  $Ha = 20$ ,  $d = 10\text{nm}$ ,  $\phi = 0.04$ ,  $\lambda = 0.5$ , and  $\tau = 1$ . 80
- 5.7 Average Nusselt number ( $Nu_{av}$ ) along heated bottom diameter with uniform thermal boundary condition (case I) for different values of nanoparticles volume fraction ( $\phi$ ) and various Rayleigh number ( $Ra$ ) for “without Brownian motion” and “with Brownian motion” effects for Cu-H<sub>2</sub>O nanofluid when  $Ha = 20$ ,  $d = 10\text{nm}$ ,  $Pr = 6.8377$ ,  $n = 3$ ,  $\lambda = 0.5$ , and  $\tau = 1$ . 81

## LIST OF FIGURES

Figure No.	Caption	Page No.
1.1	Mechanism of natural convection heat transport from a hot body.	2
1.2	Steady and Unsteady Flow	4
1.3	Making of Nanofluid	7
1.4	Copper oxide nanoparticles	9
2.1	Finite element discretization of a domain	23
2.2	Flow chart of the computational procedure.	24
3.1	Schematic view of the semi-circular enclosure with boundary conditions	27
4.1	Convergence of average Nusselt number for various elements number for Cu-H <sub>2</sub> O nanofluid for uniform thermal boundary condition (case I) when $Ra = 10^5$ , $Ha = 20$ , $\lambda = 0.5$ , $Pr = 6.8377$ , $n = 3$ , $\phi = 0.04$ , $d = 10\text{nm}$ , and $\tau = 1$ .	41
4.2	Comparison of the present results (bottom row) with the previously published paper of Mehryan <i>et al.</i> [43] (top row) concerning streamline contours and isothermal lines for $Ra = 10^6$ , $Ha = 25$ , $\phi = 0.04$ , $n = 3$ , $\lambda = 1$ .	42
5.1	Average Nusselt number ( $Nu_{av}$ ) along bottom heated diameter for different Rayleigh number ( $Ra$ ) and different dimensionless time ( $\tau$ ) for Cu-H <sub>2</sub> O nanofluid for uniform thermal boundary condition (case I) when $Pr = 6.8377$ , $Ha = 20$ , $d = 10\text{nm}$ , $n = 3$ , and $\phi = 0.04$ .	47
5.2	Average Nusselt number ( $Nu_{av}$ ) along bottom heated diameter for different nanoparticles volume fraction ( $\phi$ ) and different dimensionless time ( $\tau$ ) at (a) $Ra = 10^5$ , and (b) $Ra = 10^6$ for Cu-H <sub>2</sub> O nanofluid for uniform thermal boundary condition (case I) when $Pr = 6.8377$ , $Ha = 20$ , $d = 10\text{nm}$ , $n = 3$ , and $\phi = 0.04$ .	48
5.3	Variation of average Nusselt number ( $Nu_{av}$ ) along bottom heated diameter for different diameter of nanoparticles ( $d$ ) and dimensionless time ( $\tau$ ) for Cu-H <sub>2</sub> O	49

- nanofluid for uniform thermal boundary condition (case I) when  $n = 3$ ,  $Pr = 6.8377$ ,  $Ra = 10^5$ ,  $Ha = 20$ ,  $\lambda = 0.5$ , and  $\phi = 0.04$ .
- 5.4 Streamlines evolutions at different dimensionless time ( $\tau$ ) for Cu-H<sub>2</sub>O nanofluid for uniform thermal boundary condition (case I) when  $Pr = 6.8377$ ,  $Ra = 10^5$ ,  $Ha = 20$ ,  $d = 10\text{nm}$ ,  $n = 3$ ,  $\lambda = 0.5$ , and  $\phi = 0.04$ . 50
- 5.5 Isothermal lines evolution at different dimensionless time ( $\tau$ ) for Cu-H<sub>2</sub>O nanofluid for uniform thermal boundary condition (case I) when  $Pr = 6.8377$ ,  $Ra = 10^5$ ,  $Ha = 20$ ,  $d = 10\text{nm}$ ,  $n = 3$ ,  $\lambda = 0.5$ , and  $\phi = 0.04$ . 51
- 5.6 Effect of Hartmann number ( $Ha$ ) on streamlines for (a) uniform magnetic field (umf), and non-uniform magnetic field with different periods (b)  $\lambda = 0.1$ , (c)  $\lambda = 0.25$ , (d)  $\lambda = 0.5$  and (e)  $\lambda = 1$  for Cu-H<sub>2</sub>O nanofluid for uniform thermal boundary condition (case I) when  $Ra = 10^5$ ,  $\phi = 0.04$ ,  $d = 10\text{nm}$ ,  $Pr = 6.8377$ ,  $n = 3$ , and  $\tau = 0.1$ . 52
- 5.7 Effect of Hartmann number ( $Ha$ ) on streamlines for (a) uniform magnetic field (umf), and non-uniform magnetic field with different periods (b)  $\lambda = 0.1$ , (c)  $\lambda = 0.25$ , (d)  $\lambda = 0.5$  and (e)  $\lambda = 1$ , for Cu-H<sub>2</sub>O nanofluid for uniform thermal boundary condition (case I) when  $Ra = 10^5$ ,  $\phi = 0.04$ ,  $d = 10\text{nm}$ ,  $Pr = 6.8377$ ,  $n = 3$  and  $\tau = 1$ . 53
- 5.8 Effect of Hartmann number ( $Ha$ ) on isothermal lines for (a) uniform magnetic field (umf), and non-uniform magnetic field with different periods (b)  $\lambda = 0.1$ , (c)  $\lambda = 0.25$ , (d)  $\lambda = 0.5$  and (e)  $\lambda = 1$ , for Cu-H<sub>2</sub>O nanofluid with uniform thermal boundary condition (case I) when  $Ra = 10^5$ ,  $\phi = 0.04$ ,  $d = 10\text{nm}$ ,  $Pr = 6.8377$ ,  $n = 3$  and  $\tau = 0.1$ . 54
- 5.9 Effect of Hartmann number ( $Ha$ ) on isotherms for (a) uniform magnetic field (umf), and non-uniform magnetic field with different periods (b)  $\lambda = 0.1$ , (c)  $\lambda = 0.25$ , (d)  $\lambda = 0.5$ , and (e)  $\lambda = 1$ , for Cu-H<sub>2</sub>O nanofluid for uniform thermal boundary condition (case I) when  $Ra = 10^5$ ,  $\phi = 0.04$ ,  $d = 10\text{nm}$ ,  $Pr = 6.8377$ ,  $n = 3$  and  $\tau = 1$ . 55

- 5.10 Variation of average Nusselt number ( $Nu_{av}$ ) for uniform magnetic field (umf) and non-uniform magnetic field with different periods ( $\lambda$ ), and Hartmann number ( $Ha$ ) for Cu-H<sub>2</sub>O nanofluid for uniform thermal boundary condition (case I) when  $\phi = 0.04$ ,  $Pr = 6.8377$ ,  $Ra = 10^5$ ,  $d = 10\text{nm}$ ,  $n = 3$ , and  $\tau = 1$ . 56
- 5.11 Effect of Rayleigh number ( $Ra$ ) on streamlines for (a) uniform magnetic field (umf), and non-uniform magnetic field with different periods (b)  $\lambda = 0.1$ , (c)  $\lambda = 0.25$ , (d)  $\lambda = 0.5$ , and (e)  $\lambda = 1$ , for Cu-H<sub>2</sub>O nanofluid for uniform thermal boundary condition (case I) when  $Ha = 20$ ,  $\phi = 0.04$ ,  $d = 10\text{nm}$ ,  $Pr = 6.8377$ ,  $n = 3$ , and  $\tau = 0.1$ . 57
- 5.12 Effect of Rayleigh number ( $Ra$ ) on streamlines for (a) uniform magnetic field (umf), and non-uniform magnetic field with different periods (b)  $\lambda = 0.1$ , (c)  $\lambda = 0.25$ , (d)  $\lambda = 0.5$ , and (e)  $\lambda = 1$ , for Cu-H<sub>2</sub>O nanofluid for uniform thermal boundary condition (case I) when  $Ha = 20$ ,  $\phi = 0.04$ ,  $d = 10\text{nm}$ ,  $Pr = 6.8377$ ,  $n = 3$ , and  $\tau = 1$ . 58
- 5.13 Effect of Rayleigh number ( $Ra$ ) on isotherms for (a) uniform magnetic field (umf), and non-uniform magnetic field with different periods (b)  $\lambda = 0.1$ , (c)  $\lambda = 0.25$ , (d)  $\lambda = 0.5$ , and (e)  $\lambda = 1$ , for Cu-H<sub>2</sub>O nanofluid for uniform thermal boundary condition (case I) when  $Ha = 20$ ,  $\phi = 0.04$ ,  $d = 10\text{nm}$ ,  $Pr = 6.8377$ ,  $n = 3$ , and  $\tau = 0.1$ . 59
- 5.14 Effect of Rayleigh number ( $Ra$ ) on isotherms for (a) uniform magnetic field (umf), and non-uniform magnetic field with different periods (b)  $\lambda = 0.1$ , (c)  $\lambda = 0.25$ , (d)  $\lambda = 0.5$ , and (e)  $\lambda = 1$ , for Cu-H<sub>2</sub>O nanofluid for uniform thermal boundary condition (case I) when  $Ha = 20$ ,  $\phi = 0.04$ ,  $Pr = 6.8377$ ,  $d = 10\text{nm}$ ,  $n = 3$ , and  $\tau = 1$ . 60
- 5.15 Variation of average Nusselt number ( $Nu_{av}$ ) along bottom heated diameter with uniform thermal boundary condition (case I) for different volume fraction of nanoparticles ( $\phi$ ) and differnt Rayleigh number ( $Ra$ ) for Cu-H<sub>2</sub>O nanofluid when  $Pr = 6.8377$ ,  $Ha = 20$ ,  $d = 10\text{nm}$ ,  $n = 3$ , and  $\tau = 1$ . 61



- 5.16 Effect of nanoparticles volume fraction ( $\phi$ ) on streamlines for (a) uniform magnetic field (umf), and non-uniform magnetic field with different periods (b)  $\lambda = 0.1$ , (c)  $\lambda = 0.25$ , (d)  $\lambda = 0.5$ , and (e)  $\lambda = 1$ , for Cu-H<sub>2</sub>O nanofluid for uniform thermal boundary condition (case I) when  $Ha = 20$ ,  $Ra = 10^5$ ,  $d = 10\text{nm}$ ,  $n = 3$ ,  $Pr = 6.8377$ , and  $\tau = 0.1$ . 62
- 5.17 Effect of nanoparticles volume fraction ( $\phi$ ) on streamlines for (a) uniform magnetic field (umf), and non-uniform magnetic field with different periods (b)  $\lambda = 0.1$ , (c)  $\lambda = 0.25$ , (d)  $\lambda = 0.5$ , and (e)  $\lambda = 1$ , for Cu-H<sub>2</sub>O nanofluid for uniform thermal boundary condition (case I) when  $Ha = 20$ ,  $Ra = 10^5$ ,  $d = 10\text{nm}$ ,  $n = 3$ ,  $Pr = 6.8377$ , and  $\tau = 1$ . 63
- 5.18 Effect of nanoparticles volume fraction ( $\phi$ ) on isotherms for (a) uniform magnetic field (umf), and non-uniform magnetic field with different period (b)  $\lambda = 0.1$ , (c)  $\lambda = 0.25$ , (d)  $\lambda = 0.5$ , and (e)  $\lambda = 1$ , for Cu-H<sub>2</sub>O nanofluid for uniform thermal boundary condition (case I) when  $Ha = 20$ ,  $Ra = 10^5$ ,  $d = 10\text{nm}$ ,  $n = 3$ ,  $Pr = 6.8377$  and  $\tau = 0.1$ . 64
- 5.19 Effect of nanoparticles volume fraction ( $\phi$ ) on isotherms for (a) uniform magnetic field (umf), and non-uniform magnetic field with different periods (b)  $\lambda = 0.1$ , (c)  $\lambda = 0.25$ , (d)  $\lambda = 0.5$ , and (e)  $\lambda = 1$ , for Cu-H<sub>2</sub>O nanofluid for uniform thermal boundary condition (case I) when  $Ha = 20$ ,  $Ra = 10^5$ ,  $d = 10\text{nm}$ ,  $n = 3$ ,  $Pr = 6.8377$ , and  $\tau = 1$ . 65
- 5.20 Variation of average Nusselt number ( $Nu_{av}$ ) along bottom heated diameter with uniform thermal boundary condition (case I) for different volume fraction of nanoparticles ( $\phi$ ) and Rayleigh number ( $Ra$ ) for Cu-H<sub>2</sub>O nanofluid when  $Pr = 6.8377$ ,  $Ha = 20$ ,  $d = 10\text{nm}$ ,  $n = 3$ , and  $\tau = 1$ . 66
- 5.21 Streamline contours of Hartmann number ( $Ha$ ) for different thermal boundary conditions (a)  $\theta = 1$  (case I), (b)  $\theta = 1 - X$  (case II), (c)  $\theta = X(1 - X)$  (case III), (d)  $\theta = A \sin(2\pi X)$  (case IV) and (e)  $\theta = A \sin^2(2\pi X)$  (case V) for Cu-H<sub>2</sub>O nanofluid when  $Ra = 10^5$ ,  $\phi = 0.04$ ,  $d = 10\text{nm}$ ,  $\lambda = 0.5$ ,  $n = 3$ , and  $\tau = 1$ . 67

- 5.22 Isotherms of Hartmann number ( $Ha$ ) for different thermal boundary conditions 68  
(a)  $\theta = 1$  (case I), (b)  $\theta = 1 - X$  (case II), (c)  $\theta = X(1 - X)$  (case III), (d)  $\theta = A \sin(2\pi X)$  (case IV) and (e)  $\theta = A \sin^2(2\pi X)$  (case V) for Cu-H<sub>2</sub>O nanofluid when  $Ra = 10^5$ ,  $\phi = 0.04$ ,  $d = 10\text{nm}$ ,  $\lambda = 0.5$ ,  $n = 3$ , and  $\tau = 1$ .
- 5.23 Streamlines of Rayleigh number ( $Ra$ ) for different thermal boundary conditions 69  
(a)  $\theta = 1$  (case I), (b)  $\theta = 1 - X$  (case II), (c)  $\theta = X(1 - X)$  (case III), (d)  $\theta = A \sin(2\pi X)$  (case IV) and (e)  $\theta = A \sin^2(2\pi X)$  (case V) for Cu-H<sub>2</sub>O nanofluid when  $Ha = 20$ ,  $\phi = 0.04$ ,  $d = 10\text{nm}$ ,  $\lambda = 0.5$ ,  $n = 3$ , and  $\tau = 1$ .
- 5.24 Isothermal lines of Rayleigh number ( $Ra$ ) for different thermal boundary 70  
conditions (a)  $\theta = 1$  (case I), (b)  $\theta = 1 - X$  (case II), (c)  $\theta = X(1 - X)$  (case III), (d)  $\theta = A \sin(2\pi X)$  (case IV) and (e)  $\theta = A \sin^2(2\pi X)$  (case V) for Cu-H<sub>2</sub>O nanofluid when  $Ha = 20$ ,  $\phi = 0.04$ ,  $d = 10\text{nm}$ ,  $\lambda = 0.5$ ,  $n = 3$ , and  $\tau = 1$ .
- 5.25 Streamlines of volume fraction of nanoparticles ( $\phi$ ) for different thermal 71  
boundary conditions (a)  $\theta = 1$  (case I), (b)  $\theta = 1 - X$  (case II), (c)  $\theta = X(1 - X)$  (case III), (d)  $\theta = A \sin(2\pi X)$  (case IV) and (e)  $\theta = A \sin^2(2\pi X)$  (case V) for Cu-H<sub>2</sub>O nanofluid when  $Ha = 20$ ,  $Ra = 10^5$ ,  $d = 10\text{nm}$ ,  $\lambda = 0.5$ ,  $n = 3$ , and  $\tau = 1$ .
- 5.26 Isothermal lines of nanoparticles volume fraction ( $\phi$ ) for different thermal 72  
boundary conditions (a)  $\theta = 1$  (case I), (b)  $\theta = 1 - X$  (case II), (c)  $\theta = X(1 - X)$  (case III), (d)  $\theta = A \sin(2\pi X)$  (case IV), and (e)  $\theta = A \sin^2(2\pi X)$  (case V) for Cu-H<sub>2</sub>O nanofluid when  $Ha = 20$ ,  $Ra = 10^5$ ,  $d = 10\text{nm}$ ,  $\lambda = 0.5$ ,  $n = 3$ , and  $\tau = 1$ .
- 5.27 Variation of average Nusselt number ( $Nu_{av}$ ) along bottom heated diameter for 77  
different nanoparticles volume fraction ( $\phi$ ) and different nanoparticles diameter ( $d$ ) for Cu-H<sub>2</sub>O nanofluid and uniform thermal boundary condition (case I) when  $Pr = 6.8377$ ,  $Ra = 10^5$ ,  $Ha = 20$ ,  $n = 3$ ,  $\lambda = 0.5$ , and  $\tau = 1$ .
- 5.28 Variation of average Nusselt number ( $Nu_{av}$ ) along bottom heated diameter for 79  
uniform thermal boundary condition (case I) for different shape of nanoparticles ( $n$ ) and different volume fraction of nanoparticles ( $\phi$ ) for Cu-H<sub>2</sub>O nanofluid when  $Pr = 6.8377$ ,  $Ra = 10^5$ ,  $Ha = 20$ ,  $d = 10\text{nm}$ ,  $\lambda = 0.5$ , and  $\tau = 1$ .

# CHAPTER ONE

## Fundamental of Nanofluids and Literature Review

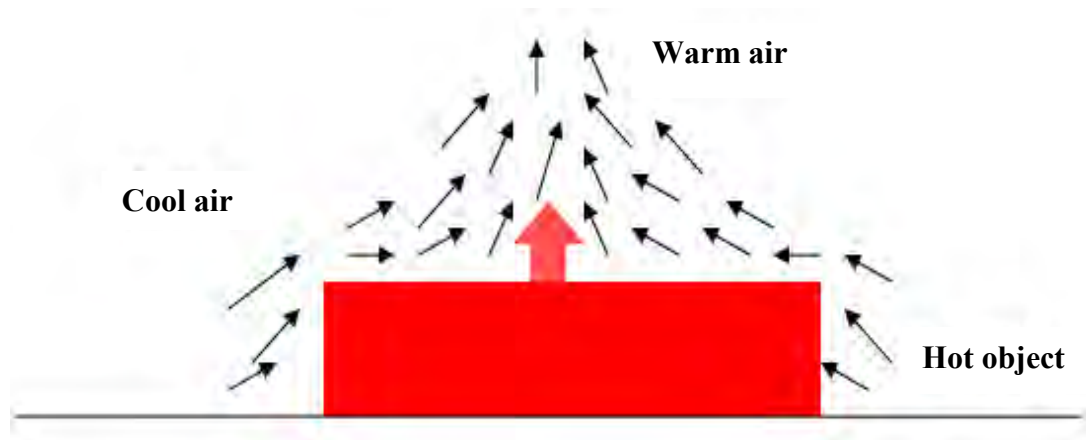
### 1.1 Introduction

Fluid dynamics is a vital science used to solve many aeronautical, chemical, mechanical, civil engineering, and many other engineering applications. A subject discipline, fluid dynamics that deals with fluids in motion and aerodynamics study air and other gases in motion. In temperature transport science that inquires, the temperature is transferred due to the difference of temperature from one system to another, not only in thermal energy but also in predicting the rate of heat exchanges that occur under particular conditions. In any industrial process, the temperature must be moved, removed, or added from one system to another. The significant issues in industrial processes are the saving of energy, enhancement of thermal rating, minimization of process time, the performance of the equipment with the extension of working life that may be created by the augmentation of cooling or heating in any industrial process. Consequently, heat transfer turns into a leading task in industrial essentiality. A considerable amount of research has been done on thermal performance to understand the thermal performance in many engineering applications, which is one of the most elementary concerns to researchers.

The investigation of heat transport has an extensive significance to engineers due to its almost universal occurrence in various branches of engineering. The primary limitation of increasing temperature transport performance is the low thermal conductivity of base fluids. Nanofluids are a novel class of liquid that can be employed to augment the heat transport rate. On account of the tiny sizes and very specific surface areas of the nanoparticles, there are some superior characteristics of nanofluids, such as higher thermal conductivity. Furthermore, metallic nanoparticles have more significant thermal conductivity than base fluids. Free convection within different cavities has recently obtained great attention due to its direct application in various engineering fields such as solar engineering applications, thermal insulation systems, geophysical fluid mechanics, etc. Understanding natural convection within the semi-circular enclosure is also helpful for the design and operation of heat exchangers or solar collectors. The main advantages of natural convection cooling systems are their simplicity, low noise, and minimum cost.

## 1.2 Natural Convection Heat Transfer

Convection is a mode of temperature transport in the form of thermal energy from a solid surface to neighboring moving fluids or gas. The motion of fluid that occurs by natural like buoyancy force is known as natural convection. The most common examples of free convection are the phenomena of the land and sea breeze. The key driving mechanism of natural convection is the difference in density due to the temperature difference. Natural convection is such a mode of flow or motion of a liquid (air, gas, water, etc.) in which the movement of the fluid is not generated by an external source such as a suction device or fan or pump, etc. In natural convection, the driven force is gravity. Natural Convection has attracted a great deal of attention from researchers due to its wide engineering applications.



**Figure 1.1:** Mechanism of natural convection heat transport from a hot body.

Suppose a heated substance is revealed in cold air (see Figure 1.1). The temperature of adjoining air will increase due to the heat drop outside of the heated substance. Consequently, a thin layer of heated air surrounding the substance is formed, and heat will be transferred to the adjacent outer comparatively cold layer from this heated layer. The density of the adjoining air of the heated substance is lower because of the higher heat of the adjacent of the heated substances. As a result, the heated air moves upwards. This type of movement of air/fluid is known as natural convection. Natural convection is used in various engineering applications such as heat loss from steam pipelines in power plants, heating of houses by electrical baseboard heaters, cooling of commercial high voltage electrical power transformers, cooling of nuclear power plants, household ventilation, solar ponds, cooling of electronic apparatus named transistors, chips using temperature sink fin, and fluid flows around shrouded heat dissipation fins.

### **1.3 Magnetohydrodynamics (MHD)**

Magnetohydrodynamics (MHD) is derived from the words magneto, hydro, and dynamics, where the phrase magneto means magnetic field, hydro indicates liquid or fluid, and dynamics implies movement. It is a branch of magneto fluid dynamics that deals with the flow of electrically conducting fluids, whether liquid or gaseous, in electric and magnetic fields. For example, plasmas, liquid metals, salt water, liquid air, electrolytes, etc. It discusses the dynamics of the substance in moving in an electromagnetic field where currents are established in the substance by induction modified field so that the flow field and dynamics equations are coupled. Hannes Alfvén received Nobel Prize for introducing MHD in 1971. MHD creates currents in moving conducting fluids and propagates forces into the liquid, changing the magnetic fields themselves. An essential new process named magnetohydrodynamics power generation that receives attention worldwide.

The electrical currents are generated with the effect of the magnetic field by the movement of the conducting fluid that modifies the magnetic field as well as magnetic field action. The action of the magnetic field assists in rising the mechanical forces, which modify the flow of the fluid. For the poor conductor of electricity, whether it is gases or liquids, electromagnetic forces will be generated, which may be the same order of magnitude as the hydro-dynamical and inertia forces. Thus, the equation of motions or other forces will have to take these electromagnetic forces into account. Various engineering problems and naturalistic real-life phenomena are susceptible to the analysis of MHD. Geophysicists employ MHD in the interactions of magnetic fields and conducting fluids present in the around heavenly bodies. The principle of the characteristics of MHD phenomenon is widely applied by engineers in space vehicle propulsion, cooling of a nuclear reactor by liquid sodium, heat exchangers, pumps, and flow meters, fusion technology, and creating novel power generating systems,.

In summary, the equations that describe MHD combine the Navier-Stokes equations of fluid dynamics and Maxwell's equations of electromagnetism. These partial differential equations can be solved simultaneously, either analytical or numerical. The phenomenon of MHD is the outcome of the mutual effect of a magnetic field and conducting fluid flowing across it. In this way, an electromagnetic force is created in a fluid flowing across a transverse magnetic field, and the resulting current and magnetic field combine to create a workforce that resists the motion of the fluids. The current also generates its own magnetic field, which distorts the original magnetic field.

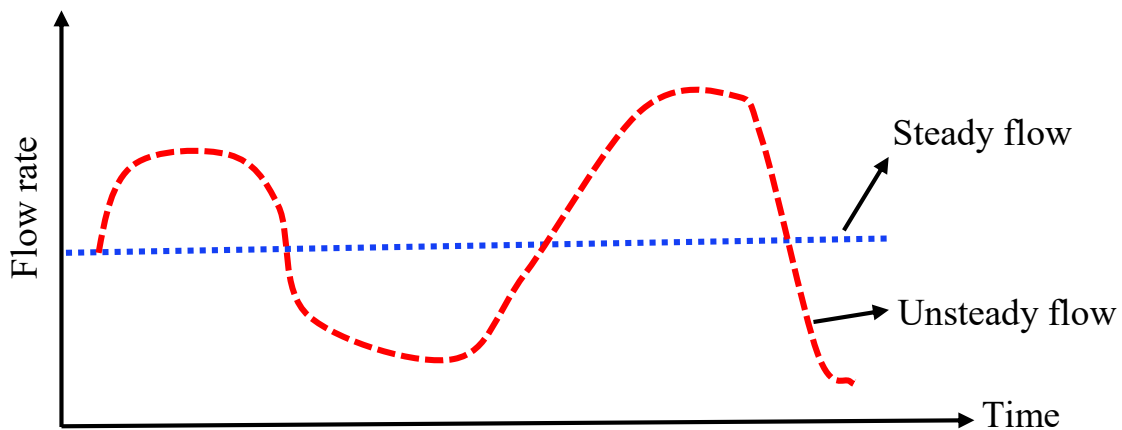
Magnetohydrodynamics wave and downstream and upstream wave phenomenon can be produced by the disturbance of the effect of magnetic field or the movement of liquids by the MHD. This phenomenon is very common in various engineering applications and occurs in nature. The science of MHD is able to describe this engineering processes and natural phenomenon.

## 1.4 Steady and Unsteady Flow

The properties of the fluid (i.e., pressure, velocity, temperature, density, and other properties) can be functions of time or space. If the flow characteristics of liquids at every point in the flow field do not depend on time, it is known as steady flow. Mathematically, steady flow can be written as:

$$\frac{\partial P}{\partial t} = 0 \quad (1.1)$$

where  $P$  represents the properties such as density, velocity, or pressure, etc. Thus,  $P = P(x, y, z)$ .



**Figure 1.2:** Steady and unsteady flow

Non-steady or unsteady flow is such flow in which the flow characteristics of the fluid (i.e., pressure, velocity, temperature, density, and other properties) depend on time. At the beginning of any process, the flow is unsteady, and it may become steady or zero flow in time. For Instance, the flow of water in a tap that has just been opened is unsteady to start with and becomes steady after a few times. The analysis of unsteady flows is undoubtedly more complex to calculate than steady flows because irregular flow conditions vary concerning both space and time, i.e., they function both space and time. The unsteadiness can be due to natural processes, human actions, or accidents and incidents. In the processes of the unsteady flow, energy, and mass within the control volume

vary continuously. It is a transient phenomenon. Flood-wave movement is a real-life example of unsteady flow. Mathematically, the unsteady flow can be written as:

$$\frac{\partial P}{\partial t} \neq 0 \quad (1.2)$$

where  $P$  represents the properties such as density, velocity, or pressure, etc. Thus,  $P = P(x, y, z)$ .

## 1.5 Prandtl Number

The Prandtl number ( $Pr$ ) is a non-dimensional number which approximates the ratio of momentum diffusivity (kinematic viscosity) and thermal diffusivity. It is named after German physicist Ludwig Prandtl, who initiated the concept of the boundary layer in 1904 and made a significant contributions on the theory of the boundary layer. Small Prandtl number ( $Pr \ll 1$ ) represents the dominant thermal diffusivity, i.e., heat diffuses very quickly throughout the liquids. In contrast, a large Prandtl number ( $Pr \gg 1$ ) represents the momentum diffusivity that dominates the behavior, i.e., heat diffuse very slowly in liquid relative to momentum.  $Pr = 1$  (approximately) indicates the rate of diffusion of heat and momentum throughout the fluid are approximately the same. It can be expressed as follows:

$$Pr = \frac{\text{Momentum diffusivity}}{\text{Thermal diffusivity}} = \frac{\nu}{\alpha} = \frac{\mu / \rho}{k / \rho c_p} = \frac{\mu c_p}{k} \quad (1.3)$$

where,  $\nu$  represents kinematic viscosity [ $\text{m}^2\text{s}^{-1}$ ],  $\alpha$  indicates thermal diffusivity [ $\text{m}^2\text{s}^{-1}$ ],  $c_p$  represents specific heat at constant pressure [ $\text{Jkg}^{-1}\text{k}^{-1}$ ], and  $k$  represents thermal conductivity [ $\text{Wm}^{-1}\text{k}^{-1}$ ]

## 1.6 Hartmann Number

The Hartmann number ( $Ha$ ) is a non-dimensional number which indicates the ratio of electromagnetic force and viscous force. This non-dimensional number measures the importance of drag forces resulting from viscous forces and induction of magnetic effects. In addition, it characterizes the flow of conducting fluid in a transverse magnetic field. Because it is a product of the magnetic flux density, a characteristics length, and square root of the ratio of electrical conductivity to viscosity. It is defined as:

$$Ha = \frac{\text{Electromagnetic force}}{\text{Viscous force}} = B_0 L \sqrt{\frac{\sigma}{\mu}} \quad (1.4)$$

where,  $B_0$  represents magnetic field [ $\text{Nm}^{-1}\text{A}^{-1}$ ],  $L$  represents characteristics length [ $\text{m}$ ],  $\sigma$  indicates

electrical conductivity [ $\Omega\text{-m}$ ], and  $\mu$  represents dynamical viscosity [ $\text{kgm}^{-1}\text{s}^{-1}$ ].

## 1.7 Rayleigh Number

The Rayleigh number ( $Ra$ ) is a non-dimensional number connected with the flow of fluids by buoyancy force. It is involved with free convection or natural convection. The value of Rayleigh number indicates wheater the fluid is convection or conduction. It is the property of a fluid that determines how heat is transferred through the liquid. It represents the product of the Grashof number and Prandtl number. The ratio of buoyancy forces and viscous forces multiplied by the percentage of momentum diffusion and thermal diffusion. The values of the Rayleigh number is below a critical value indicates the primary heat transfer mood is conduction, whereas it exceeds the critical value indicates that temperature transport is mainly by convection. The most significant use of the Rayleigh number is that it characterizes the laminar to turbulence transition of a natural convection boundary layer flow. It can be expressed as:

$$Ra = Gr.Pr = \frac{g\beta(T_h - T_c)L^3}{\nu^2} \cdot \frac{\nu}{\alpha} = \frac{g\beta(T_h - T_c)L^3}{\nu\alpha} \quad (1.5)$$

where,  $Gr$  represents Grashof number,  $Pr$  represents Prandtl number,  $g$  represents gravitational acceleration [ $\text{ms}^{-2}$ ],  $\beta$  represents the coefficient of thermal expansion [ $\text{K}^{-1}$ ],  $\alpha$  represents thermal diffusivity [ $\text{m}^2\text{s}^{-1}$ ],  $T_h$  represents surface temperature [ $\text{K}$ ],  $T_c$  represents bulk temperature [ $\text{K}$ ],  $L$  represents characteristics length [ $\text{m}$ ] and  $\nu$  is kinematic viscosity [ $\text{m}^2\text{s}^{-1}$ ].

## 1.8 Nusselt Number

The Nusselt number ( $Nu$ ) is a non-dimensional number that illustrates augmentation of temperature transport throughtout the fluid layer because of convection comparative to conduction across the same layer of the fluid. It represents how much heat is transferred due to fluid motion compared to the heat transfer by fluid by the process of conduction. It is defined as follows:

$$Nu = \frac{hL}{k} \quad (1.6)$$

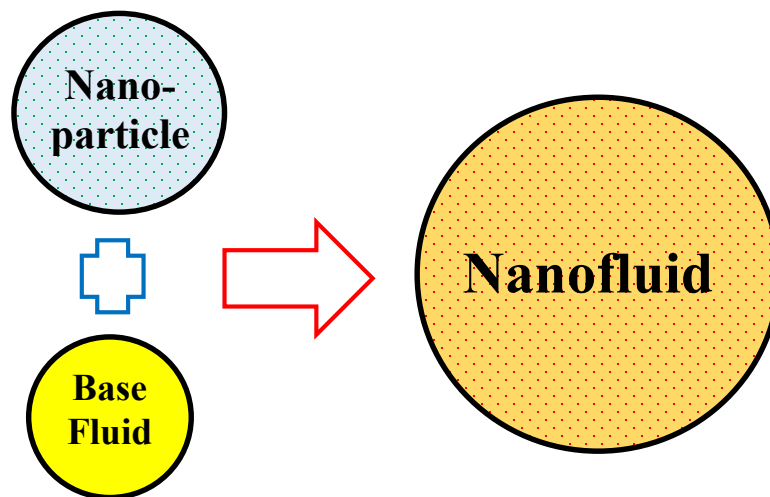
where  $k$  represents the thermal conductivity of the fluid,  $h$  represents the heat transfer coefficient, and  $L$  represents characteristics length. At the beginning of twenty century, Wilhelm Nusselt first introduced this non-dimensional number, which made significant contributions to convection temperature transport. It is viewed as the non-dimensional convection heat transfer coefficient.



The more significant Nusselt number indicates a large temperature gradient at the surface and high-temperature transport by convection. The Nusselt number  $Nu = 1$ , indicates that all temperature is transported through conduction and fluid is stationary. The higher the Nusselt number ( $Nu > 1$ ), the motion of the fluid augments the temperature transport through advection.

## 1.9 Definition of Nanofluids

For industrial, engineering, and energy system, the augmentation of heat transfer within enclosures is a burning issue. Generally, to transfer the temperature from one system to another, water, ethylene glycol, mineral oils are used as a fluid. But these fluids are not enough to fulfill the demand for higher heat exchangers in modern technology, for instance, microelectronics, power stations, production of chemicals, etc. The fluid, as mentioned above, is not more effective in the case of the heat exchanger. To fulfill the demand, it is essential for such fluid that has an efficiency of containing higher temperature. Nanofluids are used to satisfy the need for modern technology. The important class of fluids such as nanofluids which helps to advance nanotechnology in various ways. Generally, it is a dilute liquid suspension of conventional fluid and nano-shaped particles where nanoparticle size is smaller than 100nm. Nanofluid is a new class of nanotechnology-based temperature transport fluid.



**Figure 1.3: Making of Nanofluid**

The thermal conductivity of water containing three different nanoparticle suspensions such as Cu,  $TiO_2$ ,  $Al_2O_3$ , and  $SiO_2$  is more remarkable than pure water, where the size of the nanoparticles has

been maintained between 1nm to 100nm. Nanofluids are a novel that contains nanoparticle fluid suspensions, which was first introduced by Choi in 1995 at Argonne national laboratory, USA to denominate a novel class of nanotechnology-based temperature transport liquids. The destination of this novel fluid consisting of conventional fluid and nano sized particles is that achieving the maximum feasible heated characteristics at the most negligible possible concentrations (preferably < 1% by volume) by stable suspension of nanoparticles (preferably < 10nm) and uniform dispersion of it into the base fluid. Much research on nanofluids has been done to understand nanofluids' behavior to utilize them as temperature transport augmentation in various industrial processes such as transportation, heat exchanger, biomedicine, electronics, and nuclear reactors.

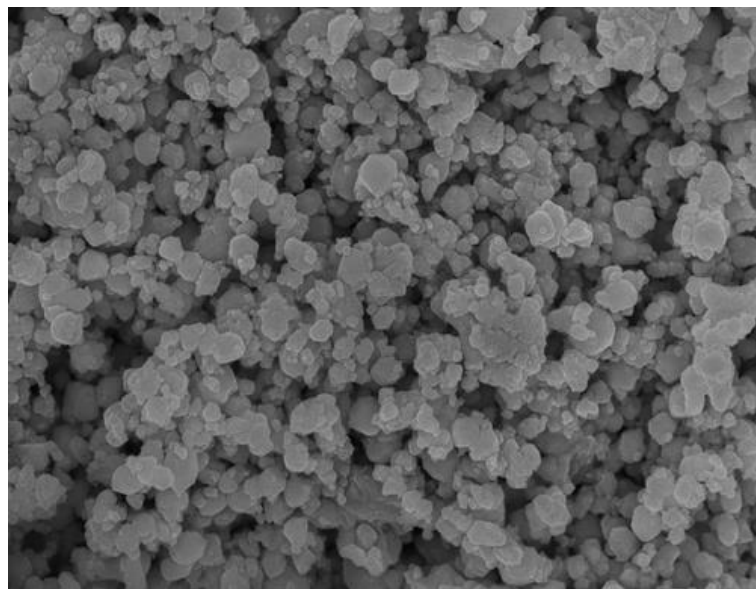
The heat transfer performance of nanofluids is significantly increased by suspending nanophase particles in heating or cooling fluids. The principle causes are listed follow as:

- The suspension of nano-sized particles into base fluid enhance the area of the surface as well as the capacity of the temperature of the liquid.
- The suspending nano sized particles augment the effectiveness of the thermal conductivity of the fluids.
- The mixing fluctuation and turbulence of the fluids are intensified.
- The dispersed nano shaped particles fatten the gradient of the transverse temperature of the liquids.

## **1.10 Nanoparticles**

Nanoparticles are widely engaged in many industrial and engineering processes to fulfill the higher heat transfer rate demand. Nanoparticles that are employed to produced nanofluid is made from different material like oxide ceramics, for examples, CuO, Al<sub>2</sub>O<sub>3</sub>, and ZnO; chemically stable metals, for examples, aluminum, gold, silver, copper; nitride ceramics, for examples, AlN, and SiN; metal carbides, for examples, SiC, carbide ceramics, for examples, SiC, and TiC); semiconductors, for examples, TiO<sub>2</sub>, and SiC; metals, for examples, Cu, Au, and Ag; metal oxides, for examples, alumina, titanium, silica, zirconia, and copper oxide; carbon in different forms, for examples, carbon nanotubes, graphite, and diamond. The principal factors of nanoparticles that are taken into account are ease of availability, costs, thermal conductivity, the tendency of the particles

to hold them into the base fluid with negligible agglomeration, etc. There are two methods of production of nanoparticles such as (i) physical methods, including inert-gas condensation (IGC): mechanical grinding, and (ii) chemical methods, including chemical vapor deposition (CVD): spray pyrolysis, thermal spray, microemulsions, and chemical precipitation, etc. Most of the nanoparticle shows better heat transfer characteristics which are widely engaged in practical applications. Some of them also less costly and environmentally friendly. Most of the nanoparticles are made up of a few hundred of atoms. The diameter of the small molecules and the atoms is 0.1nm, but the diameter of the nanoparticles and the atom is 1-100nm.



**Figure 1.4:** Copper oxide nanoparticles

## **1.11 Nanoparticles Size**

A nanoparticle is a tiny particle that is undetectable by the human eye, ranging between 1 to 100 nanometers. The physical and chemical properties of nanoparticles can exhibit significantly different from their larger material counterparts. The particle size is significant for preparing a practical nanofluid. The reasons for fixing up the size of the nanoparticles are listed below:

- (i) The size of the particles is important in making nanofluids stable. Dense nanoparticles can be suspended in liquids because the particles have an extremely high ratio of surface area to volume so that the interaction of the particle surface with the fluids is strong enough to overcome differences in density.

- (ii) The size of the particles is essential in making nanofluids with novel properties. The tiny size of the particles is affected by transport mechanisms at the nanoscale.
- (iii) The size of the particles is significant in making nanofluids useful. For instance, the nano-sized particles are similar to bio-molecules employed successfully in various biomedical applications such as drug delivery.

## 1.12 Base Fluids

The Base fluid is conventional fluid. Many types of liquids with low thermal conductivity can be used successfully, and effectively as base fluid, such as engine oil (EO), water (H<sub>2</sub>O), ethylene glycol (EG), glycerol, pump oil, oil, kerosene, and other lubricants, polymer solutions, bio-fluids, glycerine and so on. Many of them are widely engaged in different industrial processes and engineering applications.

## 1.13 Solid Volume Fraction of Nanoparticles

The characteristics of nanofluid are changed by nanoparticles volumetric fraction, nanoparticles size, and nanoparticles shape. The nanoparticle volume fraction ( $\phi$ ) is divided by the volume of all constituents of the nanofluids. In an ideal solution, volume fraction coincides with the volume concentration, where the volumes of the constituents are additive. That is, the volume of the solution is equal to the sum of the volumes of the nanoparticles. The sum of volume fractions of the solution is equal to 1. i.e.

$$\sum_{i=1}^N \phi_i = 1 \quad (1.7)$$

## 1.14 Background of the Study

Natural convection temperature transport is a widespread phenomenon in many engineering applications. Various researchers have given it abundant importance. Different researchers have performed various experimental and numerical studies to understand the free convection temperature transport phenomenon properly. Velocity distribution and temperature distributions in natural convection have a vital role in controlling components of various industries. For instance, nuclear reactor cooling, electrical systems, fire engineering, enhancing cooling systems in the vehicle, heat exchangers, petroleum reservoirs, and so on are real-life examples. The benefits

of the use of natural convection are its simplicity. The fundamental problem of free convection in enclosures has been accepted significant consideration to researchers. Many investigations on the natural convection mechanism of nanofluids within different chambers were investigated very recently. Most of these enclosures commonly used effectively in industries are triangular, trapezoidal, cylindrical and rectangular, semi-circular etc.

During the last two decades, the investigation of nanofluids' apparent thermal conductivity, which contains different solid nanoparticles, has been applied effectively to produce improvements in heat transfer procedures. A novel generation of fluids called nanofluids is replaced instead of conventional thermal fluids. To investigate the impacts of nanofluids, much research is carried out by different researchers [1-2]. They investigated augmentation of thermal conductivity of the fluids that contain nano-sized particles is more significant. By suspending metallic nanoparticles into base liquid, a new class of fluid introduced by them has higher thermal conductivity compared to conventional liquids and can be employed as temperature transport fluids. Das *et al.* [3] theoretically performed the effects of nanofluids on convective temperature transport modeling of thermal conductivity of nanofluid and the application of nanofluids in science and engineering. Ma *et al.* [4] also performed about the temperature transport capability of a nanofluid in an oscillating heated pipe. This investigation tried to develop highly efficient cooling devices.

Nowadays, Nanofluids are commonly engaged in the enhancement of temperature transport. Different types of nanoparticles such as  $\text{Al}_2\text{O}_3$ , Cu,  $\text{TiO}_2$ ,  $\text{Fe}_3\text{O}_4$ , CuO, Co,  $\text{Fe}_2\text{O}_3$ , silver, silicon, carbon nanotubes are available commercially. Water, kerosene, engine oil, pump oil, kerosene, and so on are used widely as conventional fluids. The very common nanofluids such as  $\text{TiO}_2$ -water, Cu-water,  $\text{Al}_2\text{O}_3$ - ethylene glycol, CuO-water,  $\text{Al}_2\text{O}_3$ -water are used successfully for the augmentation of heat transfer. Buongiorno [5] performed convective temperature transports of nanofluids. The results narrated that nanofluids have higher heated conductivity compared to the base fluid. Murshed *et al.* [6] also investigated the thermal conductivity enhancement of titanium dioxide and water-based nanofluids. The outcomes illustrated that the shape and size of nanoparticles significantly affect the enhancement of thermal conductivity. Ece and Buyuk [7] performed about time-independent free convective laminar flowing within an inclined rectangle shape enclosure, including the influence of the magnetic field.

Extensive attention to the field of nanofluids has been obtained because of their enriched thermo-physical properties. Nanofluids are used effectively as heat exchangers in industries to harvest solar energy to produce renewable energy. The application of nanofluids in various heat transfer devices is widely engaged, such as solar collectors, heat exchangers, electronic cooling, thermal storage system, radiators, and refrigeration systems. Nanoparticles can improve the thermal characteristics of conventional fluid. Hwang *et al.* [8] performed the characteristics of buoyancy-driven temperature transport of  $\text{Al}_2\text{O}_3$ -water nanofluids within a rectangle shape enclosure. The results indicate that  $\text{Al}_2\text{O}_3$ -water nanofluid is more stable for enhancing nanoparticles volume fraction and smaller size of nanoparticles. Jou and Tzeng [9] investigated numerically two-dimensional free convection temperature transfer within a rectangular cavity which contains nanofluids. The numerical outcomes displayed that the mean rate of temperature transport augments with the increase of the buoyancy parameter and the addition of nanoparticles.

The heat transport and fluid flow introduced by the buoyancy-driven parameter in a heated cavity is an important topic due to wide applications in the cooling of electronic heaters. Oztop and Nada [10] investigated the characteristics of free convective fluid flow and temperature transport of nanofluids inside a rectangle enclosure numerically. Different types of nanoparticles were used for this numerical investigation. The output of this investigation showed that the average Nusselt number increases for the increase of nanoparticles volume fraction and Rayleigh number. The outcomes also showed that the highest heat transfer was also observed for copper nanoparticles. Ghasemi and Aminossadati [11] investigated free convective heat transfer within an inclined cavity which contains  $\text{CuO}$ -water nanofluids. The results indicate that the addition of nanoparticles enhances the heat transfer rate and the Rayleigh number significantly increases the performance of heat transfer and fluid flow.

Aminossadati and Ghasemi [12] also studied the enhancement of the natural convective flow of nanofluids within an isosceles triangle shape enclosure. They found that thermal performance increases with the increase in the Rayleigh number and solid volume fraction of nanofluids within the chamber. Saleh *et al.* [13] performed free convective temperature transport within the trapezoidal cavity containing copper-water and  $\text{Al}_2\text{O}_3$ -water nanofluids. They showed that the rate of heat transfer enhances more with the increase of copper nanoparticles. Rashmi *et al.* [14] performed about the study of computational fluid dynamics on free convective temperature

transport using  $\text{Al}_2\text{O}_3$ -water nanofluids. The simulated numerical values of effective thermal conductivity show that heat transfer decrease with the increase of volume fraction of nanoparticles. Sheikhzadeh *et al.* [15] investigated numerically the heat transfer and buoyancy-driven fluid flow within a rectangle shape enclosure that contains  $\text{TiO}_2$ -water nanofluid. This study predicts that the mean Nusselt number augments with the increment of nanoparticle volume fraction.

Buoyancy initiated natural convective fluid flow, and temperature transport is a significant phenomenon in science and engineering for its numerous potential applications such as electronic cooling, electronics, heat exchangers, automotive, etc. Buoyancy forces and temperature differences are the leading causes of natural convective heat transfer. Arani *et al.* [16] studied the numerically free convective flow of laminar and incompressible Ag-water nanofluids inside a square enclosure. The outcomes predict that heat transfer rate along heated walls enhances with the increase of nanoparticle volume fraction. Solemani *et al.* [17] investigated finite element analysis of natural convective heat transport of Cu-water nanofluid within a semi-annulus cavity. Nasrin and Parvin [18] analyzed the heat transfer mechanism of free convection within a trapezoidal cavity, which contains copper-water nanofluid, by using the finite element technique. The numerical results showed that the physical parameters named Rayleigh number, Prandtl number, and nanoparticles volume friction significantly impact heat transfer.

The science which conducts the reciprocal interaction of the conducting liquid and magnetic field is known as MHD. Various investigations have been done on MHD regarding different geometry and various boundary conditions. MHD has many applications like crystal process, solar technologies, boiler, manufacturing technology, chemical and food processing, etc. MHD convection plays a vital role in materials engineering. Sheikholeslami *et al.* [19] researched MHD free convection using Cu-water nanofluid within an inclined half annulus based on the finite element method. The parameters such as Rayleigh number and Hartmann number significantly control the convection flow and the rate of heat transfer. Nasrin and Alim [20] performed natural convective flow and heat transport of nanofluids inside a cavity using two different nanoparticles. Hussain and Hussain [21] investigated heat transfer enhancement on free convective within a parallel shape cavity using Cu-water nanofluid. The results show that the addition of copper-water nanofluid remarkably increases the rate of heat transfer.

Malvandi *et al.* [22] performed the impact of magnetic fields on convection temperature transport within an annulus using  $\text{Al}_2\text{O}_3$ -water nanofluid. Rahman and Al-Hatmi [23] investigated a comprehensive study about the characteristics of magneto-hydrodynamics temperature flow. The results show that the velocity of the nanofluids enhances for buoyancy parameter and volume fraction of nanoparticles whereas decreases with the increase of Hartmann number. In addition, the heat transfer rate is higher in  $\text{TiO}_2$ -water nanofluid compared to the heat transfer rate in  $\text{Al}_2\text{O}_3$ -water and Cu-water nanofluids. Koopaee and Jelodari [24] investigated the impact of the inclination angle of magnetic field on time-dependent free convective temperature transport of nanofluids within an enclosure where  $\text{Al}_2\text{O}_3$  was used as nanoparticles. Mejri *et al.* [25] investigated the effect of magnetic field on laminar natural convection of  $\text{Al}_2\text{O}_3$  nanofluid within the cavity heated sinusoidally. The heat transfer rate enhances with the increase of Hartmann number and Rayleigh number, whereas it decreases with the addition of nanoparticles.

Sheikholeslami *et al.* [26] performed MHD effects on CuO–water nanofluid flow and heat transfer with Brownian motion. This study predicts that the Rayleigh number enhances heat transfer whereas decreases with a higher Hartmann number. Rahman *et al.* [27] investigated time-dependent MHD convection using Cobalt–kerosene ferrofluid within a semi-circular cavity employing finite element analysis. This study predicts that the rate of heat transfer decreases for the intensity of the magnetic field. Rahman *et al.* [28] performed about time-dependent free convective temperature flow of CNT-water nanofluid within an enclosure. The results predict that the volume fraction of nanoparticles can control the flow field, temperature distribution, and heat transfer. Alsabery *et al.* [29] performed the free convection flow of nanofluids within a square cavity, including sinusoidal temperature variations. The results show that sinusoidal temperature variations significantly enhance the convection heat transfer rate.

Ouyahia *et al.* [30] investigated the MHD thermal conductivity of titanium dioxide nanofluids within a triangle cavity. They found that the thermal performance within the enclosure was significantly changed by the solid volume fraction of nanoparticles and Rayleigh number. Mojumder *et al.* [31] investigated the effects of the magnetic field upon the free convective of ferrofluid within a half-moon-shaped enclosure. The results indicate the rate of heat transfer reduces significantly with the increment of the magnetic field. Kalbani *et al.* [32] performed about the time-dependent MHD free convective fluid flow and temperature transfer of nanofluids



within a square cavity, taking into account the Brownian motion of the nanoparticles. The results indicated that the enhancement of heat transfer strongly depends on nanoparticles diameter and nanoparticles Brownian motion. In addition, the rate of heat transfer increases for the increment of nanoparticle volume fraction and Rayleigh number, whereas it decreases for higher Hartmann numbers. The highest heat transfer rate is observed for Kerosene-based nanofluids than for engine oil or water-based nanofluids.

Uddin *et al.* [33] performed a comprehensive study of the fundamental and development biosphere of the nanofluids. This study narrated widely the properties and fundamental concepts of nanofluids and the potential application and advantages of nonofluids in various sectors. Parvin *et al.* [34] investigated the performance of natural convective heat transfer in nanofluid within an enclosure considering non-isothermal boundary conditions. They stated that heat transfer increases with the increase of the volume fraction of nanoparticles. Rahman *et al.* [35] investigated time-dependent free convective heat transfer of nanofluid within a cavity. They studied that heat transfer rate increases with the increase of nanoparticle volume fraction. Sheikha *et al.* [36] analyzed the free convective temperature flow of nine different nanofluids, including various shapes of the nanoparticles within a trapezoidal enclosure. This research shows the solution becomes the steady-state with a strong buoyancy force, and the highest heat transfer rate is observed for cobalt-engine oil nanofluid and blade shape nanoparticles.

In thermal engineering, the enhancement of heat transfer is essential. Heat transfer is a science which deals with the transfer of thermal energy. Energy is such a necessary quantity that must be transferred before performing work on any system. The energy transformation is created by heat or work. Heat transfer occurred from one system to another for the temperature difference between two systems. Heat transfer is necessary for our daily life for drying, refrigeration, cooking, etc. Qi *et al.* [37] investigated about free convective temperature flow of Cu/diamond–gallium nanofluids within a rectangle cavity. The results show that the enhancement of heat transfer can be improved 73.0% by Cu–Ga nanofluid compared to liquid metal gallium at the low-temperature difference ( $\Delta T = 1K$ ). Parvin and Akter [38] performed the impact of MHD on the natural convective flow of nanofluids within a prismatic enclosure. The results indicated that the rate of heat transfer changed significantly for the increment of Hartmann number. Uddin and Rahman [39] also investigated finite element analysis of free convective flow nanofluids within an annulus.

In everyday life, temperature interchanges are the principal components of many devices. For example, domestic water heating, air-conditioning, oil refineries, marine gas turbines, power plants, and land vehicles. These devices' mechanism depends on providing a flow of thermal energy of two or more systems of heat differences. Kalbani *et al.* [40] also investigated MHD buoyancy introduced heat transfer of nanofluids within a square enclosure. This investigation predicts that heat transfer rate increases significantly with the increment of nanoparticle volume fraction and Rayleigh number, whereas it decreases for Hartmann number. The maximum rate of heat transfer was observed for blade shape nanoparticles than other shapes of nanoparticles. Uddin and Rasel [41] investigated unsteady free convection heat transfer of copper oxide-water nanofluid within a cavity. Uddin [42] investigated the unsteady MHD natural convective temperature flow of copper-water nanofluid within a semi-circular enclosure. The results show that the heat transport rate significantly depends on the magnetic field.

Mehryan *et al.* [43] investigated the effects of horizontal magnetic field on the free convection flow of ferrofluid within a square enclosure. This investigation predicts that the magnetic field period enhances the intensity of convective flow circulation and heat transfer rate. Mahian *et al.* [44] performed a comprehensive study of nanofluids and mathematical modeling and its numerical simulation, challenges of nanofluids, improvement of the nanofluid flow, and heat transfer modeling. Kalbani and Rahman [45] also investigated the effects of MHD on the convective flow of nanofluids within an inclined square cavity. They studied that heat transfer rate within the cavity significantly depends on nanoparticles volume fraction, Hartmann number, and Rayleigh number. Balushi *et al.* [46] performed unsteady free convection flow of magnetic nanoparticles within a square cavity. They investigated that the highest heat transfer rate is observed for Kerosene-based nanofluids. Also, the mean heat transfer rate increase for the volume fraction of nanoparticles and Rayleigh number, and it becomes highest for the blade shape of nanoparticles.

The performance of heat transfer in many engineering systems is an essential topic from an energy-saving perspective. The elementary limitation of the conventional fluids named water, oils, and kerosene is low thermal conductivity. Generally, thermal conductivity is higher of solid particles than liquids. For instance, the thermal conductivity of copper is 700 times greater than water and 3000 times greater than engine oil. Izadi *et al.* [47] performed the effects of periodic magnetic field

on the free convective flow of hybrid nanofluids within a permeable chamber. They conclude that the periodic magnetic field has a non-monotonic influence on convective heat transfer performance. Marzougui *et al.* [48] performed MHD convective flow of copper-water nanofluids within an enclosure. They showed that heat transmission and flow field affects significantly by nanoparticle volume fraction and Hartmann number. Giwa *et al.* [49] investigated the heat transfer performance of nanofluids in a magnetic field in a square enclosure. They studied that heat transfer rate significantly depends on the types of nanofluids and the Brownian motion of nanoparticles. They conclude that magnetic field strength enhances heat transport rate.

From the above literature survey, it is obvious the convective heat transfer under the influence of magnetic field depends in a cavity with nanofluids depends on several mode parameters such as Rayleigh number, Hartmann number, the solid volume fraction of nanoparticles, Brownian motion of the nanoparticles, shape of the nanoparticle and size of the nanoparticles, etc. The characteristics of heat transfer and fluid flow depend on types of nanoparticles and base fluid and cavity geometry with the variation of the above-mentioned parameters. This numerical study aims to examine the unsteady natural convection flow and heat transfer of a copper-water nanofluid in a semi-circular enclosure under the influence of a periodic magnetic field. Different types of nanofluids, for instance, Cu, Co, Fe<sub>3</sub>O<sub>4</sub>, Al<sub>2</sub>O<sub>3</sub>, Ag, Zn, CuO, and TiO<sub>2</sub>, and different types of base fluid such as water, kerosene, engine oil, and ethylene glycol are used to investigate the best heat transfer performance where Cu-H<sub>2</sub>O nanofluids have been employed as the default nanofluids. Different types of thermal boundary conditions are also used to analyze the best heat transport performance. This study has much specific importance because this phenomenon is a widespread practice in many industrial and engineering applications.

## **1.15 Motivation of Research**

The literature review shows that the MHD natural convection heat transfer and fluid flow in cavities have received considerable attention due to its application in several thermal engineering problems. It is also mentioned that several authors considered natural convection, different types of nanofluids, and different types of enclosures, with or without uniform MHD and time-independent cases individually. But no study was investigated about the unsteady natural convection fluid flow and heat transfer within a semi-circular cavity filled with nanofluids under the influence of the periodic magnetic field, including Brownian motion of nanoparticles. This

study has many engineering applications and real-life applications such as heat exchangers, cooling or heating electrical equipment, biomedical engineering, etc. Therefore, extensive numerical studies are essential to ensure efficient performance of fluid flow and heat transfer, to observe characteristics of vertically periodic magnetic field on natural convection, to understand the variation of fluid flow and heat transfer of nanofluids under the influence of non-uniform magnetic effect and Brownian motion of nanoparticles for different physical changes such as Rayleigh number, Hartmann number, nanoparticles volume fraction, and so on with different boundary conditions that form the basis of the motivation of behind the selection of the present study.

## **1.16 Main Objectives of the Study**

The present study investigates numerically time-dependent natural convective heat transfer inside a semi-circular cavity filled with nanofluids (copper-water) with Brownian motion of nanoparticles via the periodic magnetic field. The outcomes of different model parameters such as Hartmann number, nanoparticles volume fraction, and Rayleigh number will be presented in terms of streamlines, isotherms, and heat transfer rate, local and average Nusselt number. The main objectives of the proposed study are as follows:

- To formulate the mathematical model for the physical problem regarding natural convection heat transfer and fluid flow and transfer the governing equations into the non-dimensional form using appropriate transformations.
- To solve the governing equations numerically using finite element method (FEM) of Galerkin weighted residual type.
- To validate the computational procedure and results found from this study with existing literature or other published works.
- To investigate the effects of various physical parameters such as Hartmann number, Period of the non-uniform magnetic field, Rayleigh number, the solid volume fraction of nanoparticles, and nanoparticles diameter, Brownian motion of the nanoparticles on the streamlines and isotherms inside the cavity.
- To illustrate the numerical results of the heat transfer rate concerning the average Nusselt number graphically for the parameters mentioned earlier.

## **1.17 Outline of the Thesis**

This investigation is concerned with the effects of unsteady natural convective heat transfer and fluid flow of copper-water nanofluid within a semi-circular enclosure under the influence of periodic magnetic field considering the Brownian motion of the nanoparticles. In chapter one, some basic concepts related to this study and the fundamentals of nanofluids have been presented and discussed, and relevant discussion on dimensionless parameters. A brief discussion of the literature review of the past studies on fluid flow and heat transfer in various cavities or channels under different boundary conditions is presented. Also, a brief introduction is given with the main objectives and inspiration behind selecting the present study. In chapter two, the computational techniques of the current problem have been discussed. The finite element method has been carried out elaborately. The solution domain has been discretized into finite element meshes of non-uniform triangular elements. In chapter three, the nonlinear governing partial equations with boundary conditions have been transferred into a non-dimensional form using a set of transformation variables. The finite element formulation of the non-dimensional partial differential equations is also performed. In chapter four, numerical analysis and comparison with other previously published work have been discussed. In chapter five, the outcomes of different physical parameters, for example, Rayleigh number, Hartmann number, nanoparticles volume fraction, size of the nanoparticles, the diameter of the nanoparticles, are presented in terms of streamlines, isotherms, and average Nusselt number and discussed them from a physical point of views. Different types of nanoparticles are also considered to calculate the heat transfer performance regarding the average Nusselt number. Different types of thermal boundary conditions are also taken into consideration to examine the best heat transfer performance. In chapter six, finally, the main achievements and some ideas of further work have been summarized.

# **CHAPTER TWO**

## **Computational Procedure**

### **2.1 Computational Fluid Dynamics**

The computational Fluid Dynamics (CFD) method is becoming very popular for technological and scientific interests without doing any experiments because it is time-consuming and economical for solving fluid flow problems. Experimental investigation of temperature transport and fluid flow could not be adequately achieved in fluid dynamics due to their limited flexibility. The analytical methods of solution are not also more helpful due to the engagement of complex geometric bodies, a large number of variables, different boundary shapes, and conditions. Consequently, numerical methods are the best alternative for performing the solution of practical problems of partial differential equations. For complicated geometry or some vital feature that cannot be solved with a standard method, CFD is used to solve such engineering problems by computer-based simulation. CFD involves the information of a set of algebraic equations, which constitutes a practical approximation of a natural living system. The outcomes of the computational procedure can understand the performance of a system. Thereby, researchers apply CFD simulation codes with finite grids to make realistic solutions physically with reasonable accuracy. The exact and dependable prophecy of complex geometry greatly fulfills the intense demand for more excellent reliability and economic challenges. These behaviors frequently occur in CFD. CFD is applied for numerical calculation of fluid dynamics over the years. Now it is also used successfully for large-scale applications of industrial problems, including turbulent flows.

### **2.2 Discretization Approaches**

To solve a mathematical model of the physical phenomenon numerically, the first step of the solving procedure is numerical discretization. This means that each differential equation component is transferred into a numerical analog, represented in the computer, and then processed by a computer program built on some algorithm. There are several discretization methods available for the high-performance numerical computation in CFD, such as finite difference method (FDM), finite volume method (FVM), finite element method (FEM), boundary element method (BEM), and boundary volume method (BVM).

## 2.3 Finite Element Method

All the numerical methods have their strength and some weakness for solving the partial differential equations. FDM relies on the philosophy that the body is in one single piece. Still, the parameters are evaluated only at some selected points within the body, satisfying the governing differential equations. In contrast, the FVM relies on the philosophy that the body is divided into a finite number of control volumes. On the other hand, in the FEM, the body is divided into several elements. FEM works when all other methods fail, and it's managing complex geometrical bodies and boundaries. The advantage of this method, it considers the body is not in one piece. Still, it is an assemblage of elements connected only at nodes, and the finite element solution is highly dependent on the element type. Another advantage of FEM is that of the specific model to deduce the equations for each element that are then assembled. FEM is comparatively simple to analyze mathematical problems.

In current numerical computation, Galerkin weighted residual finite element technique has been used. It is a most powerful numerical computational technique for finding the approximate solutions of a system of PDEs. For solving fluid dynamics problems, the popularity of FEM increases over time. This technique is adequately global for dealing with time-dependent and non-linear flow problems in irregular domains. By clipping together the local approximations of the phenomena under consideration, the mathematical model generation is formed, which is a fundamental characteristic of FEM. The significant advantage of FEM is the ability to deal with arbitrary complex geometries.

Furthermore, every element can subdivide easily, and the grid can simply redefine. FEM produces equations for each component independently of all other elements. Only when the equations are collected together and assembled into a global matrix are the interactions between elements taken into account. FEM dominates most of the computational procedures for these ideal characteristics. For FEM, there are no restrictions on the connection of the elements when the sides of the elements are correctly aligned and have the same nodes for the neighboring elements. This flexibility allows us to model very complex geometry.

In FEM, the domain is subdivided into a set of discrete volumes of finite elements, which are usually unstructured. For two-dimensional geometry, finite elements are generally formed by

triangles or quadrilaterals. In three-dimensional geometry, the finite elements are traditionally created tetrahedral or hexahedra. The distinctive feature of the weighted residual finite element method is that the equations are multiplied by a weight function before they are integrated over the entire domain. A linear shape function approximates the solution within each element to guarantee continuity of a solution across element boundaries. The weight function is generally of the same form of shape function. Then the approximation is substituted into the weighted integral of the conservation equations. In the natural study, potential flow problems are elaborately discussed using FEM by Kalbani *et al.* [32]. Finite element models of unsteady compressible and incompressible flow problems were obtained by Uddin *et al.* [39]. The implementations of FEM problems in fluid mechanics have been discussed by Zienkiewicz and Taylor [51].

The primary idea of FEM is to view a given domain as an assemblage of simple geometric shapes called finite elements, for which it is possible to systemically generate the approximation functions needed in the solution of PDEs by the variation or weighted residual method. The computational domains with irregular geometries by a collection of finite elements make the method a valuable practical tool for the solution of initial, boundary, and eigenvalue problems arising in various engineering fields. The approximation functions, which satisfy the governing equations and boundary conditions, are often constructed using ideas from interpolation theory. Approximating functions in finite elements and determined in terms of nodal values of a physical field is sought. A persistent physical problem is transferred into a discretized limited element problem with unknown nodal values. For a linear problem, a system of linear algebraic equations should be solved. Values inside finite elements can be recovered using nodal values. The significant steps involved in FEM of a typical problem are:

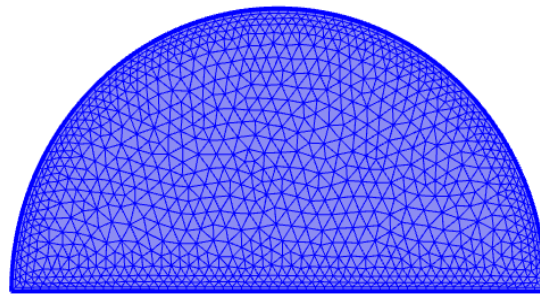
- Discretization of the domain into a set of finite elements (mesh generation).
- Weighted integral or weak formulation of the differential equation to be analyzed.
- Development of the FEM of the problem using its weighted integral or weak form.
- Development of an element shape function.
- Assembly of the finite element to obtain the global system of algebraic equations.
- Imposition of boundary conditions.
- Solution of equations.



- Post-computation of solution and quantities of interest.

## 2.4 Mesh Generation

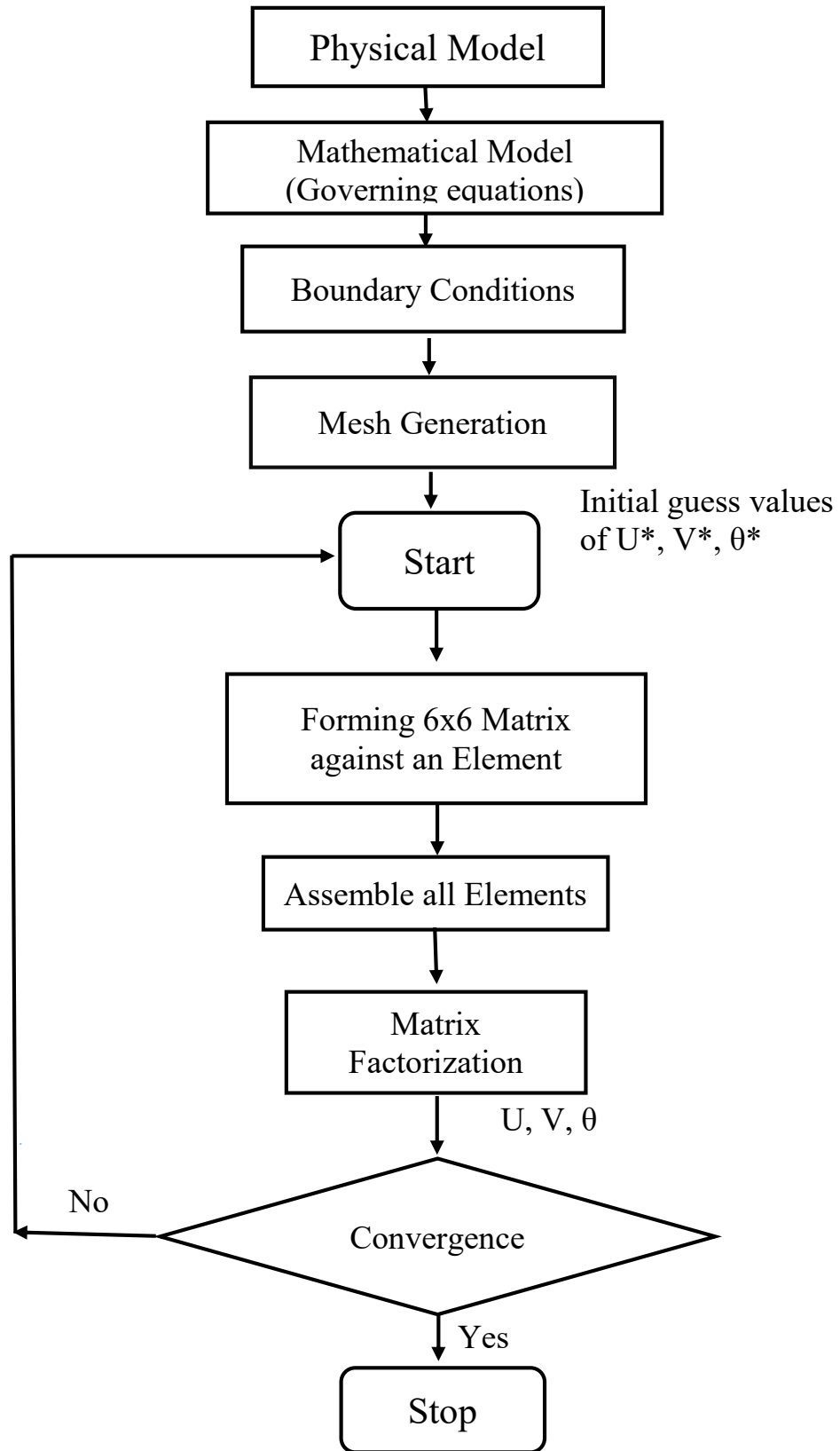
In FEM, the mesh generation or grid generation is the technique to subdivide a domain into a set of subdomains, called finite elements. To discretize a local approximation from a large domain, mesh cells are used. The goal is to create a mesh that accurately captures the input domain geometry, with high-quality (well-shaped) cells, and without so many cells as to make subsequent calculations intractable. The mesh should also be fine (small elements) in areas that are important for the subsequent calculations. Meshes are used for rendering to a computer screen and for physical simulation such as FEM or CFD. Fig. 3.1 represents a domain is subdivided into a set of subdomains with boundary. Three-dimensional meshes created for finite element analysis need to consist of tetrahedra, pyramids, prisms, or hexahedra. Those used for the finite volume method can consist of arbitrary polyhedra. Those used for finite difference methods consist of piecewise structured arrays of hexahedra known as multi-block structured meshes. The present numerical technique will discretize the computational domain into unstructured triangles by Delaunay triangular method. The Delaunay triangulation is a geometric structure that has enjoyed great popularity in mesh generation science the mesh generation was in its infancy. In two-dimensions, the Delaunay triangulation of a vertex set maximizes the minimum angle among all possible triangulations of that vertex set.



**Figure 2.1:** Finite element discretization of a domain

## 2.5 Algorithm

The iterative Newton-Raphson algorithm originally put forward the algorithm; the discrete forms of the continuity, momentum, and energy equations are solved to determine the value of the velocity and the temperature. It is essential to guess the initial values of the variables. Then the numerical solutions of the variables are obtained while the convergent criterion is fulfilled. The simple algorithm is shown in the flow chart below.



**Figure 2.2:** Flow chart of the computational procedure.

# CHAPTER THREE

## Mathematical Model of the Problem

### 3.1 Introduction

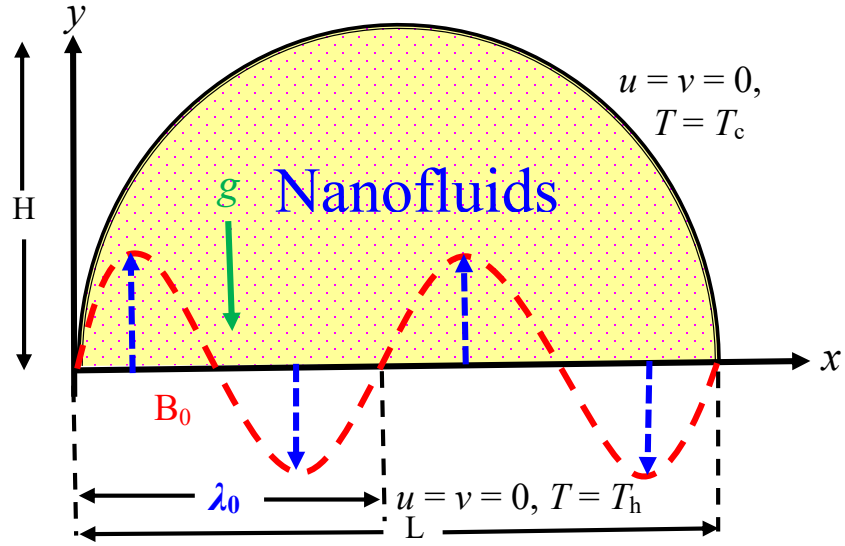
The mathematical model of any real-life physical problem consisting of a set of linear or nonlinear ordinary and partial differential equations including appropriate boundary conditions is the initial stage of any numerical procedure. The generalized governing ordinary or partial differential equations are based on mass, momentum, and energy conservation. The advancement of heat transfer rate in any thermal system or industry is a primary concern of researchers and scientists. Natural convective fluid flow and heat transfer are essential in engineering systems for numerous applications in cooling electronic appliances, air-conditioning systems, building insulation, heat exchangers and solar collectors, etc. In these systems, augmentation of heat transfer performance is an essential topic from an energy-saving perspective. Compared with generally used base fluid, improved characteristics fluids named nanofluids have many benefits in many engineering and industrial applications such as solar thermal collectors to maximize the solar energy absorption with the change of the size, shape, material, and volume fraction of nanoparticles.

Several geometric shapes of heat exchangers or solar thermal collectors, for example, triangular shape, square shape, rectangular shape, and circular shape, have been studied in literature review for different nanofluids. However, to the best of my knowledge, the literature review related to semi-circular shape solar thermal collectors filled with different nanofluids and varying the shape of nanoparticles under the influence of periodic magnetic field has not been investigated yet. Therefore, in this investigation, a numerical study of convection flow and heat transfer for semi-circular shape solar collectors filled with different nanofluids, including various shapes of nanoparticles under the influence of the periodic magnetic field, has been performed. A higher temperature transfer rate is required in solar thermal collectors, which can be possible by introducing nanofluids. The present numerical simulations provide a prediction that may be helpful for design optimization and the augmentation of thermal performance of energy systems such as solar thermal collectors, heat exchangers, cooling of electronic appliances, air conditioning systems, building insulations, biomedical engineering, boiler, and so on.

### 3.2 Physical Modeling

A time-dependent, laminar, incompressible, two-dimensional natural convection flow and heat transfer of nanofluids within a semi-circular enclosure under a periodic magnetic field influence. The dimensional coordinates  $x$ -axis measures along the bottom wall and  $y$ -axis normal to it. The cavity walls are considered fixed, and natural convection has been induced by making temperature differences between bottom hot and top circular cold walls. The circular wall is cooled at low-temperature  $T_c$ , whereas the bottom wall is heated uniformly at the temperature  $T_h$  ( $T_c < T_h$ ) (case I). In addition, the bottom border is also heated at linearly temperature:  $T = T_c + (T_h - T_c) \left(1 - \frac{x}{L}\right)$  (case II), or non-uniform temperature:  $T = T_c + (T_h - T_c) \left(\frac{x}{L}\right) \left(1 - \frac{x}{L}\right)$  (case III), or sinusoidal temperature:  $T = T_c + (T_h - T_c) \left(\frac{a}{L}\right) \sin(Kx)$  (case IV), or  $T = T_c + (T_h - T_c) \left(\frac{a}{L}\right) \sin^2(Kx)$  (case V). Here,  $a$  is the amplitude of the wave, and  $K$  is the wave number such that  $K = 2\pi/L$ . The non-uniform magnetic field has been employed as a sinusoidal function of the  $x$ -coordinate. The relation of the vertical periodic magnetic field is denoted as  $B = B_0 \sin\left(\frac{2\pi x}{\lambda_0}\right)$  where  $\lambda_0$  represents the magnetic field period and represents the amplitude of the non uniform periodic magnetic field.

In the present study, water (H<sub>2</sub>O) is taken as base fluid, and copper (Cu) is taken for nanoparticles, and copper-water nanofluid is used as default nanofluid. The nanoparticles are dispersed into the base fluid homogenously. It is also assumed that thermal equilibrium exists between the base fluids and nanoparticles, and no dynamical and thermal slip occurs between nanoparticles and base fluid. It is mentioned that the physical property density in the buoyancy term varies among the thermo-physical properties of nanofluid while other properties remain constant during convection. Since the temperature difference is limited between cold and hot walls, this condition is reasonable. The gravitational acceleration acts in the negative direction along the  $y$ -axis. All the solid boundaries are assumed to be rigid no-slip walls. The geometry and coordinate systems are schematically shown in Figure 3.1. Generally, this type of enclosure filled with nanofluids has been modeled as a solar thermal collector or heat exchanger. The nanofluids' physical properties are considered constant except the density variation in the body force term of the momentum equation estimated by Boussinesq approximation. 32-types of different nanofluids are considered to calculate the average Nusselt number on heated bottom walls for different physical nanoparticles. The reason



**Figure 3.1:** Schematic view of the semi-circular enclosure with boundary conditions

for selecting these nanoparticles and base fluid is that they are applied effectively in different industrial processes and various fields. For instance, conventional fluid water is used heavily in many engineering processes such as cooling systems, nuclear reactors, and solar thermal collectors etc. The thermo-physical properties of various nanoparticles and base fluids are listed in Table 3.1.

**Table 3.1:** Thermo-physical properties of the different base fluid and solid nanoparticles.

Base Fluid / Nanoparticles	$c_p$ [Jkg <sup>-1</sup> K <sup>-1</sup> ]	$\rho$ [kgm <sup>-3</sup> ]	$k$ [Wm <sup>-1</sup> K <sup>-1</sup> ]	$\mu$ [kgm <sup>-1</sup> s <sup>-1</sup> ]	$\beta \times 10^{-5}$ [K <sup>-1</sup> ]	$\sigma$ [Sm <sup>-1</sup> ]	$Pr$
Water (H <sub>2</sub> O)	4179	997.1	0.613	0.001003	21	$5.50 \times 10^{-6}$	6.8377
Kerosene	2090	780	0.149	0.00164	99	$6.0 \times 10^{-10}$	23.004
Ethylene Glycol	2382.1	1117.48	0.2492	0.022	57	$1.07 \times 10^{-8}$	210.3
Engine oil (EO)	1880.3	888.23	0.145	0.8451	70	23.004	10958.9
Copper (Cu)	385	8933	400	-	1.67	$5.96 \times 10^7$	-
Alumina (Al <sub>2</sub> O <sub>3</sub> )	765	3970	40	-	0.85	$3.50 \times 10^7$	-
Co	420	8900	100	-	1.3	$1.602 \times 10^7$	-
Fe <sub>3</sub> O <sub>4</sub>	670	5180	80.4	-	20.6	$1.12 \times 10^5$	-
TiO <sub>2</sub>	686.2	4250	8.9538	-	0.90	$2.60 \times 10^6$	-
Ag	233	10500	429	-	1.8	$6.30 \times 10^7$	-
Zn	387	7135	116	-	3.02	$1.69 \times 10^7$	-
CuO	531.8	6320	76.5	-	1.8	$51.28 \times 10^7$	-

### 3.3 Mathematical Modeling

To drive the governing equations in dimensional form for the present study, applying the aforementioned considerations as follows:

Continuity equation:

$$\frac{\partial u}{\partial x} + \frac{\partial v}{\partial y} = 0 \quad (3.1)$$

Momentum equation in  $x$ -direction:

$$\frac{\partial u}{\partial t} + u \frac{\partial u}{\partial x} + v \frac{\partial u}{\partial y} = -\frac{1}{\rho_{nf}} \frac{\partial p}{\partial x} + \frac{\mu_{nf}}{\rho_{nf}} \left( \frac{\partial^2 u}{\partial x^2} + \frac{\partial^2 u}{\partial y^2} \right) - \frac{1}{\rho_{nf}} \sigma_{nf} B_0^2 \sin^2 \left( \frac{2\pi x}{\lambda_0} \right) u \quad (3.2)$$

Momentum equation in  $y$ -direction:

$$\frac{\partial v}{\partial t} + u \frac{\partial v}{\partial x} + v \frac{\partial v}{\partial y} = -\frac{1}{\rho_{nf}} \frac{\partial p}{\partial y} + \frac{\mu_{nf}}{\rho_{nf}} \left( \frac{\partial^2 v}{\partial x^2} + \frac{\partial^2 v}{\partial y^2} \right) + g \frac{(\rho\beta)_{nf}}{\rho_{nf}} (T - T_c) \quad (3.3)$$

Energy equation:

$$\frac{\partial T}{\partial t} + u \frac{\partial T}{\partial x} + v \frac{\partial T}{\partial y} = \alpha_{nf} \left( \frac{\partial^2 T}{\partial x^2} + \frac{\partial^2 T}{\partial y^2} \right) \quad (3.4)$$

where  $u$ ,  $v$  are the velocity component along  $x$ ,  $y$  coordinates, respectively,  $p$  is the pressure,  $g$  is the gravity,  $T$  is the temperature,  $T_c$  is the reference temperature,  $\mu_{nf}$  is the dynamic viscosity of nanofluid,  $\rho_{nf}$  is the density of nanofluid,  $\alpha_{nf} = k_{nf} / (\rho c_p)_{nf}$  is the thermal diffusivity of nanofluid,  $k_{nf}$  is the thermal conductivity of nanofluid,  $(\rho c_p)_{nf}$  is the heat capacity of nanofluid,  $(\rho\beta)_{nf}$  is the volumetric thermal expansion of nanofluid.

### 3.4 Initial and Boundary Conditions

The initial and boundary conditions of the above-narrated model are as follows:

$$\text{For } t \leq 0; \text{ entire domain: } u = 0, v = 0, T = T_c, p = 0 \quad (3.5a)$$

For  $t > 0$ ;

$$\text{At the circular wall: } u = 0, v = 0, T = T_c \quad (3.5b)$$

At the horizontal base wall:

$$\text{Case I: } u = 0, v = 0, T = T_h \quad (3.5c)$$

$$\text{Case II: } u = 0, v = 0, T = T_c + (T_h - T_c) \left(1 - \frac{x}{L}\right) \quad (3.5d)$$

$$\text{Case III: } u = 0, v = 0, T = T_c + (T_h - T_c) \left(\frac{x}{L}\right) \left(1 - \frac{x}{L}\right) \quad (3.5e)$$

$$\text{Case IV: } u = 0, v = 0, T = T_c + (T_h - T_c) \left(\frac{a}{L}\right) \sin(Kx) \quad (3.5f)$$

$$\text{Case V: } u = 0, v = 0, T = T_c + (T_h - T_c) \left(\frac{a}{L}\right) \sin^2(Kx) \quad (3.5g)$$

### 3.5 Physical and Thermal Properties of Nanofluids

To enhance the thermal performance of nanofluids, the physical and thermal properties of nanofluids are essential. Nanofluids' material and thermal characteristics are listed as viscosity, density, thermal diffusivity, heat capacitance, thermal conductivity, and thermal expansion coefficient. The thermal performance of a solar collector predominantly depends on how thermal properties treat in varied operating conditions. Variation in temperature, ambient conditions, type of base fluid, size of particles, nanoparticles shape, and volume concentration is the main operational parameters. Therefore, the nomination of appropriate nanofluids considering all these parameters is necessary for optimum performance. To compute the physical and thermal properties of the nanofluids under considerations, the following formulas are used (see Kalbani *et al.* [32], Al-Weheibi *et al.* [36], and Uddin *et al.* [54]):

The effective viscosity of the nanofluids is expressed as follows:

$$\mu_{nf} = \mu_{bf} \frac{1}{(1 - \phi)^{2.5}} \quad (3.6)$$

where  $\phi$  represents volume fraction of nanoparticles.

The effective density of the nanofluid is expressed as follows

$$\rho_{nf} = (1 - \phi) \rho_{bf} + \phi \rho_{sp} \quad (3.7)$$

The thermal diffusivity of the nanofluid is expressed as follows

$$\alpha_{nf} = \frac{k_{nf}}{(\rho c_p)_{nf}} \quad (3.8)$$

The heat capacitance of the nanofluid is given by

$$(\rho c_p)_{nf} = (1 - \phi) (\rho c_p)_{bf} + \phi (\rho c_p)_{sp} \quad (3.9)$$

The electrical conductivity of a nanofluid is determined by the formula

$$\sigma_{nf} = \frac{\sigma_{sp} + 2\sigma_{bf} - 2(\sigma_{bf} - \sigma_{sp})\phi}{\sigma_{sp} + 2\sigma_{bf} + (\sigma_{bf} - \sigma_{sp})\phi} \sigma_{bf} \quad (3.10)$$

Thermal conductivity characterizes the ability of the material to conduct heat. The thermal conductivity of nanofluids is usually higher compared to conventional fluids. The ratio of the thermal conductivity of the nanofluids restricted to nanoparticles is expressed as follows:

$$\frac{k_{nf}}{k_{bf}} = \frac{k_{sp} + 2k_{bf} - 2(k_{bf} - k_{sp})\phi}{k_{sp} + 2k_{bf} + (k_{bf} - k_{sp})\phi} \quad (3.11)$$

where  $k_{nf}$  represents thermal conductivity of nanofluids,  $k_{bf}$  represents thermal conductivity of base fluids. This method is valid for spherical particles with a small concentration ( $\phi \ll 1$ ).

The Maxwell model of thermal conductivity is extended by including a shape factor by Hamilton and crosser [50] as follows:

$$k_{nf} = \frac{k_{sp} + (n-1)k_{bf} - (n-1)(k_{bf} - k_{sp})\phi}{k_{sp} + (n-1)k_{bf} + (k_{bf} - k_{sp})\phi} k_{bf} \quad (3.12)$$

where  $n$  is the nanoparticles shape factor. The values of nanoparticles shape factor  $n = 8.6, 5.7, 4.9, 3.7, 3$  represents blade, platelet, brick, cylinder, and sphere shape nanoparticles, respectively. The shape of the nanoparticle is defined as  $n = 3/\psi$ , where  $\psi$  represents sphericity and is defined by the ratio of sphere surface area and real particle surface area with the same volumes. The values of  $\psi$  for the blade, platelet, cylinder, brick shape of nanoparticles are evaluated as 0.36, 0.52, 0.62, and 0.81, respectively (Al-Balushi *et al.* [46], Timofeeva *et al.* [51]). For different values of  $n$ , the different shape of nanoparticles is shown in Table 3.2:

The Brownian motion of nanoparticles has not been considered in the above Maxwell model in equation (3.10). But experimentally, it has been proved that the Brownian movement of nanoparticles plays an essential role in the heat transfer enhancement of nanofluids. Therefore, an appropriate model is considered for calculating thermal conductivity, including a convective static and Brownian motion parts. Furthermore, the model of thermal conductivity of nanofluids, including this two-component thermal conductivity, takes into account the effects of particles size,



particle volume fraction, and temperature dependence as well as types of particle and base fluid combinations:

$$k_{nf} = k_{static} + k_{Brownian} \quad (3.13)$$






where  $k_{static}$  represents the static thermal conductivity based on Maxwell classical correlation that is given in equation (3.11). But,  $k_{Brownian}$  represents the dynamical part of nanofluids thermal conductivity model for the effect of Brownian motion on nanoparticles which is calculated as:

$$k_{Brownian} = \frac{\phi \rho_{sp} c_{p,sp}}{2} \sqrt{\frac{2K_B T_{ref}}{3\pi d_p \mu_{nf}}} \quad (3.14)$$

where  $K_B$  represents the Boltzmann constant and  $d_p$  represents the diameter of nanoparticles.

Therefore, nanofluids' thermal conductivity depends on nanoparticles volume fraction, the thermal conductivity of nanoparticles, temperature of the mixture, nanoparticles size, and base fluid properties considering viscosity and specific heat capacity. For the present mathematical model, the both Maxwell static part and Brownian part are considered for the thermal conductivity model of nanofluids as follows (see Uddin and Rahman [52]):

**Table 3.2:** Different shapes of nanoparticles with geometry.

Values of $n$	Shape of nanoparticles	Geometry
$n = 3$	Spherical	
$n = 4.9$	Cylindrical	
$n = 3.7$	Brick	
$n = 5.7$	Platelet	
$n = 8.6$	Blade	

$$k_{nf} = \frac{k_{sp} + (n-1)k_{bf} - (n-1)(k_{bf} - k_{sp})\phi}{k_{sp} + (n-1)k_{bf} + (k_{bf} - k_{sp})\phi} k_{bf} + \frac{\phi \rho_{sp} c_{p,sp}}{2} \sqrt{\frac{2K_B T_{ref}}{3\pi d_p \mu_{nf}}} \quad (3.15)$$

The thermal expansion coefficient is expressed as follows

$$(\rho\beta)_{nf} = (1-\phi)(\rho\beta)_{bf} + \phi(\rho\beta)_{sp} \quad (3.16)$$

### 3.6 Dimensional Analysis

In the study of fluid dynamics, one of the most important mathematical tools is dimensional analysis. Dimensional analysis has some advantages. Non-dimensionalization gives freedom to explore any system irrespective of its material properties. It reduces the number of variables and complexity of experimental variables which affect a given physical phenomenon. Non-dimensional equations also give a clear-sightedness of parameters that control the whole system. The results don't depend on the size of the geometry. One can get insight into physical problems before experimenting. The following dimensionless variables are introduced for the present study to convert the governing equations (3.1)-(3.4), including initial and boundary conditions (3.5a)-(3.5c) into non-dimensional form.

$$X = \frac{x}{L}, Y = \frac{y}{L}, A = \frac{a}{L}, U = \frac{uL}{\alpha_{bf}}, V = \frac{vL}{\alpha_{bf}}, \theta = \frac{T - T_c}{T_h - T_c}, P = \frac{\rho L^2}{\rho_{bf} \alpha_{bf}^2}, \tau = \frac{t \alpha_{bf}}{L^2}, \lambda = \frac{\lambda_0}{L} \quad (3.17)$$

Employing the equation (3.17) into (3.1)-(3.4) including initial and boundary conditions (3.5a)-(3.5c) as follows

$$\frac{\partial U}{\partial X} + \frac{\partial V}{\partial Y} = 0 \quad (3.18)$$

$$\frac{\partial U}{\partial \tau} + U \frac{\partial U}{\partial X} + V \frac{\partial U}{\partial Y} = -\frac{\rho_{bf}}{\rho_{nf}} \frac{\partial P}{\partial X} + Pr \left( \frac{\mu_{nf}}{\mu_{bf}} \right) \left( \frac{\rho_{bf}}{\rho_{nf}} \right) \left( \frac{\partial^2 U}{\partial X^2} + \frac{\partial^2 U}{\partial Y^2} \right) - Ha^2 Pr \left( \frac{\rho_{bf}}{\rho_{nf}} \right) \left( \frac{\sigma_{nf}}{\sigma_{bf}} \right) \sin^2 \left( \frac{2\pi X}{\lambda} \right) U \quad (3.19)$$

$$\frac{\partial V}{\partial \tau} + U \frac{\partial V}{\partial X} + V \frac{\partial V}{\partial Y} = -\frac{\rho_{bf}}{\rho_{nf}} \frac{\partial P}{\partial Y} + Pr \left( \frac{\mu_{nf}}{\mu_{bf}} \right) \left( \frac{\rho_{bf}}{\rho_{nf}} \right) \left( \frac{\partial^2 V}{\partial X^2} + \frac{\partial^2 V}{\partial Y^2} \right) + \frac{(\rho\beta)_{nf}}{\rho_{nf} \beta_{bf}} Ra Pr \theta \quad (3.20)$$

$$\frac{\partial \theta}{\partial \tau} + U \frac{\partial \theta}{\partial X} + V \frac{\partial \theta}{\partial Y} = \left( \frac{\alpha_{nf}}{\alpha_{bf}} \right) \left( \frac{\partial^2 \theta}{\partial X^2} + \frac{\partial^2 \theta}{\partial Y^2} \right) \quad (3.21)$$

The non-dimensional boundary condition becomes

$$\text{For } \tau = 0, \text{ whole domain: } U = 0, V = 0, \theta = 0, P = 0 \quad (3.22a)$$

For  $\tau > 0$ , the dimensionless boundary conditions:

$$\text{At the circular wall: } U = 0, V = 0, \theta = 0 \quad (3.22b)$$

At the bottom wall:

$$\text{Case I: } u = 0, v = 0, \theta = 1 \quad (3.22c)$$

$$\text{Case II: } u = 0, v = 0, \theta = 1-X \quad (3.22d)$$

$$\text{Case III: } u = 0, v = 0, \theta = X(1-X) \quad (3.22e)$$

$$\text{Case IV: } u = 0, v = 0, \theta = A \sin(2\pi X) \quad (3.22f)$$

$$\text{Case V: } u = 0, v = 0, \theta = A \sin^2(2\pi X) \quad (3.22g)$$

where, the parameters which is introduced in the above non-dimensional equation are as follows:

$A = a/L$  represents non-dimensional amplitude, the Rayleigh number is represented as

$$Ra = \frac{g\beta_{bf}(T_h - T_c)L^3}{\nu_{bf}\alpha_{bf}}, \text{ Hartmann number is represented as } Ha = B_o L \sqrt{\sigma_{bf}/\mu_{bf}}, \text{ and Prandtl}$$

number is represented as  $Pr = \nu_{nf}/\alpha_{bf}$ .

### 3.7 Calculation of Nusselt Number

For this model, the important physical parameter quantities are local Nusselt number ( $Nu_L$ ) and average Nusselt number ( $Nu_{av}$ ) along the heated bottom wall of the cavity. The local Nusselt number is defined as

$$Nu_L = \frac{Lq_w}{k_{bf}(T_h - T_c)} \quad (3.23)$$

where the heat transfer from the heated bottom wall  $q_w$  is given by

$$q_w = -k_{nf} \left( \frac{\partial \theta}{\partial Y} \right)_{Y=0} \quad (3.24)$$

The average Nusselt number on the bottom heated wall of the cavity is expressed as

$$Nu_{av} = - \left( \frac{k_{nf}}{k_{bf}} \right) \int_0^1 \frac{\partial \theta}{\partial Y} dX \quad (3.25)$$

In the present problem, the flow field or fluid motion has been visualized through a streamline that can be obtained from the mathematical trick stream function. The stream function can be derived from velocity components  $U$  and  $V$ . The relation of the stream function and velocity components in two dimensional flow is given as:  $U = \frac{\partial \psi}{\partial Y}$ ,  $V = -\frac{\partial \psi}{\partial X}$ .

### 3.8 Finite Element Formulation

Conservation of mass or continuity equation (3.1), conservation of momentum equations (3.2) & (3.3), and conservation of energy equation (3.4) are fundamental laws that form a set of coupled nonlinear partial differential equations that are used for solving the convective heat transfer. To solve both ordinary and partial differential equations which arise in science and engineering problems, the finite element method (FEM) is a powerful numerical method for solving them. In this method, the whole domain is divided into smaller elements of finite dimensions called finite elements. To analysis, the science and engineering problems finite element method is a wonderful numerical method. FEM is applied to solve the integral equations, including fluid mechanics, heat transfer, electrical systems, the process of chemical, and many other fields. Therefore, the governing dimensionless equations (3.18)-(3.21) along with the initial and boundary conditions (3.22a)-(3.22g) have been solved numerically by employing Galerkin weighted residual-based finite element technique.

An approximate solution of the governing equations over each finite element is tremendous advances in the finite element method. The approximate solutions are replaced into the governing equations to obtain an expression that will not be equal on both sides of the equations. The difference between the two sides of the equations is known as residual. The residual must be zero, in some sense, to find out the parameters of approximate solutions over the element. The residual may be zero in the weighted-integral sense. Let us consider  $N_\eta$  and  $H_\lambda$  as weight function or linear shape function, equating with the finite element method. The weighted-integral equations try to make a set of algebraic relations among the parameters of the approximate solutions. The algebraic equations are linearly independent and invertible because the weight functions are linearly independent. The weighted residual method is described by Zienkiewicz and Taylor [51]. The weighted-integral technique of the governing equations (3.18)-(3.21) is applied for deriving finite element equations as follows:

$$\int_A N_\eta \left( \frac{\partial U}{\partial X} + \frac{\partial V}{\partial Y} \right) dA = 0 \quad (3.26)$$

$$\begin{aligned} \int_A N_\eta \left( \frac{\partial U}{\partial \tau} + U \frac{\partial U}{\partial X} + V \frac{\partial U}{\partial Y} \right) dA &= -\frac{\rho_{bf}}{\rho_{nf}} \int_A H_\lambda \frac{\partial P}{\partial X} dA + \frac{\mu_{nf} \text{Pr}}{\nu_{bf} \rho_{nf}} \int_A N_\eta \left( \frac{\partial^2 U}{\partial X^2} + \frac{\partial^2 U}{\partial Y^2} \right) dA \\ &- \frac{\rho_{bf} \sigma_{nf}}{\rho_{nf} \sigma_{bf}} Ha^2 \text{Pr} \int_A N_\eta \sin^2 \left( \frac{\pi x}{\lambda} \right) U dA \end{aligned} \quad (3.27)$$

$$\begin{aligned} \int_A N_\eta \left( \frac{\partial V}{\partial \tau} + U \frac{\partial V}{\partial X} + V \frac{\partial V}{\partial Y} \right) dA &= -\frac{\rho_{bf}}{\rho_{nf}} \int_A H_\lambda \frac{\partial P}{\partial Y} dA + \frac{\mu_{nf} \text{Pr}}{\nu_{bf} \rho_{nf}} \int_A N_\eta \left( \frac{\partial^2 V}{\partial X^2} + \frac{\partial^2 V}{\partial Y^2} \right) dA \\ &+ \frac{(\rho\beta)_{nf}}{\beta_{bf} \rho_{nf}} Ra \text{Pr} \int_A N_\eta \theta dA \end{aligned} \quad (3.28)$$

$$\int_A N_\eta \left( \frac{\partial \theta}{\partial \tau} + U \frac{\partial \theta}{\partial X} + V \frac{\partial \theta}{\partial Y} \right) dA = -\frac{\alpha_{nf}}{\alpha_{bf}} \int_A N_\eta \left( \frac{\partial^2 \theta}{\partial X^2} + \frac{\partial^2 \theta}{\partial Y^2} \right) dA \quad (3.29)$$

Where  $A$  represents the element area,  $H_\lambda$  represents the element shape functions for the pressure, and  $N_\eta$  ( $\eta = 1, 2, \dots, 6$ ) represents the element shape functions or interpolation functions for the velocity components and temperature.

The equation of continuity (3.26) remains unaffected because integration by parts doesn't assist in shrinking differentiability on  $(U, V)$ . Moreover, the boundary terms will be in a struggle with physical stipulations. Therefore, to keep the boundary stresses intact, then physical problems must be integrated. The integration by parts also allows the pressure variable to have a lower-order approximation. To deal the second order derivatives as well as integration by parts, the Gauss theorem for two-dimensions and vector identity is applied. (Gauss's theorem in 2D: Gauss's theorem in 2D states that the flow  $\mathbf{F}$  across the boundary  $\Gamma^e$  dotted with a normal vector  $\mathbf{n}$  times a little chunk of the boundary and summing up to over the entire boundary is equal to summing up to over the whole region of the small chunk of the region times the divergence of  $\mathbf{F}$ . i.e.

$$\int_A \nabla \cdot \mathbf{F} dA = \int_{\Gamma^e} \mathbf{F} \cdot \mathbf{n} dA \quad (3.30)$$

Applying Gauss's divergence theorem to the second order derivative terms of the equations (3.27)-(3.29) for generating the boundary integral terms associated with the surface tractions and heat flux. The equations (3.27)-(3.29) becomes,

$$\int_A N_\eta \left( \frac{\partial U}{\partial \tau} + U \frac{\partial U}{\partial X} + V \frac{\partial U}{\partial Y} \right) dA + \frac{\rho_{bf}}{\rho_{nf}} \int_A H_\lambda \frac{\partial P}{\partial X} dA - \frac{\mu_{nf} \text{Pr}}{\nu_{bf} \rho_{nf}} \int_A N_\eta \left( \frac{\partial N_\eta}{\partial X} \frac{\partial U}{\partial X} + \frac{\partial N_\eta}{\partial Y} \frac{\partial U}{\partial Y} \right) dA$$

$$+ \frac{\rho_{bf} \sigma_{nf}}{\rho_{nf} \sigma_{bf}} Ha^2 \text{Pr} \int_A N_\eta \sin^2 \left( \frac{\pi x}{\lambda} \right) U dA = \frac{\mu_{nf} \text{Pr}}{\nu_{bf} \rho_{nf}} \int N_\eta S_x dS_0 \quad (3.31)$$

$$\int_A N_\eta \left( \frac{\partial V}{\partial \tau} + U \frac{\partial V}{\partial X} + V \frac{\partial V}{\partial Y} \right) dA + \frac{\rho_{bf}}{\rho_{nf}} \int_A H_\lambda \frac{\partial P}{\partial Y} dA - \frac{\mu_{nf} \text{Pr}}{\nu_{bf} \rho_{nf}} \int_A \left( \frac{\partial N_\eta}{\partial X} \frac{\partial V}{\partial X} + \frac{\partial N_\eta}{\partial Y} \frac{\partial V}{\partial Y} \right) dA$$

$$- \frac{(\rho\beta)_{nf}}{\beta_{bf} \rho_{nf}} Ra \text{Pr} \int_A N_\eta \theta dA = \frac{\mu_{nf} \text{Pr}}{\nu_{bf} \rho_{nf}} \int N_\eta S_y dS_0 \quad (3.32)$$

$$\int_A N_\eta \left( \frac{\partial \theta}{\partial \tau} + U \frac{\partial \theta}{\partial X} + V \frac{\partial \theta}{\partial Y} \right) dA + \frac{\alpha_{nf}}{\alpha_{bf}} \int_A \left( \frac{\partial N_\eta}{\partial X} \frac{\partial \theta}{\partial X} + \frac{\partial N_\eta}{\partial Y} \frac{\partial \theta}{\partial Y} \right) dA = \frac{\alpha_{nf}}{\alpha_{bf}} \int N_\eta q_w dS_w \quad (3.33)$$

where the surface tractions ( $S_x$ ,  $S_y$ ) along the outflow boundary  $S_0$  and the velocity components and fluid temperature or heat flux ( $q_w$ ) that flows into or out from the domain along wall boundary  $S_w$ . ( $U$ ,  $V$ ),  $\theta$ , and  $P$  are the fundamental unknowns representing velocity components, temperature, and pressure, respectively of the differential equations (3.31)-(3.33). For the development of the finite element equations, six node triangular elements are used in this study. All six nodes are connected with both velocities and temperature. The corner nodes are also associated with pressure. This means that a lower order polynomial is chosen for pressure and which is satisfied through the continuity equation. The velocity component and the temperature distributions and the linear interpolation for the pressure distribution according to their height derivative orders in the differential equations (3.18)-(3.21) as:

$$U(X, Y) = N_\delta U_\delta \quad (3.34)$$

$$V(X, Y) = N_\delta V_\delta \quad (3.35)$$

$$\theta(X, Y) = N_\delta \theta_\delta \quad (3.36)$$

$$P(X, Y) = H_\lambda P_\lambda \quad (3.37)$$

where  $\delta = 1, 2, \dots, 6$ ;  $\lambda = 1, 2, 3$

Now putting the element velocity component distributions, the temperature distribution, and pressure distribution from equations (3.34)-(3.37) into equations (3.26) and (3.31)-(3.33), the finite element equations can be written as follows:

$$K_{\eta\delta^x} U_\delta + K_{\eta\delta^y} V_\delta = 0 \quad (3.38)$$

$$\begin{aligned} & \left( K_\eta \dot{U}_\delta + K_{\eta\delta^x} U_\delta U_\zeta + K_{\eta\delta^y} V_\delta U_\zeta \right) + \frac{\rho_{bf}}{\rho_{nf}} R_{\lambda\zeta^x} P_\zeta + \frac{\mu_{nf}}{\nu_{bf} \rho_{nf}} \Pr \left( K_{\eta\delta^{xx}} + K_{\eta\delta^{yy}} \right) U_\delta \\ & + \frac{\rho_{bf} \sigma_{nf}}{\rho_{nf} \sigma_{bf}} Ha^2 \Pr N_{\eta\delta} U_\delta \sin^2 \left( \frac{\pi x}{\lambda} \right) = Q_{\eta^u} \end{aligned} \quad (3.39)$$

$$\begin{aligned} & \left( K_{\eta\delta} \dot{V}_\delta + K_{\eta\delta^x} U_\delta U_\zeta + K_{\eta\delta^y} V_\delta V_\zeta \right) + \frac{\rho_{bf}}{\rho_{nf}} R_{\lambda\zeta^y} P_\zeta + \frac{\mu_{nf}}{\nu_{bf} \rho_{nf}} \Pr \left( K_{\eta\delta^{xx}} + K_{\eta\delta^{yy}} \right) V_\delta \\ & - \frac{(\rho\beta)_{nf}}{\rho_{nf} \beta_{bf}} Ra \Pr K_{\eta\delta} \theta_\delta = Q_{\eta^v} \end{aligned} \quad (3.40)$$

$$K_{\eta\delta} \dot{\theta}_\delta + K_{\eta\delta^x} U_\delta \theta_\zeta + K_{\eta\delta^y} V_\delta \theta_\zeta + \frac{\alpha_{nf}}{\alpha_{bf}} \left( K_{\eta\delta^{xx}} + K_{\eta\delta^{yy}} \right) \theta_\delta = Q_{\eta^\theta} \quad (3.41)$$

where partial differentiation with respect to  $\tau$  is represented by superposed dot. The coefficients in the element matrices are in the form of the integral over the element area and along the element edges  $S_\theta$  and  $S_W$  as:

$$K_{\eta\delta} = \int N_\eta N_\delta dA \quad (3.42)$$

$$K_{\eta\delta^x} = \int N_\eta \frac{\partial N_\delta}{\partial X} dA \quad (3.43)$$

$$K_{\eta\delta^y} = \int N_\eta \frac{\partial N_\delta}{\partial Y} dA \quad (3.44)$$

$$K_{\eta\delta^{xx}} = \int \frac{\partial N_\eta}{\partial X} \frac{\partial N_\delta}{\partial X} dA \quad (3.45)$$

$$K_{\eta\delta^{yy}} = \int \frac{\partial N_\eta}{\partial Y} \frac{\partial N_\delta}{\partial Y} dA \quad (3.46)$$

$$K_{\eta\delta^x} = \int N_\eta N_\delta \frac{\partial N_\zeta}{\partial X} dA \quad (3.47)$$

$$K_{\eta\delta^y} = \int N_\eta N_\delta \frac{\partial N_\zeta}{\partial Y} dA \quad (3.48)$$

$$K_{\eta\delta\zeta^x} = \int N_\eta N_\delta \frac{\partial N_\zeta}{\partial X} dA \quad (3.49)$$

$$R_{\lambda\zeta^x} = \int N_\lambda \frac{\partial N_\zeta}{\partial X} dA \quad (3.50)$$

$$R_{\lambda\zeta^y} = \int N_\lambda \frac{\partial N_\zeta}{\partial Y} dA \quad (3.51)$$

$$Q_{\eta^u} = \frac{\mu_{nf}}{\nu_{bf} \rho_{nf}} \text{Pr} \int N_\eta S_x dS_0 \quad (3.52)$$

$$Q_{\eta^v} = \frac{\mu_{nf}}{\nu_{bf} \rho_{nf}} \text{Pr} \int N_\eta S_y dS_0 \quad (3.53)$$

$$Q_{\eta^w} = \frac{\alpha_{nf}}{\alpha_{bf}} \int N_\eta q_\theta dS_w \quad (3.54)$$

These element matrices are evaluated in closed form ready for numerical simulation. Details of the derivation for these element matrices are omitted here.

The derived finite element equations (3.38)-(3.41) are nonlinear. These nonlinear algebraic equations are solved by applying the Newton-Raphson iteration technique by first writing the unbalanced values from the set of the finite element equations (3.38)-(3.41) as follows,

$$F_{\eta^p} = K_{\eta\delta^x} U_\delta + K_{\eta\delta^y} V_\delta \quad (3.55)$$

$$F_{\alpha^u} = \left( K_\eta \dot{U}_\delta + K_{\eta\delta\zeta^x} U_\delta U_\zeta + K_{\eta\delta\zeta^y} V_\delta U_\zeta \right) + \frac{\rho_{bf}}{\rho_{nf}} R_{\lambda\zeta^x} P_\zeta + \frac{\mu_{nf}}{\nu_{bf} \rho_{nf}} \text{Pr} \left( K_{\eta\delta^{xx}} + K_{\eta\delta^{yy}} \right) U_\delta + \frac{\rho_{bf} \sigma_{nf}}{\rho_{nf} \sigma_{bf}} Ha^2 \text{Pr} K_{\eta\delta} U_\delta \sin^2 \left( \frac{\pi x}{\lambda} \right) - Q_{\eta^u} \quad (3.56)$$

$$F_{\alpha^v} = \left( K_{\eta\delta} \dot{V}_\delta + K_{\eta\delta\zeta^x} U_\delta V_\zeta + K_{\eta\delta\zeta^y} V_\delta V_\zeta \right) + \frac{\rho_{bf}}{\rho_{nf}} R_{\lambda\zeta^y} P_\zeta + \frac{\mu_{nf}}{\nu_{bf} \rho_{nf}} \text{Pr} \left( K_{\eta\delta^{xx}} + K_{\eta\delta^{yy}} \right) V_\delta - \frac{(\rho\beta)_{nf}}{\rho_{nf} \beta_{bf}} Ra \text{Pr} K_{\eta\delta} \theta_\delta - Q_{\eta^v} \quad (3.57)$$

$$F_{\alpha^\theta} = K_{\eta\delta} \dot{\theta}_\delta + K_{\eta\delta\zeta^x} U_\delta \theta_\zeta + K_{\eta\delta\zeta^y} V_\delta \theta_\zeta + \frac{\alpha_{nf}}{\alpha_{bf}} \left( K_{\eta\delta^{xx}} + K_{\eta\delta^{yy}} \right) \theta_\delta - Q_{\eta^\theta} \quad (3.58)$$

This leads to a set of algebraic equations with the incremental unknowns of the element nodal velocity components, temperatures, and pressures in the form,



$$\begin{bmatrix} K_{pu} & K_{pv} & 0 & 0 \\ K_{uu} & K_{uv} & 0 & K_{up} \\ K_{\theta u} & K_{\theta v} & K_{\theta\theta} & 0 \\ K_{vu} & K_{vv} & K_{v\theta} & K_{vp} \end{bmatrix} \begin{bmatrix} \Delta p \\ \Delta u \\ \Delta \theta \\ \Delta v \end{bmatrix} = - \begin{bmatrix} F_{\alpha^p} \\ F_{\alpha^u} \\ F_{\alpha^\theta} \\ F_{\alpha^v} \end{bmatrix} \quad (3.59)$$

$$\text{where, } K_{uu} = K_{\eta\delta\zeta^x} U_\delta + K_{\eta\delta\zeta^x} U_\zeta + K_{\eta\delta\zeta^y} V_\delta + \text{Pr} \left( K_{\eta\delta^{xx}} + K_{\eta\delta^{yy}} \right) + \text{Pr} Ha^2 K_{\eta\delta} \quad (3.60)$$

$$K_{uv} = K_{\eta\delta\zeta^y} U_\zeta \quad (3.61)$$

$$K_{u\theta} = 0 \quad (3.62)$$

$$K_{up} = M_{\eta\lambda^x} \quad (3.63)$$

$$K_{vu} = K_{\eta\delta\zeta^x} U_\zeta \quad (3.64)$$

$$K_{vv} = K_{\eta\delta\zeta^x} U_\zeta + K_{\eta\delta\zeta^y} V_\zeta + K_{\eta\delta\zeta^y} V_\zeta + \text{Pr} \left( K_{\eta\delta^{xx}} + K_{\eta\delta^{yy}} \right) \quad (3.65)$$

$$K_{v\theta} = -Ra \text{Pr} K_{\eta\delta} \quad (3.66)$$

$$K_{vp} = R_{\lambda\xi^y} \quad (3.67)$$

$$K_{\theta u} = K_{\eta\delta\zeta^x} \theta_\zeta \quad (3.68)$$

$$K_{\theta v} = K_{\eta\delta\zeta^y} \theta_\zeta \quad (3.69)$$

$$K_{\theta\theta} = K_{\eta\delta\zeta^x} U_\delta + K_{\eta\delta\zeta^y} V_\delta + (K_{\eta\delta^{xx}} + K_{\eta\delta^{yy}}) \quad (3.70)$$

$$K_{\theta p} = 0 \quad (3.71)$$

$$K_{pu} = K_{\eta\delta^x} \quad (3.72)$$

$$K_{pv} = K_{\eta\delta^y} \quad (3.73)$$

$$K_{p\theta} = K_{pp} = 0 \quad (3.74)$$

The iteration process is terminated if the percentage of the overall change compared to the previous iteration is less than the specified value.

To solve the sets of the global nonlinear algebraic equations in the form of matrix, the Newton-Raphson iteration technique has been adapted through PDE solver. The convergent criterion of the numerical solution along with error estimation has been set to  $|\Gamma^{n+1} - \Gamma^n| \leq 10^{-5}$ , where  $\Gamma$  is the general dependent variable ( $U, V, \theta$ ) and  $n$  is the number of iteration.

# CHAPTER FOUR

## Numerical Simulation and Comparison

### 4.1 Computational Procedure

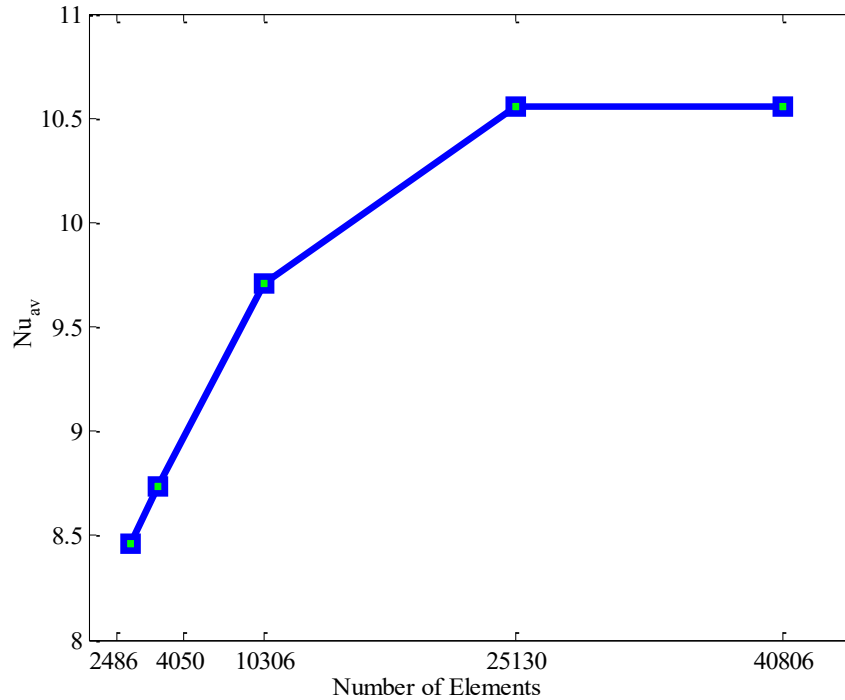
The semi-circular enclosure has been discretized into numerous triangle shape elements in which the dimensionless governing equations (3.18)-(3.21) including boundary conditions (3.22a)-(3.22g) are employed for the numerical calculations. The finite element technique of the Galerkin weighted residual form has been employed for solving these problems. This numerical method has been narrated well in the book by Zienkiewicz and Taylor [53]. Uddin and Rahman [39] have also described the finite element computational procedure step by step on the non-linear governing partial differential equations in an annulus. In this thesis work, to understand the finite element technique, all necessary calculations are performed over the dimensionless governing equations (3.18)-(3.21) and the non-dimensional boundary conditions (3.22a)-(3.22g). The domain of the solution is discretized within a limited number of grids firstly that is determined from non-uniform three-cornered elements in this method.

In this numerical method, the triangular elements of non-uniform type are constructed for the present geometric domain. The domain of the solution space is discretized into finite element meshes that are compressed of triangular elements of non-uniform style. In the current investigation, triangle shape components of six nodes are employed for improving finite element equations where all six nodes are connected with velocity and temperature. The nodes at the corner are merely associated with pressure. The matching of the pressure gradient has happened between momentum equations for continuity requirement and a shape function of lower-order selected for the pressure that is satisfied through the equation of continuity. The identical pressure is considered with linear elements, whereas it is non-continuous among the elements. After that, the technique of Galerkin weighted residual is appointed in the governing non-linear partial differential equations, which transfer the non-linear partial differential governing equations into a system of integral equations. Integral parts of these equations are accomplished employing Gauss's quadrature technique. After that, boundary conditions are also used to modify the non-linear algebraic equations. To solve these non-linear algebraic equations using matrix form, Newton-

Raphson iteration is devoted. The convergent criteria of the procedure of the numerical solution has been estimated as  $|\Gamma^{n+1} - \Gamma^n| \leq 10^{-5}$ , where  $\Gamma$  represents subordinate variables ( $U, V, \theta$ ) and  $n$  is the number of iteration.

## 4.2 Grid Independency Test

For the grid-independent test, a comprehensive non-uniform grid sensitivity study is performed for the current problem when  $Ra = 10^5$ ,  $Ha = 20$ ,  $\lambda = 0.5$ ,  $Pr = 6.8377$ ,  $n = 3$ ,  $\phi = 0.04$ ,  $d = 10$  nm, and  $\tau = 1$  in a semi-circular cavity. Five different non-uniform grid systems containing elements number such as 2486, 4050, 10306, 25130, and 40806 are examined for the present semi-circular enclosure. For the number as mentioned earlier of elements, the design of the numerical calculation of mean Nusselt number ( $Nu_{av}$ ) has been examined for checking the development of grid fineness which is shown in Figure 4.1 and Table 4.1. The value of the mean Nusselt number for elements size 25130 depicts an ordinary difference with elements size 40806. Therefore, to get accurate results, the size of the elements 25130 and 40806 can be used. In this study, the size of the elements 25130 is employed for getting grid-independent solution and computational time limits.



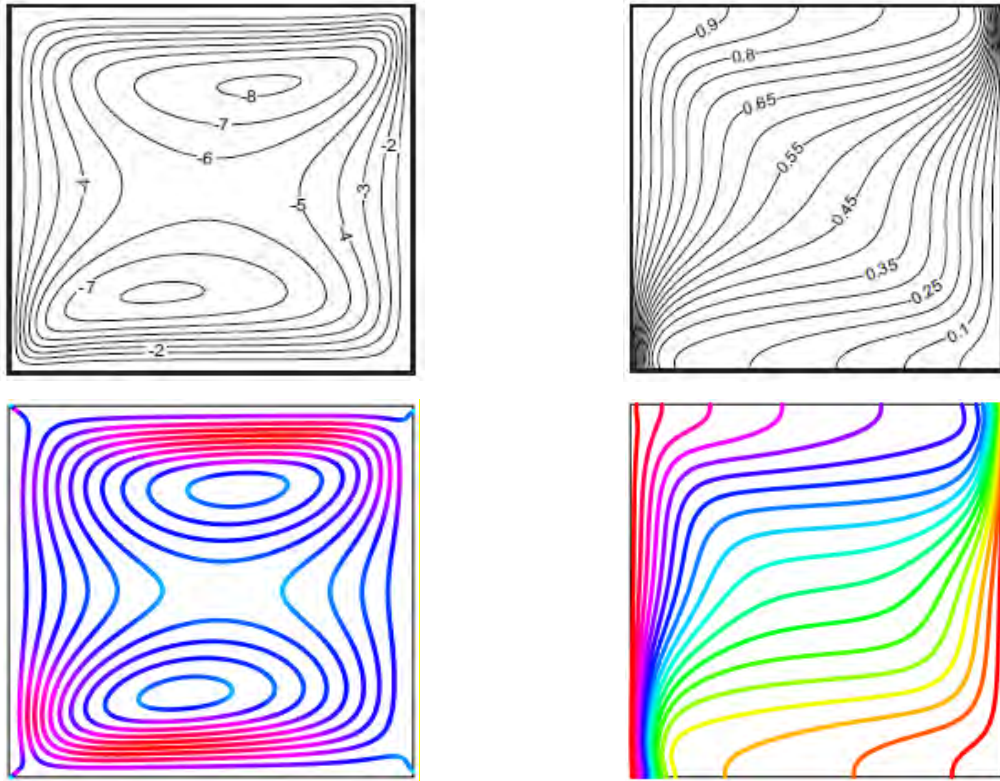
**Figure 4.1:** Convergence of average Nusselt number for various elements number for Cu-H<sub>2</sub>O nanofluid with uniform thermal boundary condition (case I) when  $Ra = 10^5$ ,  $Ha = 20$ ,  $\lambda = 0.5$ ,  $Pr = 6.8377$ ,  $n = 3$ ,  $\phi = 0.04$ ,  $d = 10$ nm, and  $\tau = 1$ .

**Table 4.1:** Grid sensitivity using average Nusselt number for Cu-H<sub>2</sub>O nanofluid for case I when  $Ra = 10^5$ ,  $Ha = 20$ ,  $\lambda = 0.5$ ,  $Pr = 6.8377$ ,  $n = 3$ ,  $\phi = 0.04$ ,  $d = 10\text{nm}$ , and  $\tau = 1$ .

Elements	2486	4050	10306	25130	40806
Nodes	1318	2118	5352	12951	20789
$Nu_{av}$	8.46282	8.73730	9.70890	10.55846	10.55895

### 4.3 Code Validation through Streamlines and Isotherms

To access the correctness of our current numerical scheme, the results generated by the present numerical scheme has been compared with the outcomes of Mehryan *et al.* [43] using streamlines and isothermal lines when  $Ra = 10^6$ ,  $Ha = 25$ ,  $\phi = 0.04$ , and  $\lambda = 1$ . Figure 4.2 represents the comparison of present results (bottom row) generated from current numerical code with regard to streamlines (left column) and isotherms (right column) with previously published work by Mehryan *et al.* [43] (top row). The results show a strong permission and boost the confidence for employing the current numerical code.



**Figure 4.2:** Comparison of the present results (bottom row) with the previously published paper of Mehryan *et al.* [43] (top row) concerning streamline contours and isothermal lines for  $Ra = 10^6$ ,  $Ha = 25$ ,  $\phi = 0.04$ ,  $n = 3$ ,  $\lambda = 1$ .

## 4.4 Code Validation through Data

After studying the grid independence, the validation of the numerical code is also imperative to practice in the computational procedure. Therefore, the present numerical code is also compared with respect to data of average Nusselt number with previously published work. Furthermore, to examine the accuracy of the current numerical code through numerical data with references to mean Nusselt number, the numerical outcomes of the parameters nanoparticles volume fraction and Rayleigh number generated by current code are compared with Ghasemi *et al.* [54] for the steady-state case.

**Table 4.2:** Comparison of the present data regarding average Nusselt number ( $Nu_{av}$ ) with previously published paper of Ghasemi *et al.* [54] for the volume fraction of nanoparticles ( $\phi$ ) and Rayleigh number ( $Ra$ ) when  $Ha = 30$ .

Ra	$\phi = 0$		$\phi = 0.02$		$\phi = 0.04$	
	Ghasemi <i>et al.</i> [54]	Present Study	Ghasemi <i>et al.</i> [54]	Present Study	Ghasemi <i>et al.</i> [54]	Present Study
$10^3$	1.002	1.002	1.060	1.060	1.121	1.121
$10^4$	1.183	1.182	1.212	1.208	1.249	1.242
$10^5$	3.150	3.138	3.138	3.097	3.124	3.057
$10^6$	7.907	7.820	7.979	7.796	8.042	7.773
$10^7$	16.929	16.317	17.197	16.992	17.449	16.865

The two-dimensional physical problem about the natural convective two-dimensional flow of  $Al_2O_3$ -water nanofluid within a square cavity with the existence of a horizontally magnetic effect was investigated by Ghasemi *et al.* [54]. The range of the numerical values of the Hartmann number and Rayleigh number are  $0 \leq Ha \leq 60$  and  $10^3 \leq Ra \leq 10^7$ , respectively, to predict the present numerical code. The numerical data of mean Nusselt number generated by current numerical code and previously published work of Ghasemi *et al.* [54] are presented in Table 4.2, Table 4.3, Weheibi *et al.* [36] in Table 4.4, and Akgün *et al.* [55] in Table 4.5. The analogy of numerical data of the current code with Ghasemi *et al.* [54], Weheibi *et al.* [36], and Akgün *et al.* [55] represent worthy compliance. The numerical outcomes of the existing code make us confident to use the current code for the numerical simulation for the present physical problem.

**Table 4.3:** Comparison of the present data of average Nusselt number ( $Nu_{av}$ ) with previously published paper of Ghasemi *et al.* [54] in steady state case for different values of Hartmann number ( $Ha$ ) and nanoparticles volume fraction ( $\phi$ ) when  $Ra = 10^5$ .

$Ha$	$\phi = 0$		$\phi = 0.02$		$\phi = 0.04$	
	Ghasemi <i>et al.</i> [54]	Present Study	Ghasemi <i>et al.</i> [54]	Present Study	Ghasemi <i>et al.</i> [54]	Present Study
0	4.738	4.721	4.820	4.717	4.896	4.814
15	4.143	4.127	4.179	4.105	4.211	4.083
30	3.150	3.138	3.138	3.097	3.124	3.057
45	2.369	2.359	2.342	2.318	2.317	2.281
60	1.851	1.843	1.831	1.815	1.815	1.794

**Table 4.4:** Comparison of the present results of average Nusselt number ( $Nu_{av}$ ) with previously published paper of Weheibi *et al.* [36] for different Rayleigh numbers ( $Ra$ ) and nanoparticles volume fraction ( $\phi$ ) when  $n = 3$  and  $\tau = 2$ .

$Ra$	Average Nusselt number ( $Nu_{av}$ )						
	Weheibi <i>et al.</i> [36]		Present Study		$\phi$	Weheibi <i>et al.</i> [36]	
$10^3$	1.61201	1.61345			0	4.79048	4.79048
$10^4$	2.23350	2.24213			0.02	4.90759	4.91454
$10^5$	5.07824	5.10549			0.05	5.07824	5.10549
$10^6$	9.82489	9.83726			0.1	5.35063	5.38245

**Table 4.5:** Comparison of the present data of average Nusselt number ( $Nu_{av}$ ) with previously published paper of Akgün *et al.* [55] for various Hartmann numbers and volume fraction of nanoparticles when  $Ra = 10^5$ .

$Ha$	Average Nusselt number ( $Nu_{av}$ )					
	$\phi = 0$			$\phi = 0.04$		
	Akgün <i>et al.</i> [55]	Present results	Error (%)	Akgün <i>et al.</i> [55]	Present results	Error (%)
0	4.998	4.721	5.54	5.309	4.814	9.32
15	4.276	4.127	3.48	4.491	4.083	9.08
30	3.139	3.138	0.03	3.238	3.057	5.59
60	1.774	1.843	3.89	1.808	1.794	0.77

# CHAPTER FIVE

## Results and Discussion

In this section, a two-dimensional numerical study is performed using the finite element method to analyze the laminar, incompressible, unsteady, natural convection flow and heat transfer within the semi-circular enclosure under the influence of a non-uniform periodic magnetic field. This problem is analyzed for copper-water nanofluid as default, with the spherical shape of nanoparticles varying the other physical model parameters. The simulated numerical results are analyzed to investigate the effects of Rayleigh number ( $10^3 \leq Ra \leq 10^6$ ), Hartman number ( $0 \leq Ha \leq 80$ ), the solid volume fraction of nanoparticles ( $0 \leq \phi \leq 0.1$ ), period of the magnetic field ( $0.1 \leq \lambda \leq 1$ ), and different diameters of nanoparticles ( $1\text{nm} \leq d \leq 100\text{nm}$ ). The numerical calculations are expressed in terms of streamlines, isotherms, and average Nusselt number. In the numerical simulations, four different types of base fluid such as water ( $\text{H}_2\text{O}$ ), kerosene, Ethylene Glycol (EG), and Engine Oil (EO) with eight different types of nanoparticles such as Cu, Co,  $\text{Fe}_3\text{O}_4$ ,  $\text{Al}_2\text{O}_3$ ,  $\text{TiO}_2$ , Ag, Zn, and CuO also considered to check the augmentation of heat transfer. The thermos-physical properties of the nanoparticles as mentioned above and base fluids, which are used for controlling the flow and heat transport in the present problem, are listed in Table 3.1.

Firstly, the numerical outcomes focus on the time evolution of the solution using average Nusselt number with dimensionless time ( $\tau$ ), and evolution of streamlines and isotherms with non-dimensional time ( $\tau$ ) are calculated for those as mentioned earlier different physical model parameters. Secondly, the outcomes focus on identifying the flow and temperature transport characteristics using streamline contours and isothermal lines for above mentioned parameters. Then, it is focused on heat transfer rate through the average Nusselt number along the heated bottom diameter of the enclosure to investigate heat transport performance for various physical parameters. The results are taken for Cu- $\text{H}_2\text{O}$  nanofluid and then compare the average Nusselt number using different nanofluids for different nanoparticles volume fractions, nanoparticle diameters, Rayleigh number, Hartmann number, period of the magnetic field, and Brownian effects of nanoparticles. In addition, the five different shapes of nanoparticles like spherical, brick, cylinder, blade, and platelet are examined regarding the average Nusselt number to understand the

effects of shape and size factor of nanoparticles on heat transfer rate. The outcomes are presented using the line graph and tabulated form. Moreover, the most significant features of nanofluids are the impact of nanoparticles are also investigated and displayed graphically in terms of amount, shape, and size of nanoparticles. Finally, different types of thermal boundary conditions such as uniformly (case I), linearly (case II), parabolically (case III), sinusoidally (case IV or case V) are also examined regarding the average Nusselt number along the heated bottom wall for copper-water nanofluid to calculate the augmentation of heat transfer performance.

### 5.1 Time Evolution of Solution

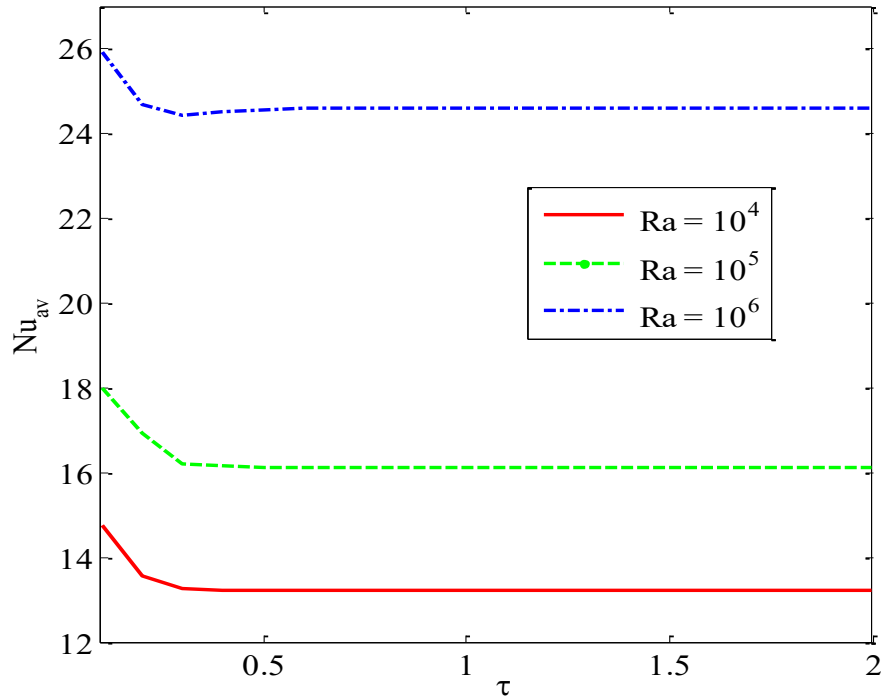
Figure 5.1 displays the variation of the average Nusselt number ( $Nu_{av}$ ) on heated wall against non-dimensional time ( $\tau$ ) for different Rayleigh number ( $10^4 \leq Ra \leq 10^6$ ) for Cu-H<sub>2</sub>O for uniform thermal boundary condition (case I) when  $Ha = 20$ ,  $\phi = 0.04$ ,  $n = 3$ , and  $d = 10\text{nm}$ . This figure clearly shows the time evolution of the average Nusselt number on the heated bottom wall from unsteady to steady-state. The temperature increases suddenly at the bottom diameter; consequently, the average Nusselt number is higher at the bottom wall for the increment of the Rayleigh number. The average Nusselt number diminishes with the increment of time and approaches the steady-state after a certain period of time. In the steady-state part, for  $Ra = 10^4$ , the transport of heat is lowest and as  $Ra$  enhances, the heat transfer enhances due to increment of buoyancy effect.

Figure 5.2 represents the effects of different nanoparticles volume fraction on average Nusselt number on bottom heated wall for (a)  $Ra = 10^5$ , and (b)  $Ra = 10^6$  with different dimensionless time for Cu-H<sub>2</sub>O nanofluid for uniform thermal boundary condition (case I) when  $Pr = 6.8377$ ,  $Ha = 20$ ,  $d = 10\text{nm}$ , and  $n = 3$ . These figures show the average Nusselt number decreases initially and then reaches a steady state after a certain amount of time. The steady-state time is calculated approximately at  $\tau = 0.4$ , and  $\tau = 0.65$  from these figures with respect to different values of nanoparticle volume fraction. These figures clearly depict that the solution takes more time to reaches an unsteady state to state for the absence of nanoparticles in the base fluid. Therefore, the additional nanoparticles into the base fluid assist the unsteady solution to reach a steady state. These figures show that the addition of nanoparticles into the base fluid significantly enhances the rate of heat transfer. Also, the Rayleigh number ( $Ra$ ) has a positive impact on the average Nusselt number rate. At the unstable flow, when the process is beginning, the average Nusselt number

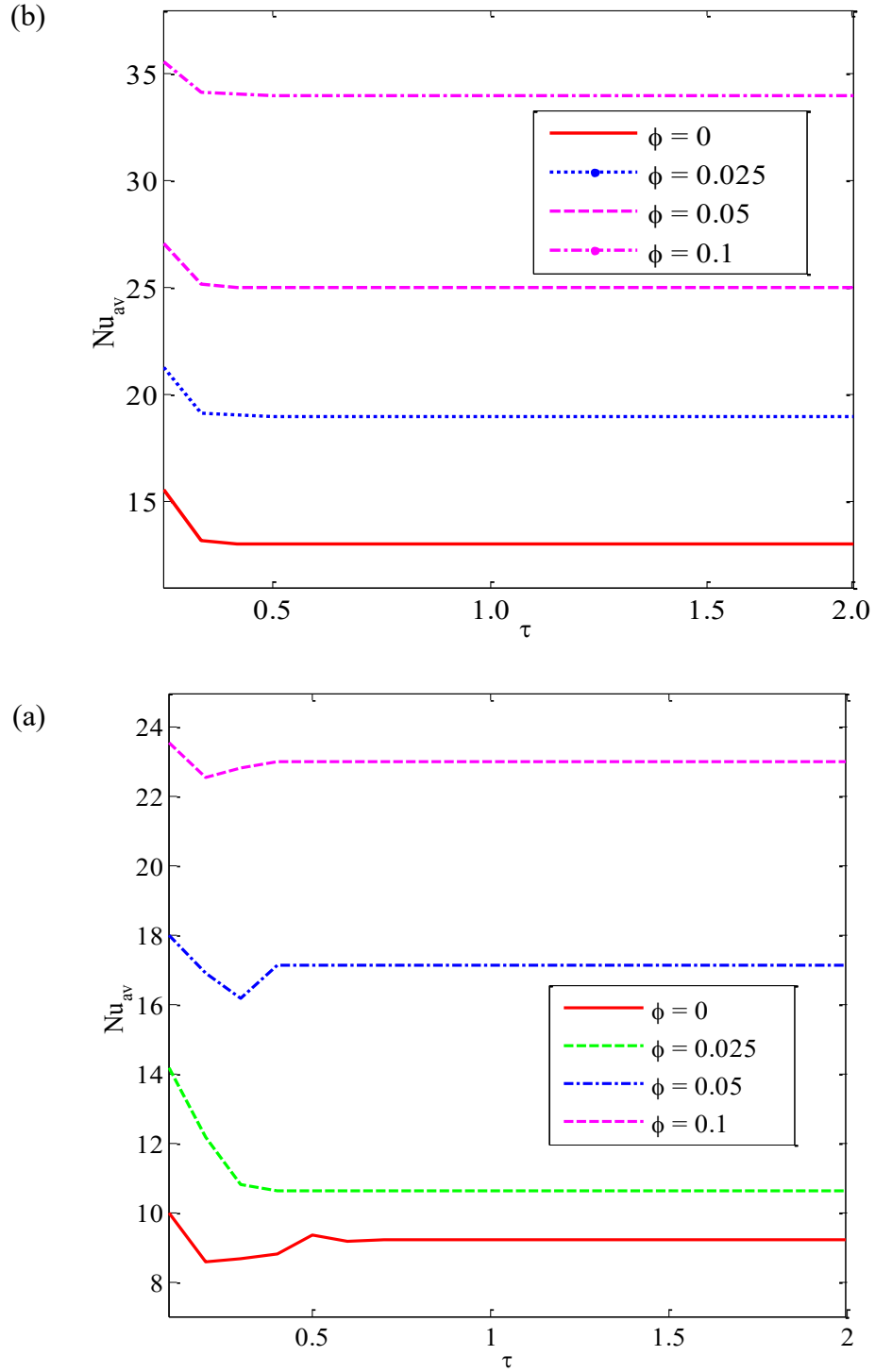


$(Nu_{av})$  is quite higher, and it becomes constant after passing dimensionless time. In addition, the higher nanoparticles into the base fluid create a particle tapping; consequently, the characteristics of nanofluid may change from Newtonian to non-Newtonian. In the present numerical calculations, the volume fraction of nanoparticles has been varied from 0 to 10%. To check the qualitative change in the solution, we have used an extreme case of 10%. Furthermore, the flow takes less time to reaches a steady state from an unsteady state for a higher Rayleigh number ( $Ra$ ) because a strong buoyancy force assists the flow in reaching a steady state faster.

Figure 5.3 represents the average Nusselt number ( $Nu_{av}$ ) with non-dimensional time ( $\tau$ ) for different diameter of nanoparticles ( $d$ ) for Cu-H<sub>2</sub>O nanofluid for uniform thermal boundary condition (case I) when  $Pr = 6.8377$ ,  $Ra = 10^5$ ,  $Ha = 20$ ,  $n = 3$ , and  $\phi = 0.04$ . The figure shows that the average Nusselt number oscillates significantly for a certain initial period of time for different diameters of nanoparticles. After a certain period of time, the distributions of the average Nusselt number is the almost straight line which means that the solution reaches a steady state for the diameter of nanoparticles. It is also observed that the average Nusselt number oscillates more for



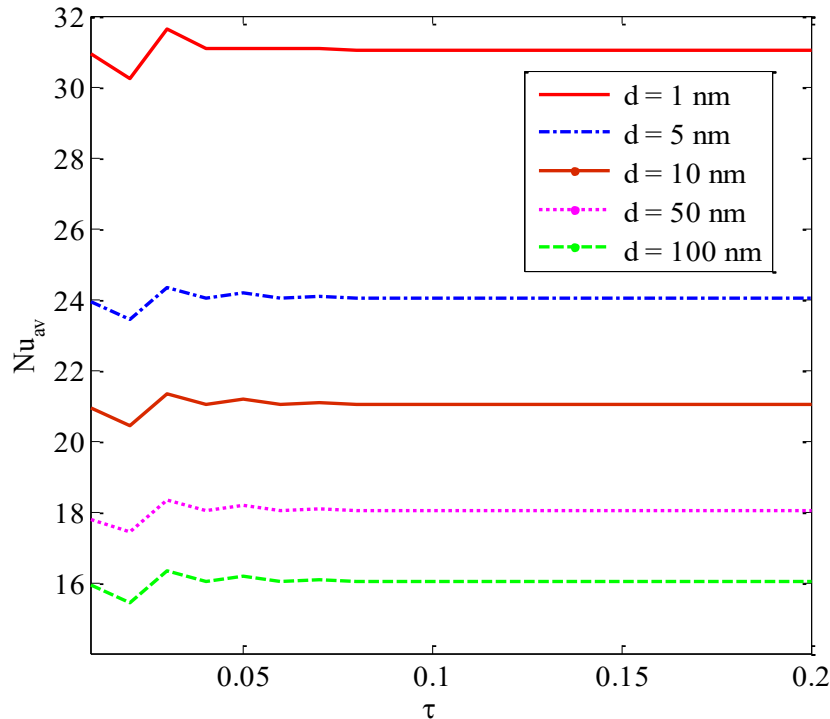
**Figure 5.1:** Average Nusselt number ( $Nu_{av}$ ) along bottom heated diameter for different Rayleigh number ( $Ra$ ) and different dimensionless time ( $\tau$ ) for Cu-H<sub>2</sub>O nanofluid for uniform thermal boundary condition (case I) when  $Pr = 6.8377$ ,  $Ha = 20$ ,  $d = 10\text{nm}$ ,  $n = 3$ , and  $\phi = 0.04$ .



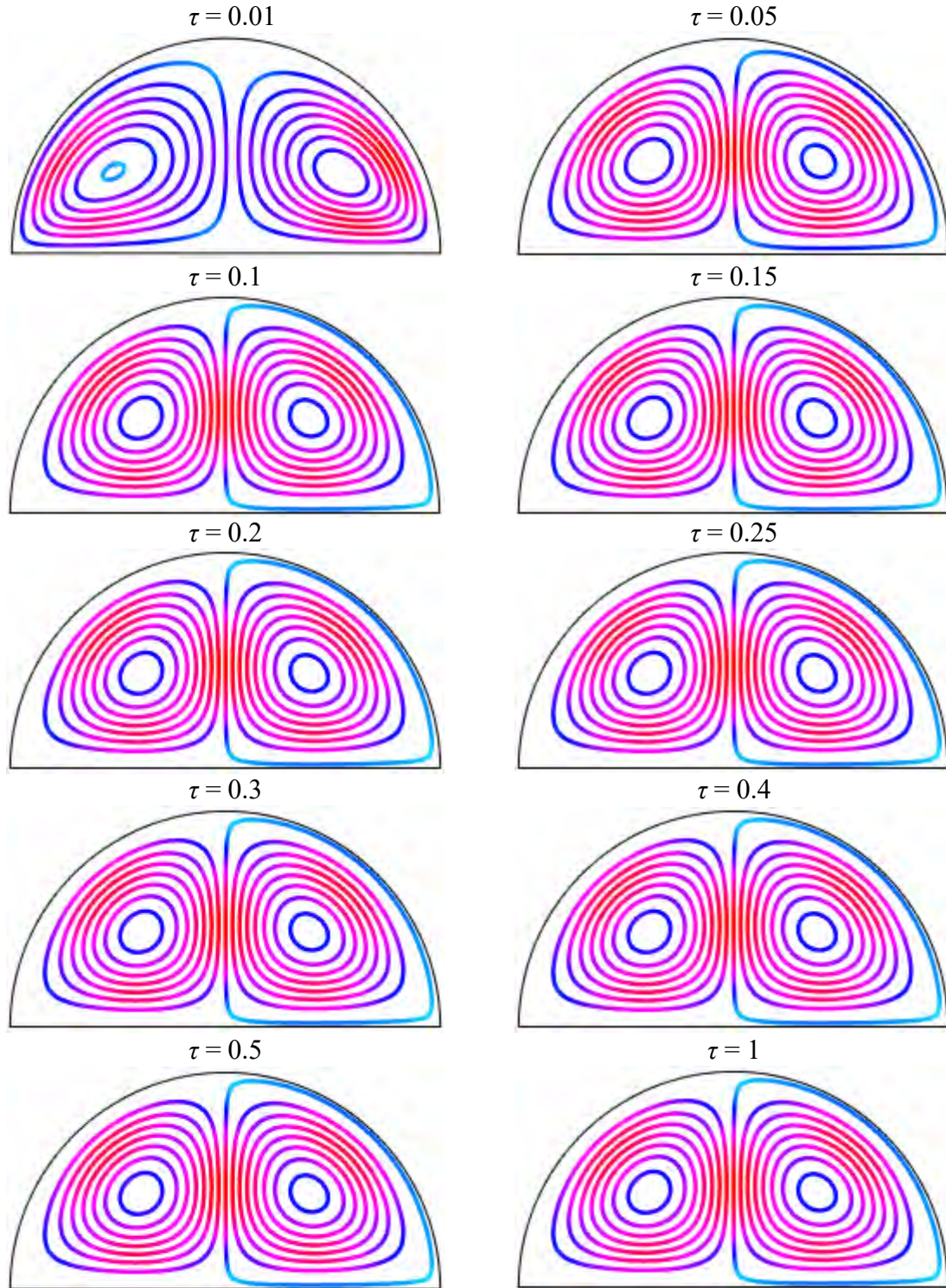
**Figure 5.2:** Average Nusselt number ( $Nu_{av}$ ) along bottom heated diameter for different nanoparticles volume fraction ( $\phi$ ) and different dimensionless time ( $\tau$ ) at (a)  $Ra = 10^5$ , and (b)  $Ra = 10^6$  for Cu-H<sub>2</sub>O nanofluid for uniform thermal boundary condition (case I) when  $Pr = 6.8377$ ,  $Ha = 20$ ,  $d = 10\text{nm}$ ,  $n = 3$ , and  $\phi = 0.04$ .

the small size of nanoparticles compared to the large size of nanoparticles. Therefore, the small size of nanoparticles helps the solution to attain in steady than large nanoparticles because the settling velocity is negligible for the small size of nanoparticles. For getting a steady-state solution quickly, it can be assisted by the possible smaller size of nanoparticles.

Figure 5.4 displays the evolution of streamline contours with non-dimensional time ( $\tau$ ) for uniform thermal boundary condition (case I) for Cu-H<sub>2</sub>O nanofluids when  $Ra = 10^5$ ,  $Ha = 20$ ,  $\phi = 0.04$ , and  $d = 10\text{nm}$  taking into account the time step  $\Delta\tau = 0.01$ . In a shorter time, it is seen that there are two symmetrical circulating vortices within the enclosure are formed where the eyes of the rotating cells of the streamlines near the heated wall. The rotating zone changed and intensify at the heated wall and cooled wall. The eyes of the symmetrical circulation move to central circulation with the increase of non-dimensional time ( $\tau$ ), which indicates a higher velocity of the flow. For the increases of dimensionless time ( $\tau$ ), the streamlines pattern shows no significant changes until it reaches to steady state. It is further mentioned that there are no streamlines that do not change when approximately  $\tau = 0.65$  for the solution of Cu-H<sub>2</sub>O nanofluid.

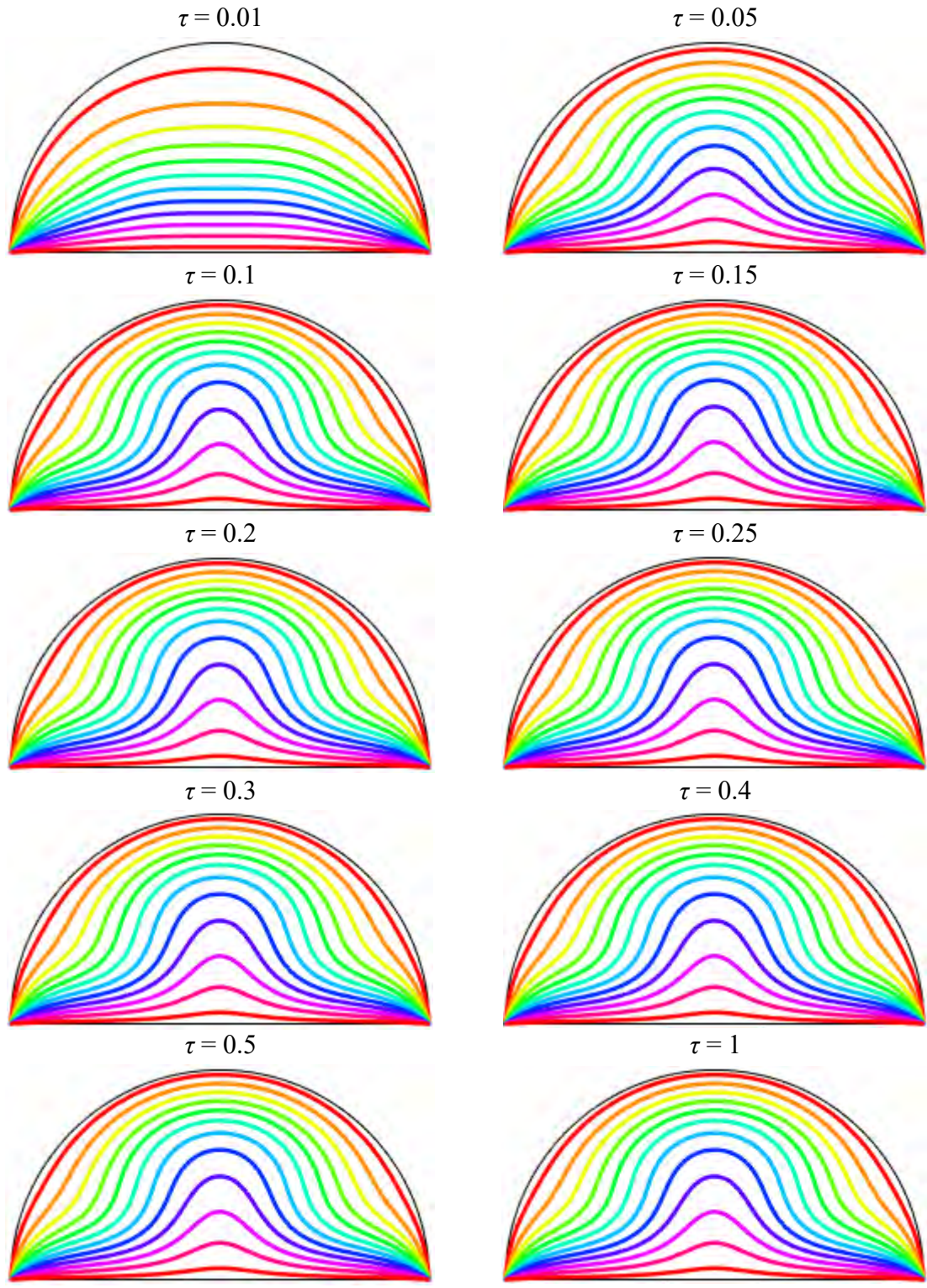


**Figure 5.3:** Variation of average Nusselt number ( $Nu_{av}$ ) along bottom heated diameter for different diameter of nanoparticles ( $d$ ) and dimensionless time ( $\tau$ ) for Cu-H<sub>2</sub>O nanofluid for uniform thermal boundary condition (case I) when  $n = 3$ ,  $Pr = 6.8377$ ,  $Ra = 10^5$ ,  $Ha = 20$ ,  $\lambda = 0.5$ , and  $\phi = 0.04$ .



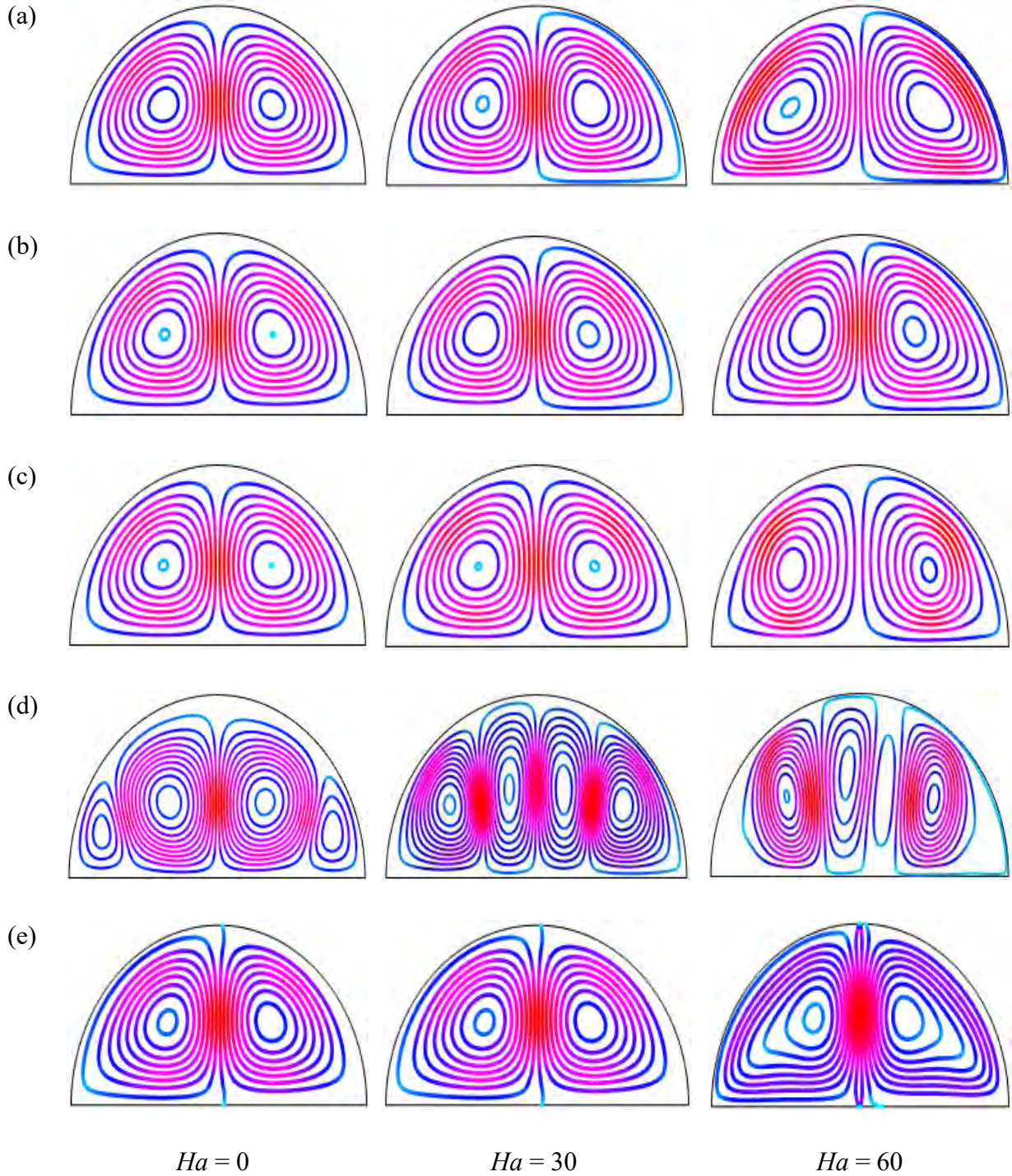
**Figure 5.4:** Streamlines evolutions at different dimensionless time ( $\tau$ ) for Cu-H<sub>2</sub>O nanofluid for uniform thermal boundary condition (case I) when  $Pr = 6.8377$ ,  $Ra = 10^5$ ,  $Ha = 20$ ,  $d = 10\text{nm}$ ,  $n = 3$ ,  $\lambda = 0.5$ , and  $\phi = 0.04$ .





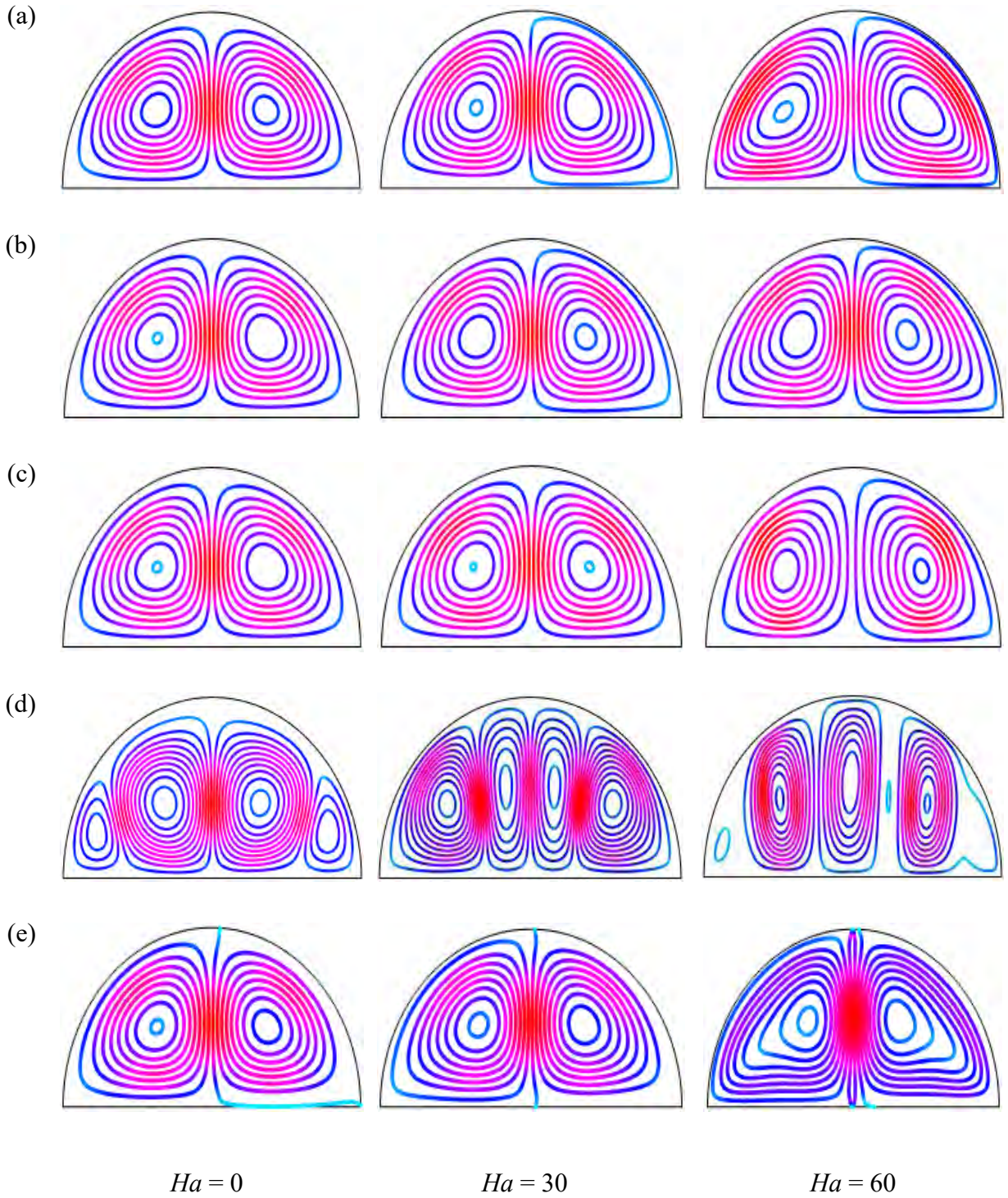
**Figure 5.5:** Isothermal lines evolution at different dimensionless time ( $\tau$ ) for Cu-H<sub>2</sub>O nanofluid for uniform thermal boundary condition (case I) when  $Pr = 6.8377$ ,  $Ra = 10^5$ ,  $Ha = 20$ ,  $d = 10\text{nm}$ ,  $n = 3$ ,  $\lambda = 0.5$ , and  $\phi = 0.04$ .





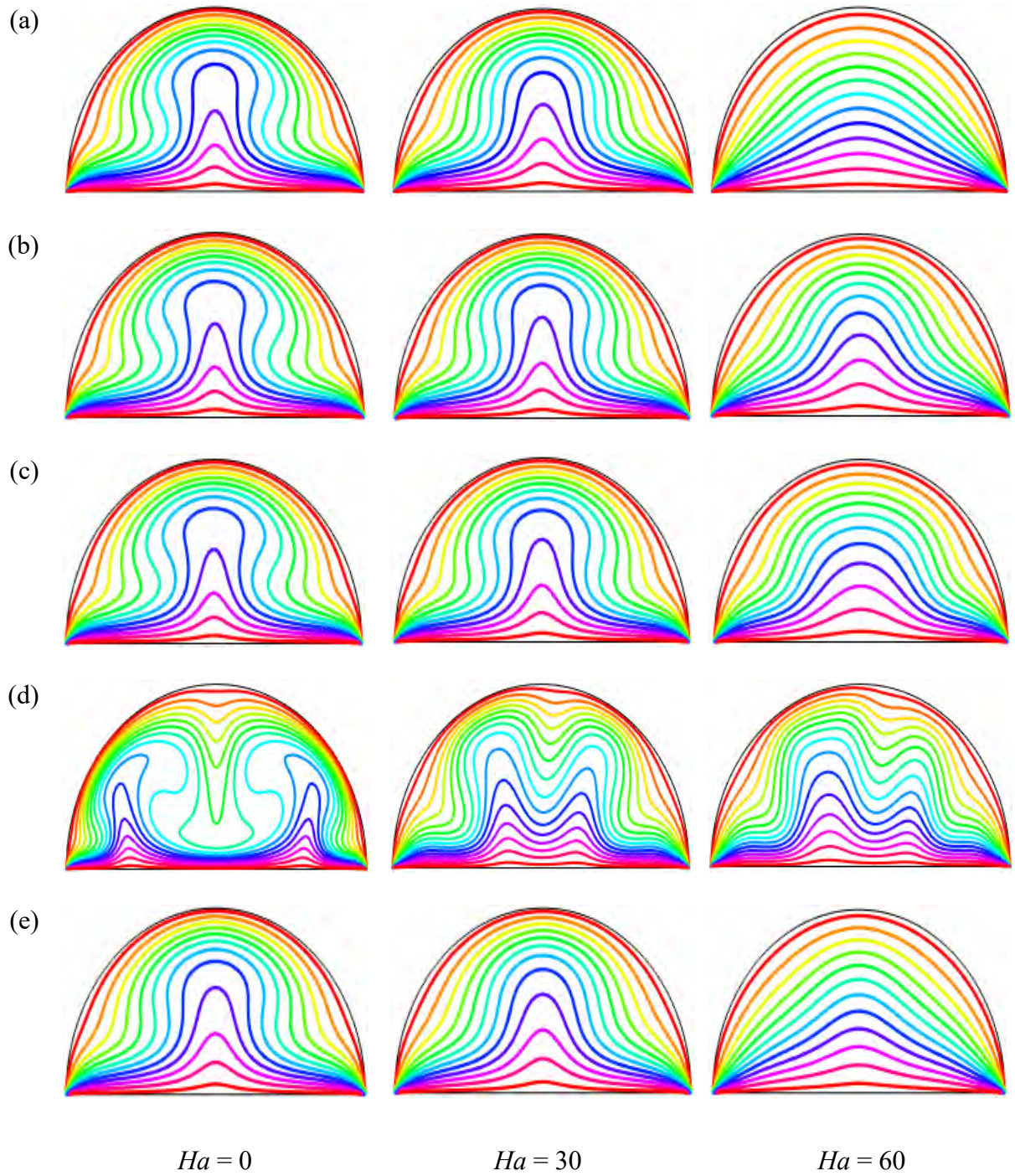
**Figure 5.6:** Effect of Hartmann number ( $Ha$ ) on streamlines for (a) uniform magnetic field (umf), and non-uniform magnetic field with different periods (b)  $\lambda = 0.1$ , (c)  $\lambda = 0.25$ , (d)  $\lambda = 0.5$  and (e)  $\lambda = 1$  for Cu-H<sub>2</sub>O nanofluid for uniform thermal boundary condition (case I) when  $Ra = 10^5$ ,  $\phi = 0.04$ ,  $d = 10\text{nm}$ ,  $n = 3$ ,  $Pr = 6.8377$ , and  $\tau = 0.1$ .





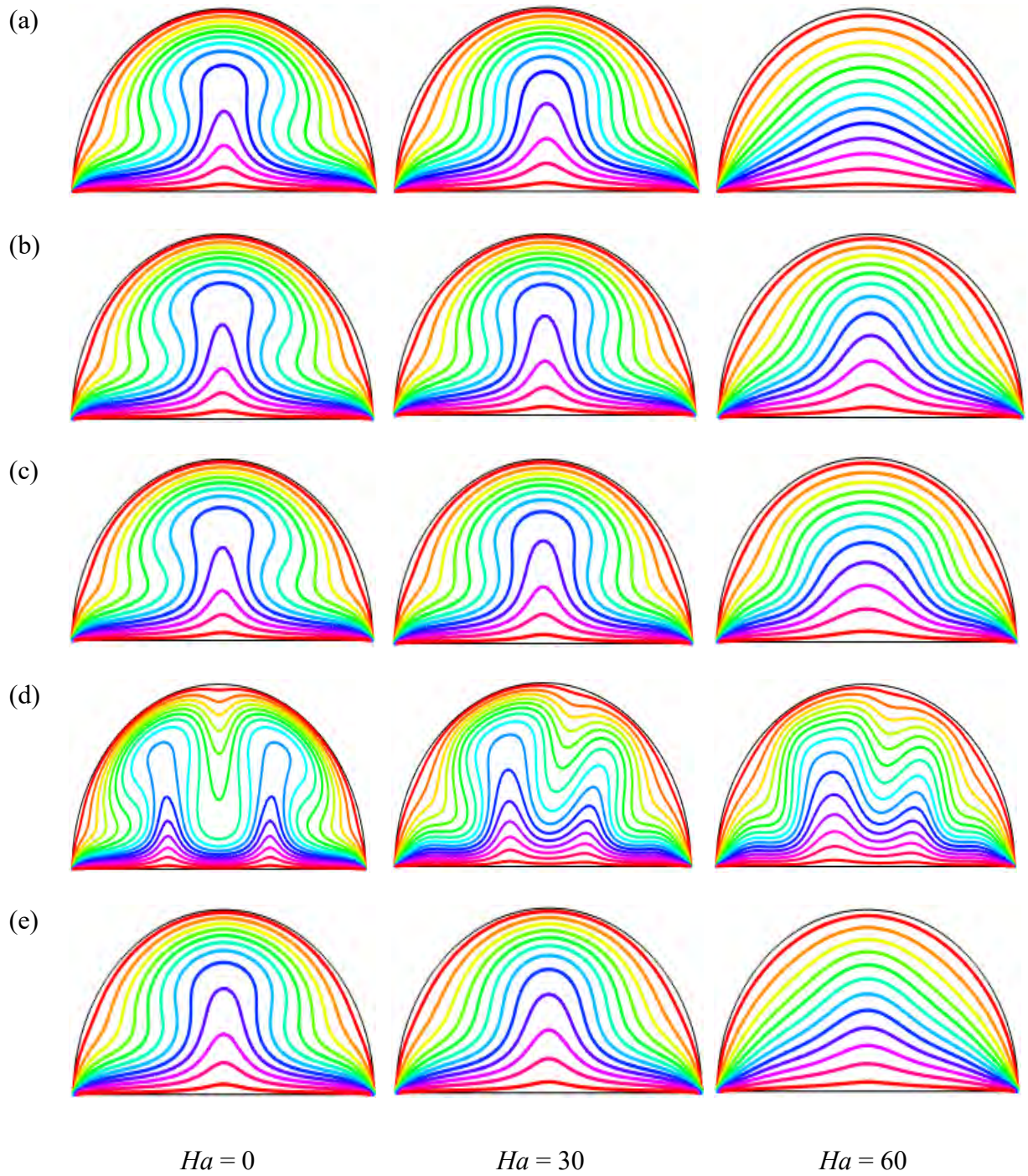
**Figure 5.7:** Effect of Hartmann number ( $Ha$ ) on streamlines for (a) uniform magnetic field (umf), and non-uniform magnetic field with different periods (b)  $\lambda = 0.1$ , (c)  $\lambda = 0.25$ , (d)  $\lambda = 0.5$  and (e)  $\lambda = 1$ , for Cu-H<sub>2</sub>O nanofluid for uniform thermal boundary condition (case I) when  $Ra = 10^5$ ,  $\phi = 0.04$ ,  $d = 10\text{nm}$ ,  $Pr = 6.8377$ ,  $n = 3$  and  $\tau = 1$ .



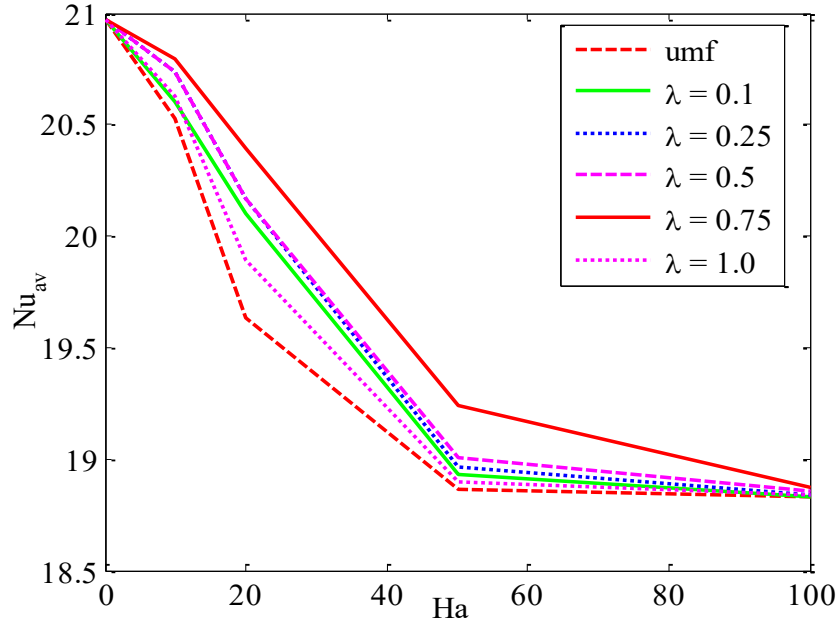


**Figure 5.8:** Effect of Hartmann number ( $Ha$ ) on isothermal lines for (a) uniform magnetic field (umf), and non-uniform magnetic field with different periods (b)  $\lambda = 0.1$ , (c)  $\lambda = 0.25$ , (d)  $\lambda = 0.5$  and (e)  $\lambda = 1$ , for Cu-H<sub>2</sub>O nanofluid with uniform thermal boundary condition (case I) when  $Ra = 10^5$ ,  $\phi = 0.04$ ,  $d = 10\text{nm}$ ,  $Pr = 6.8377$ ,  $n = 3$  and  $\tau = 0.1$ .





**Figure 5.9:** Effect of Hartmann number ( $Ha$ ) on isotherms for (a) uniform magnetic field (umf), and non-uniform magnetic field with different periods (b)  $\lambda = 0.1$ , (c)  $\lambda = 0.25$ , (d)  $\lambda = 0.5$ , and (e)  $\lambda = 1$ , for Cu-H<sub>2</sub>O nanofluid for uniform thermal boundary condition (case I) when  $Ra = 10^5$ ,  $\phi = 0.04$ ,  $d = 10\text{nm}$ ,  $Pr = 6.8377$ ,  $n = 3$  and  $\tau = 1$ .



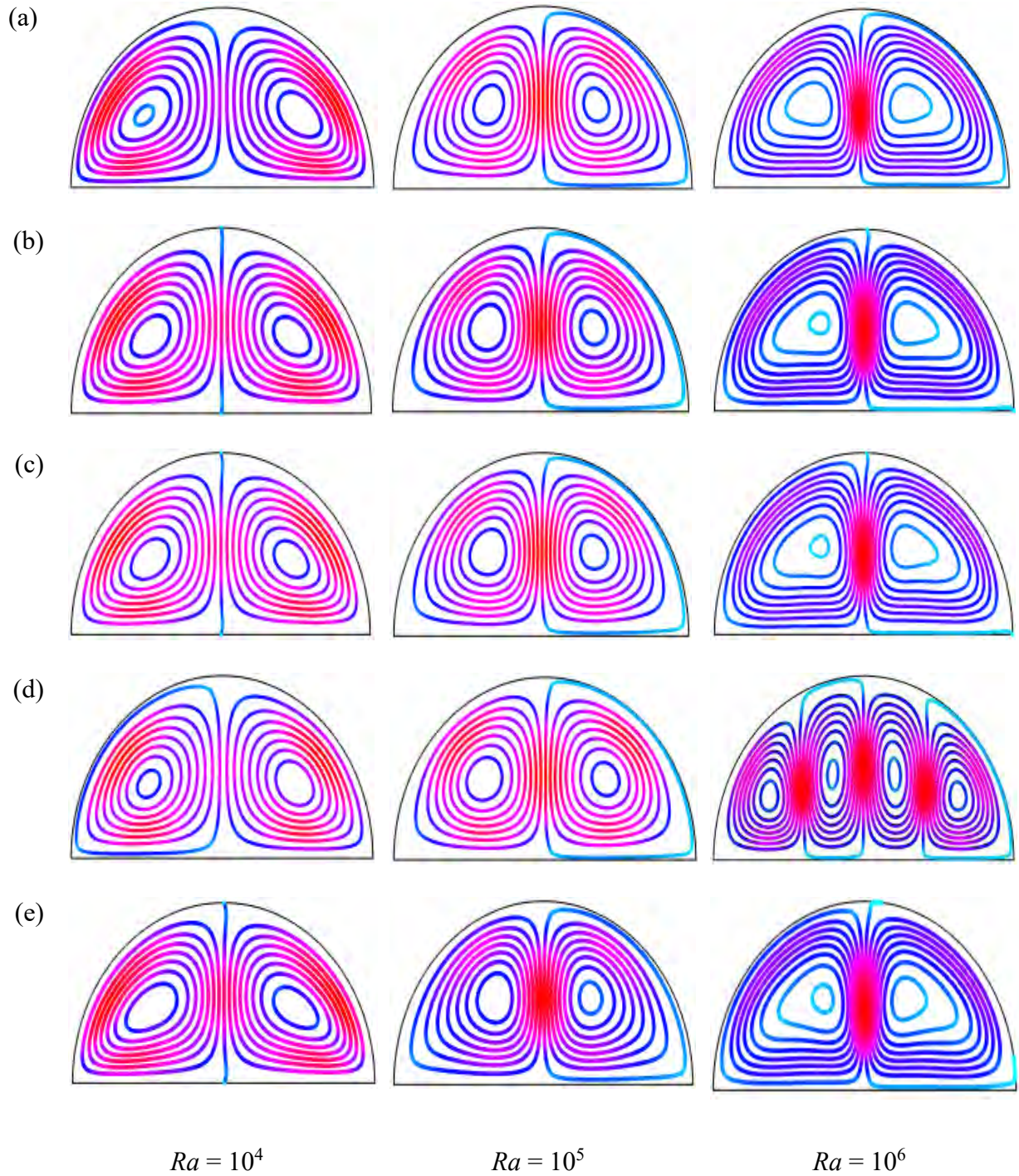
**Figure 5.10:** Variation of average Nusselt number ( $Nu_{av}$ ) for uniform magnetic field (umf) and non-uniform magnetic field with different periods ( $\lambda$ ), and Hartmann number ( $Ha$ ) for Cu-H<sub>2</sub>O nanofluid for uniform thermal boundary condition (case I) when  $\phi = 0.04$ ,  $Pr = 6.8377$ ,  $Ra = 10^5$ ,  $d = 10\text{nm}$ ,  $n = 3$ , and  $\tau = 1$ .

Figure 5.5 shows the distribution of isothermal lines within the semi-circular enclosure for different non-dimensional time ( $\tau$ ) for Rayleigh number,  $Ra = 10^5$  for Cu-H<sub>2</sub>O nanofluids when  $Ha = 20$ ,  $\phi = 0.04$ , and  $d = 10\text{nm}$  for uniform thermal boundary condition (case I). At  $\tau = 0.01$ , the flow is unsteady, and the isothermal lines are concentrated near the hot bottom wall that represents a higher temperature gradient due to buoyancy effects. As dimensionless time ( $\tau$ ) increases, the isothermal lines move upward at the middle of the bottom wall, representing the flow of temperature higher in that region. The intensity of the isothermal line increases with the increase of non-dimensional time until it reaches a steady-state. In addition, the isothermal lines change over few time and show a marginal variation until it reaches the steady-state.

## 5.2 Effects of magnetic field and its period

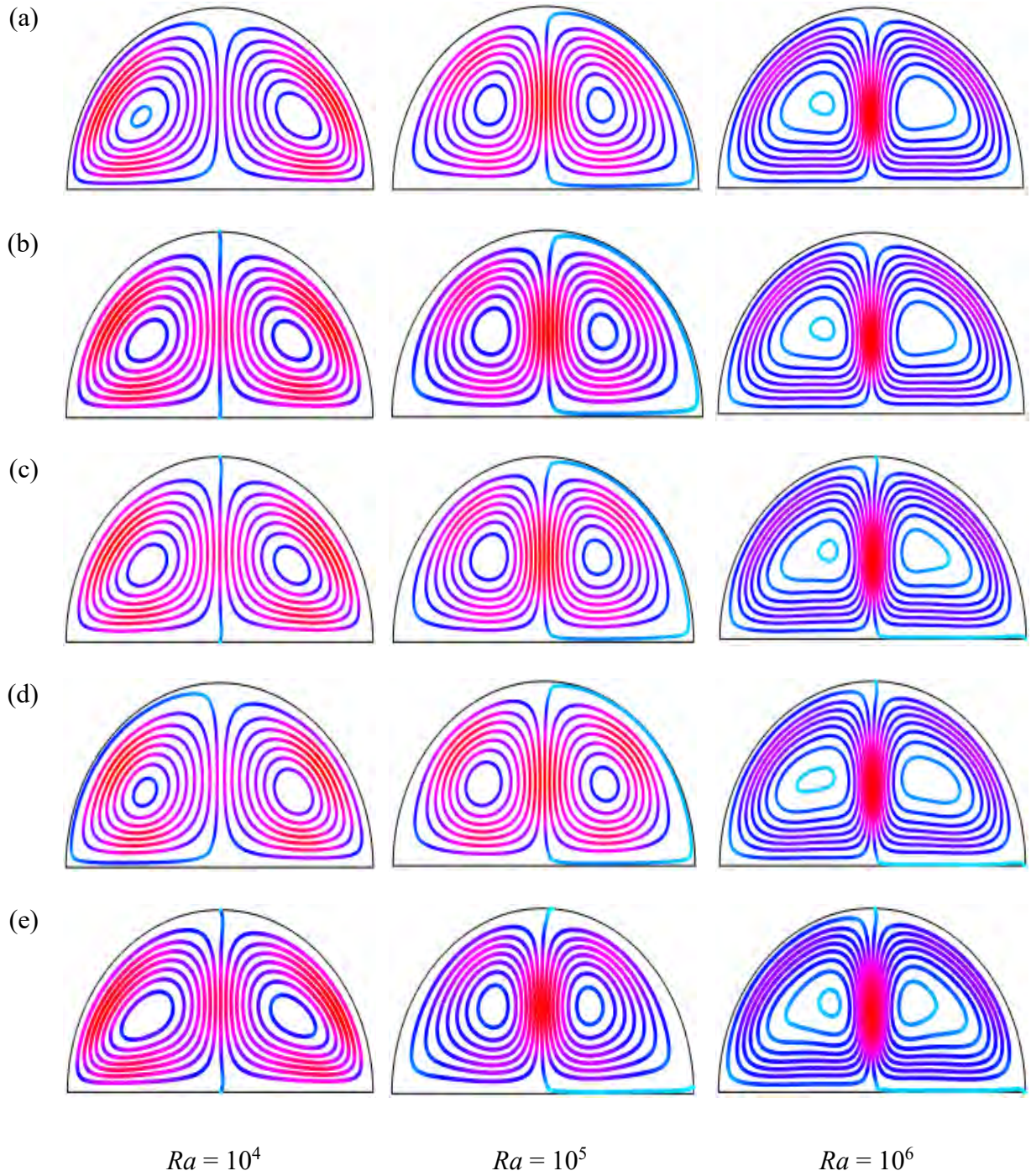
Figures 5.6-5.7, respectively, represent the influence of streamlines for different Hartmann number ( $Ha$ ) or both unsteady case ( $\tau = 0.1$ ) and steady case ( $\tau = 1$ ) for Cu-H<sub>2</sub>O nanofluid for uniform thermal boundary condition (case I) when  $Pr = 6.8377$ ,  $Ra = 10^5$ ,  $d = 10\text{nm}$  and,  $n = 3$ . These figures actually represent the evaluation of streamlines under the strong magnetic field. Two-





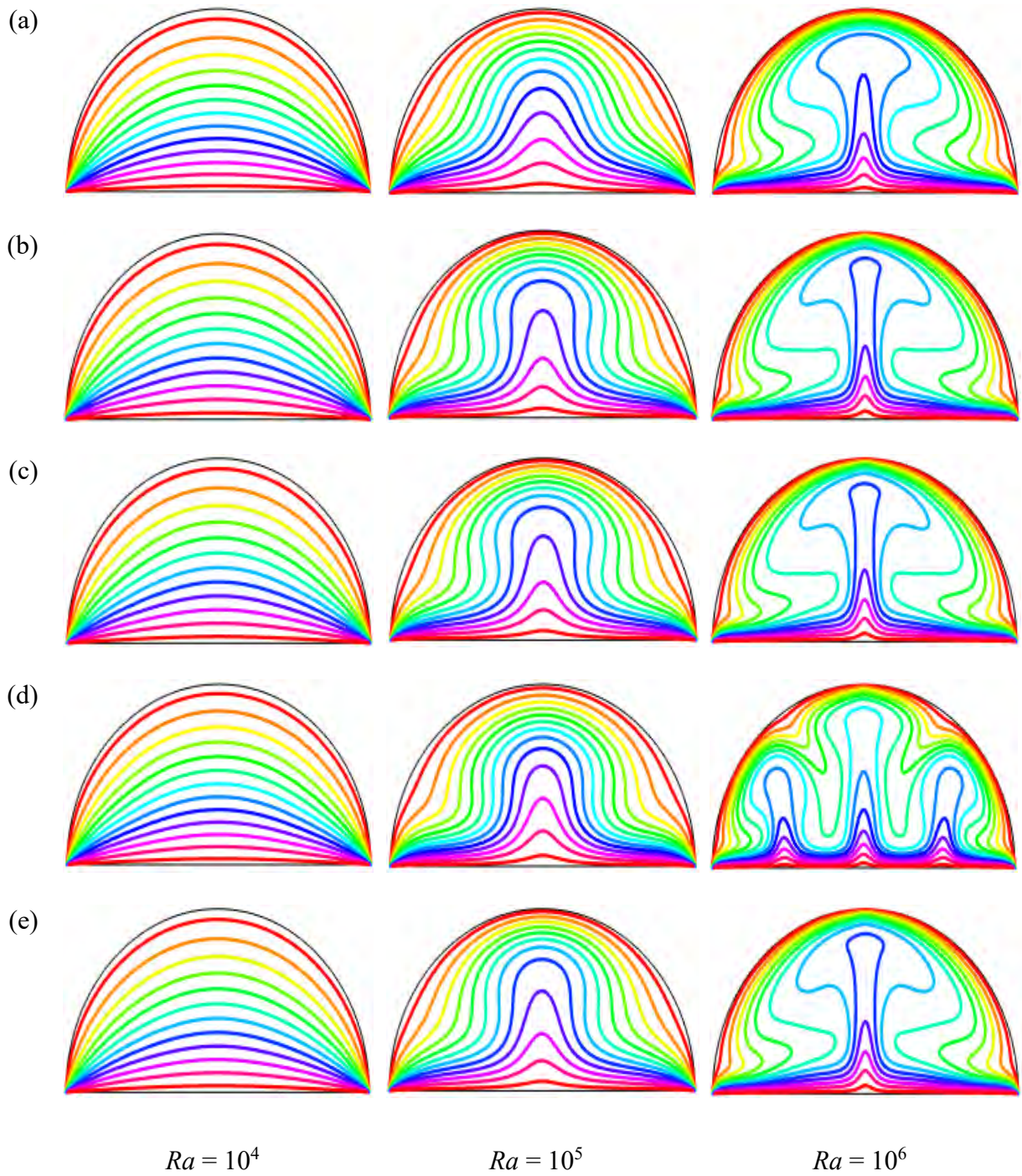
**Figure 5.11:** Effect of Rayleigh number ( $Ra$ ) on streamlines for (a) uniform magnetic field (umf), and non-uniform magnetic field with different periods (b)  $\lambda = 0.1$ , (c)  $\lambda = 0.25$ , (d)  $\lambda = 0.5$ , and (e)  $\lambda = 1$ , for Cu-H<sub>2</sub>O nanofluid for uniform thermal boundary condition (case I) when  $Ha = 20$ ,  $\phi = 0.04$ ,  $d = 10\text{nm}$ ,  $Pr = 6.8377$ ,  $n = 3$ , and  $\tau = 0.1$ .



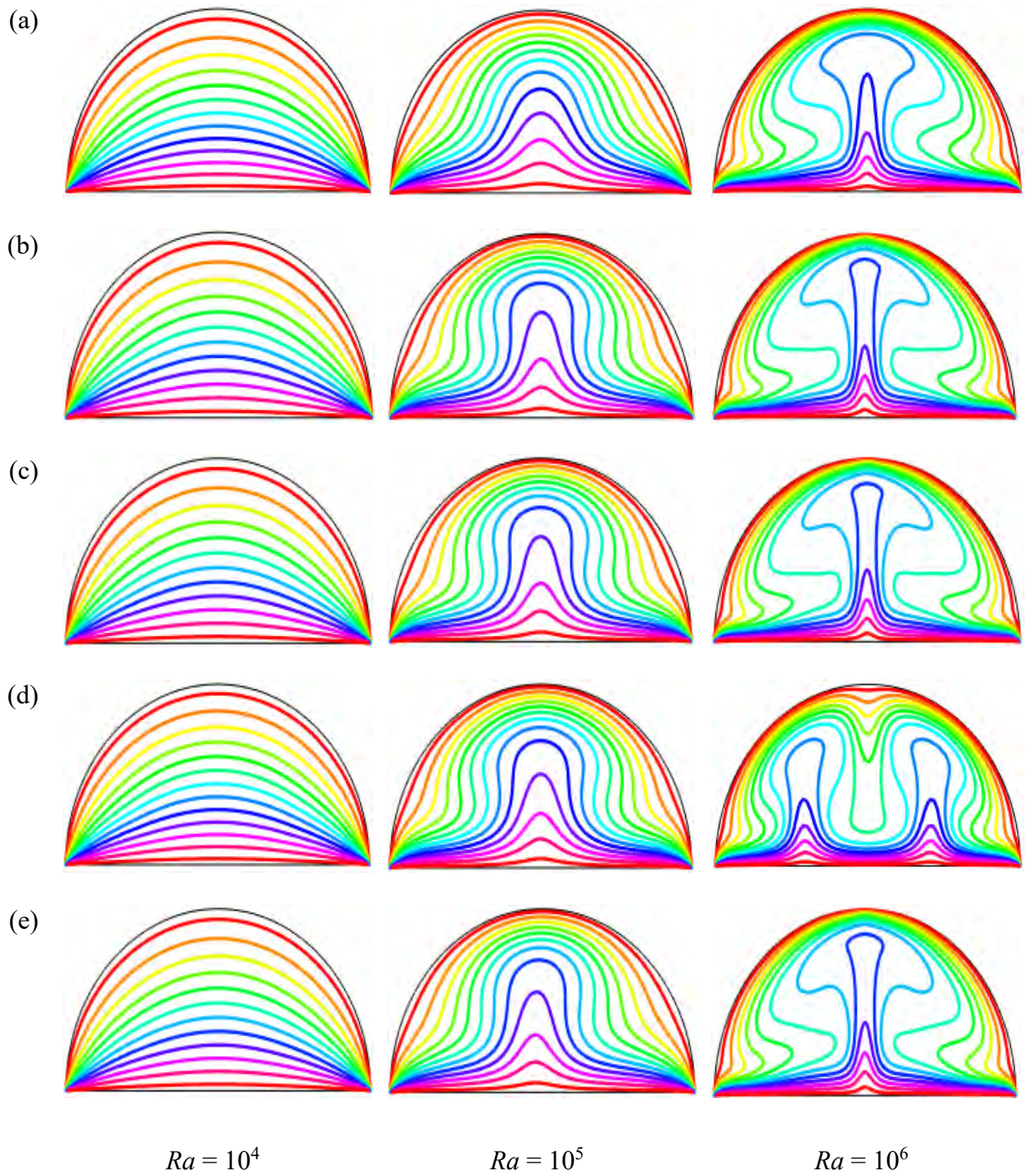


**Figure 5.12:** Effect of Rayleigh number ( $Ra$ ) on streamlines for (a) uniform magnetic field (umf), and non-uniform magnetic field with different periods (b)  $\lambda = 0.1$ , (c)  $\lambda = 0.25$ , (d)  $\lambda = 0.5$ , and (e)  $\lambda = 1$ , for Cu-H<sub>2</sub>O nanofluid for uniform thermal boundary condition (case I) when  $Ha = 20$ ,  $\phi = 0.04$ ,  $d = 10\text{nm}$ ,  $Pr = 6.8377$ ,  $n = 3$ , and  $\tau = 1$ .



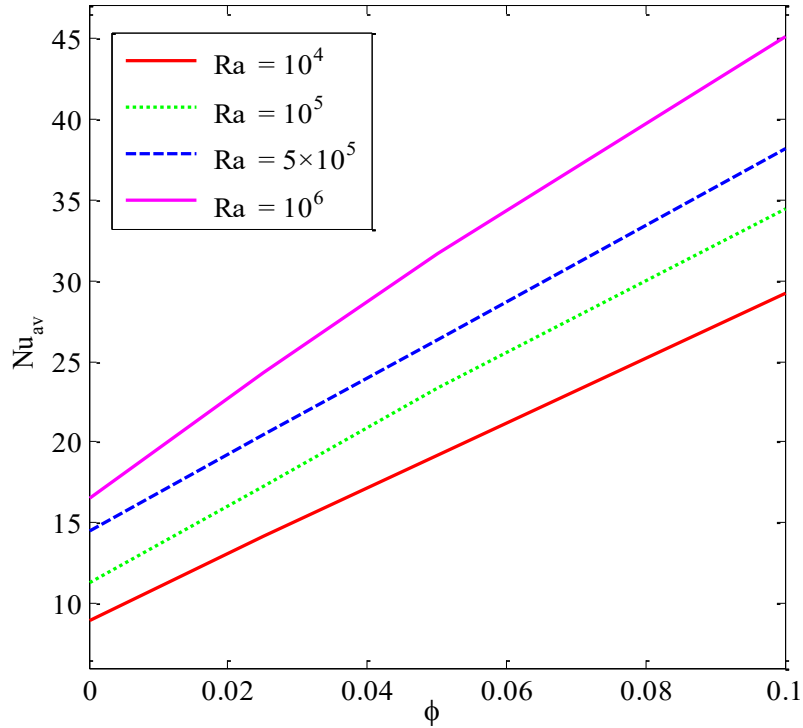


**Figure 5.13:** Effect of Rayleigh number ( $Ra$ ) on isotherms for (a) uniform magnetic field (umf), and non-uniform magnetic field with different periods (b)  $\lambda = 0.1$ , (c)  $\lambda = 0.25$ , (d)  $\lambda = 0.5$ , and (e)  $\lambda = 1$ , for Cu-H<sub>2</sub>O nanofluid for uniform thermal boundary condition (case I) when  $Ha = 20$ ,  $\phi = 0.04$ ,  $d = 10\text{nm}$ ,  $Pr = 6.8377$ ,  $n = 3$ , and  $\tau = 0.1$ .



**Figure 5.14:** Effect of Rayleigh number ( $Ra$ ) on isotherms for (a) uniform magnetic field (umf), and non-uniform magnetic field with different periods (b)  $\lambda = 0.1$ , (c)  $\lambda = 0.25$ , (d)  $\lambda = 0.5$ , and (e)  $\lambda = 1$ , for Cu-H<sub>2</sub>O nanofluid for uniform thermal boundary condition (case I) when  $Ha = 20$ ,  $\phi = 0.04$ ,  $Pr = 6.8377$ ,  $d = 10\text{nm}$ ,  $n = 3$ , and  $\tau = 1$ .

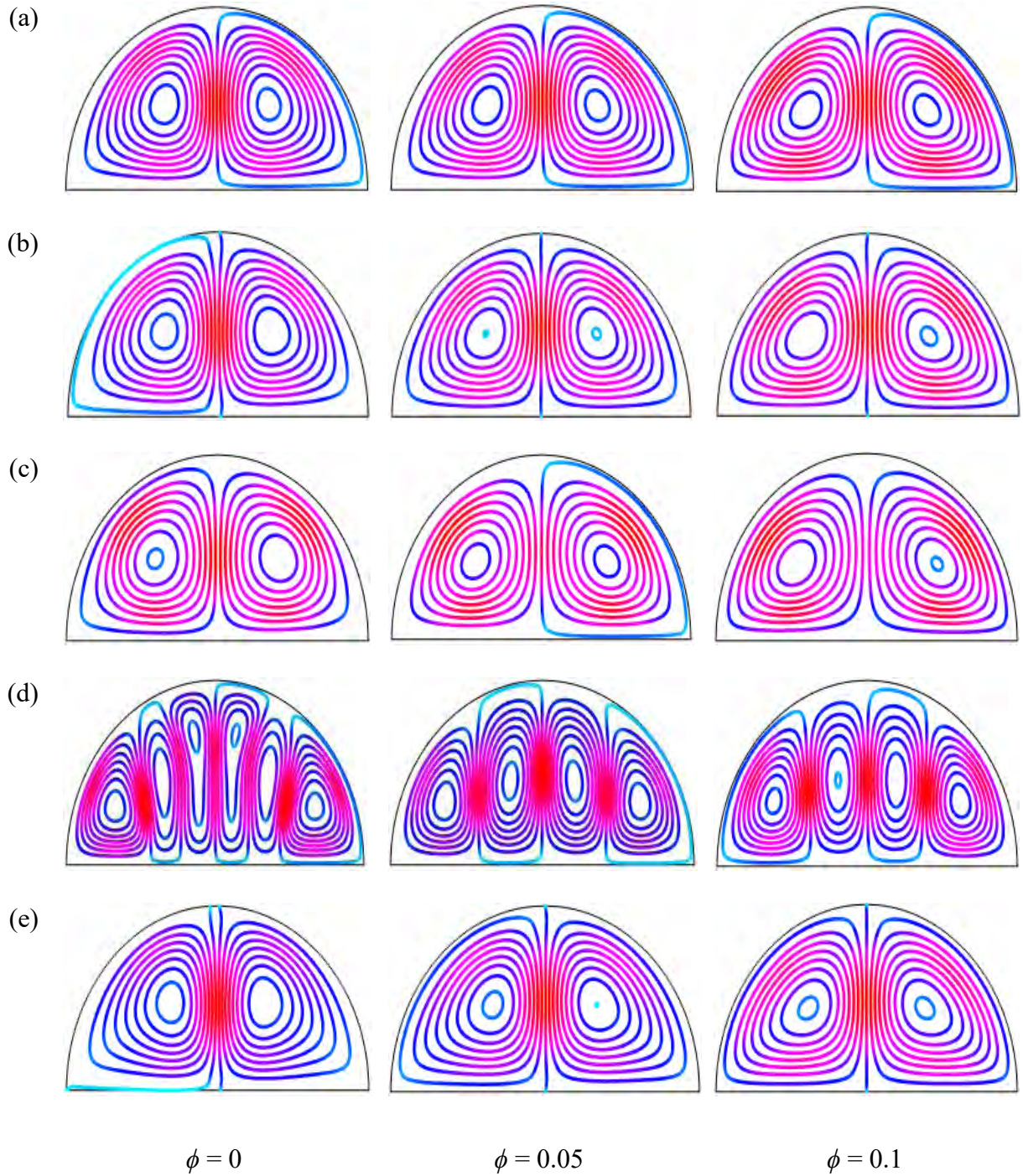




**Figure 5.15:** Variation of average Nusselt number ( $Nu_{av}$ ) along bottom heated diameter with uniform thermal boundary condition (case I) for different volume fraction of nanoparticles ( $\phi$ ) and different Rayleigh number ( $Ra$ ) for Cu-H<sub>2</sub>O nanofluid when  $Pr = 6.8377$ ,  $Ha = 20$ ,  $d = 10\text{nm}$ ,  $n = 3$ , and  $\tau = 1$ .

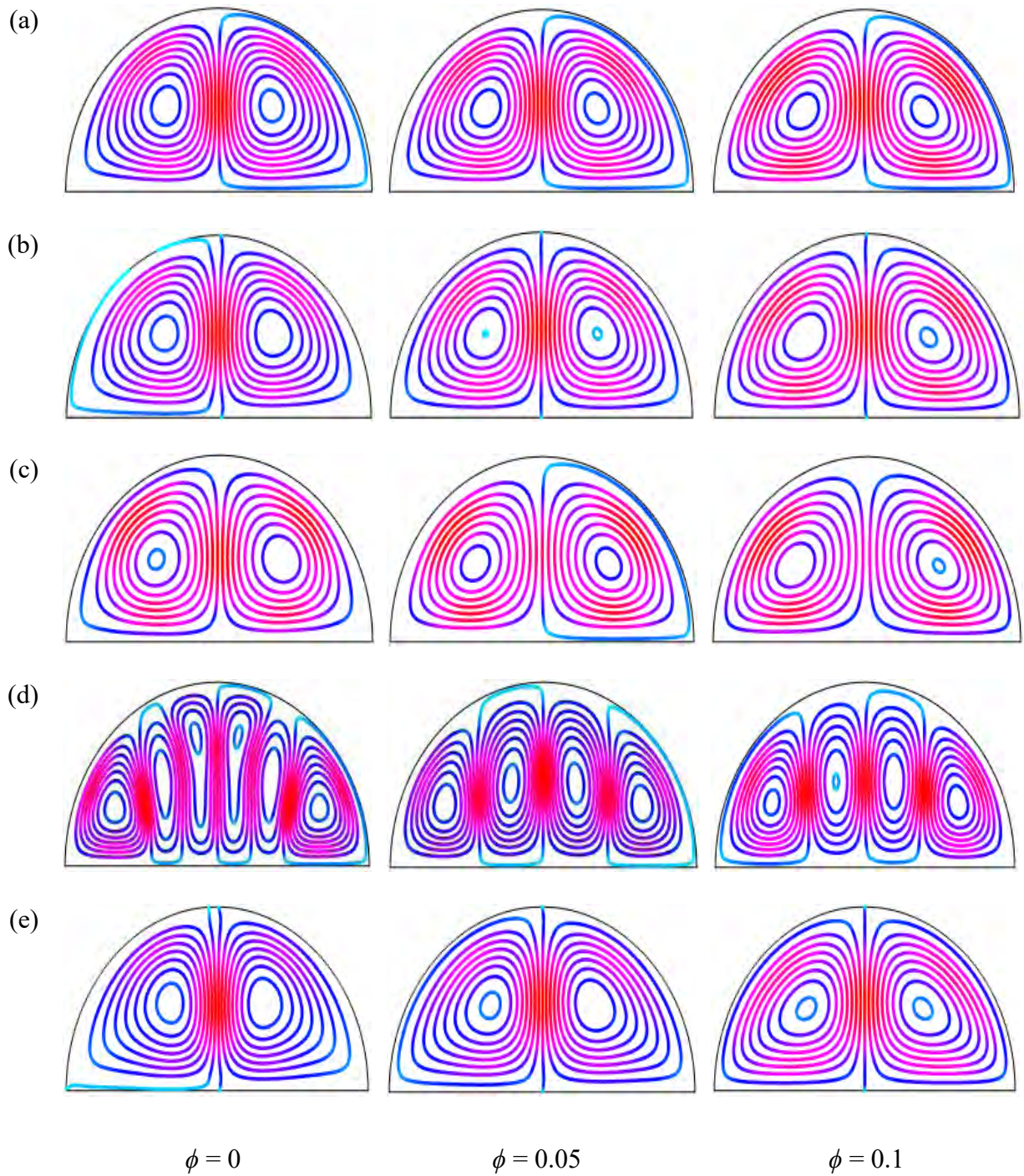
symmetrical vortices are observed for both uniform magnetic field and non-uniform magnetic field except for the period of the magnetic field  $\lambda = 0.5$ . The strength of the flow diminishes with a stronger applied magnetic field, i.e., increase of Hartmann number. A strong field is imposed over the moving fluid by imposing an external applied magnetic field that has magnetic impressionability. The Lorentz force generated by applied magnetic field has a nature to oppose the varying its generation in fluid movement. This force field weakens the streams within the enclosure. Figure 5.7 shows the pattern of the streamlines after the system has reached a steady state. There is a little change in the strength of the streamlines with time within the cavity. In addition, at  $\lambda = 0.5$ , the intensity of the pattern of the streamlines increase inside the enclosure.

Figures 5.8-5.9 exhibit the effect of isothermal lines for different values of Hartmann number ( $Ha$ ) and different period of the non-uniform magnetic field when  $Pr = 6.8377$ ,  $Ra = 10^5$ ,  $d = 10\text{nm}$ ,  $n = 3$  and  $\tau = 0.1$  and  $\tau = 1$ , respectively for Cu-H<sub>2</sub>O nanofluid for uniform thermal boundary condition



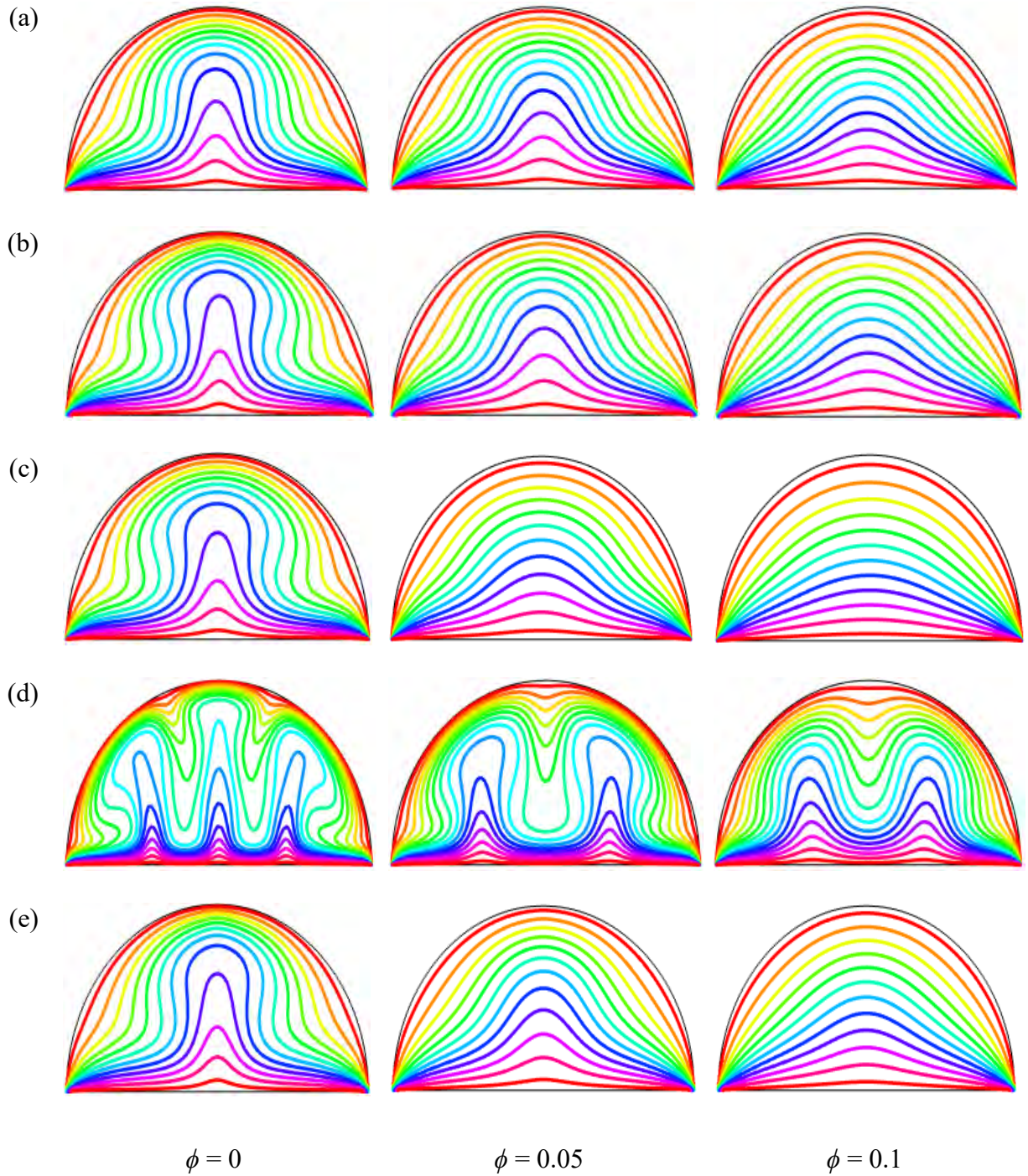
**Figure 5.16:** Effect of nanoparticles volume fraction ( $\phi$ ) on streamlines for (a) uniform magnetic field (umf), and non-uniform magnetic field with different periods (b)  $\lambda = 0.1$ , (c)  $\lambda = 0.25$ , (d)  $\lambda = 0.5$ , and (e)  $\lambda = 1$ , for Cu-H<sub>2</sub>O nanofluid for uniform thermal boundary condition (case I) when  $Ha = 20$ ,  $Ra = 10^5$ ,  $d = 10\text{nm}$ ,  $n = 3$ ,  $Pr = 6.8377$ , and  $\tau = 0.1$ .



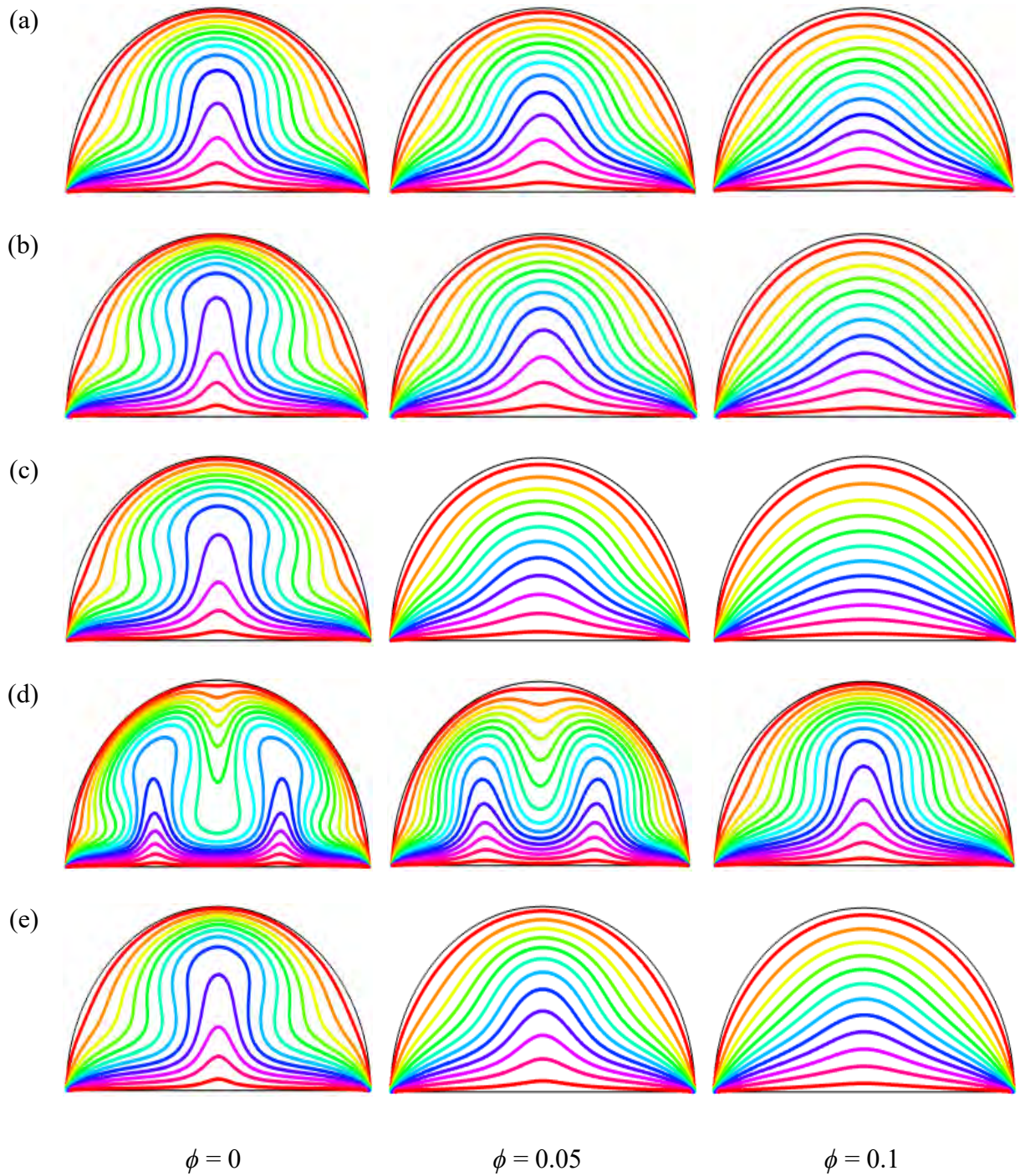


**Figure 5.17:** Effect of nanoparticles volume fraction ( $\phi$ ) on streamlines for (a) uniform magnetic field (umf), and non-uniform magnetic field with different periods (b)  $\lambda = 0.1$ , (c)  $\lambda = 0.25$ , (d)  $\lambda = 0.5$ , and (e)  $\lambda = 1$ , for Cu-H<sub>2</sub>O nanofluid for uniform thermal boundary condition (case I) when  $Ha = 20$ ,  $Ra = 10^5$ ,  $d = 10\text{nm}$ ,  $n = 3$ ,  $Pr = 6.8377$ , and  $\tau = 1$ .



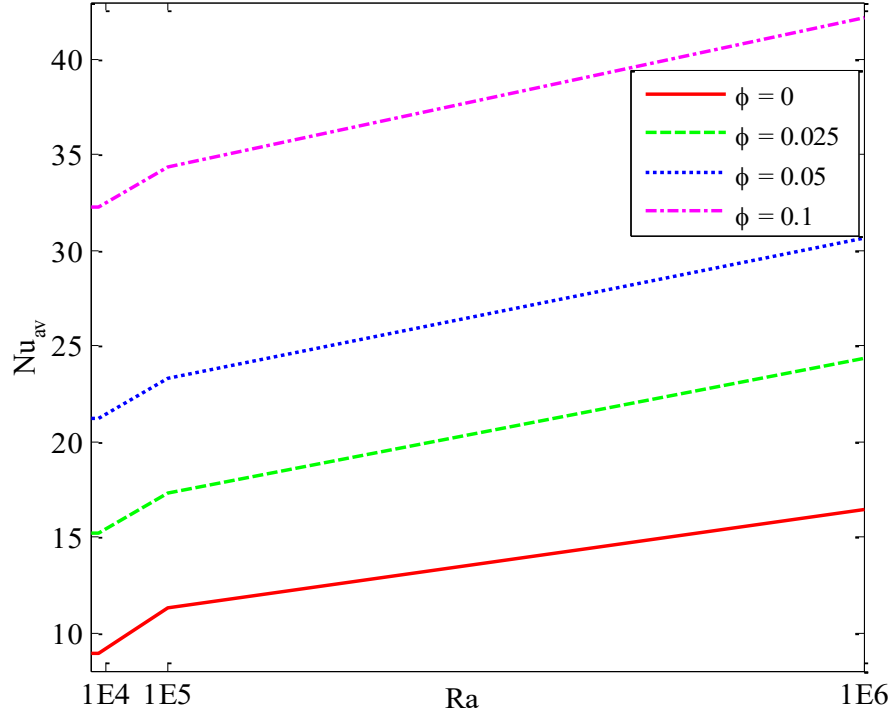


**Figure 5.18:** Effect of nanoparticles volume fraction ( $\phi$ ) on isotherms for (a) uniform magnetic field (umf), and non-uniform magnetic field with different period (b)  $\lambda = 0.1$ , (c)  $\lambda = 0.25$ , (d)  $\lambda = 0.5$ , and (e)  $\lambda = 1$ , for Cu-H<sub>2</sub>O nanofluid for uniform thermal boundary condition (case I) when  $Ha = 20$ ,  $Ra = 10^5$ ,  $d = 10\text{nm}$ ,  $n = 3$ ,  $Pr = 6.8377$  and  $\tau = 0.1$ .



**Figure 5.19:** Effect of nanoparticles volume fraction ( $\phi$ ) on isotherms for (a) uniform magnetic field (umf), and non-uniform magnetic field with different periods (b)  $\lambda = 0.1$ , (c)  $\lambda = 0.25$ , (d)  $\lambda = 0.5$ , and (e)  $\lambda = 1$ , for Cu-H<sub>2</sub>O nanofluid for uniform thermal boundary condition (case I) when  $Ha = 20$ ,  $Ra = 10^5$ ,  $d = 10\text{nm}$ ,  $n = 3$ ,  $Pr = 6.8377$ , and  $\tau = 1$ .

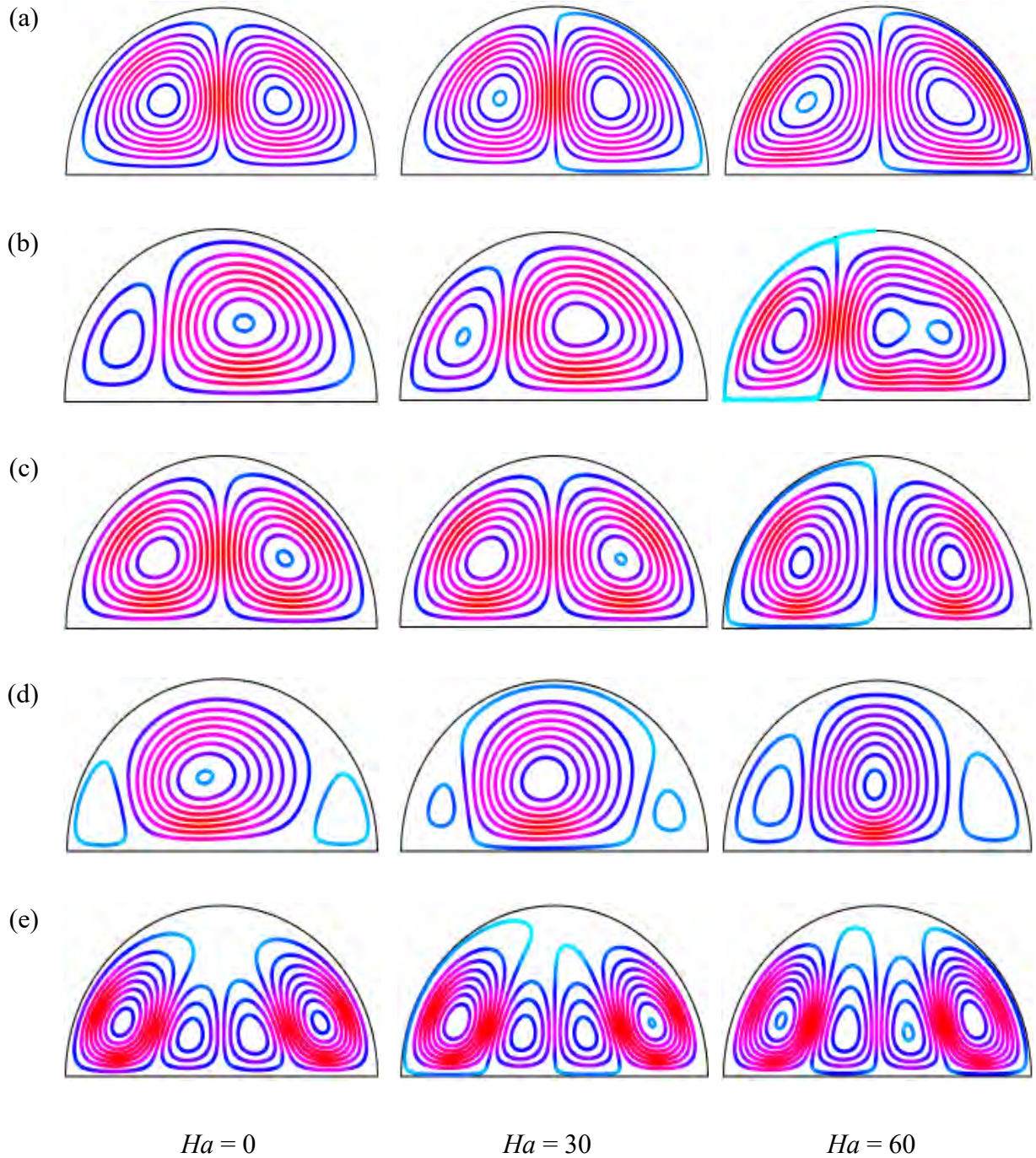




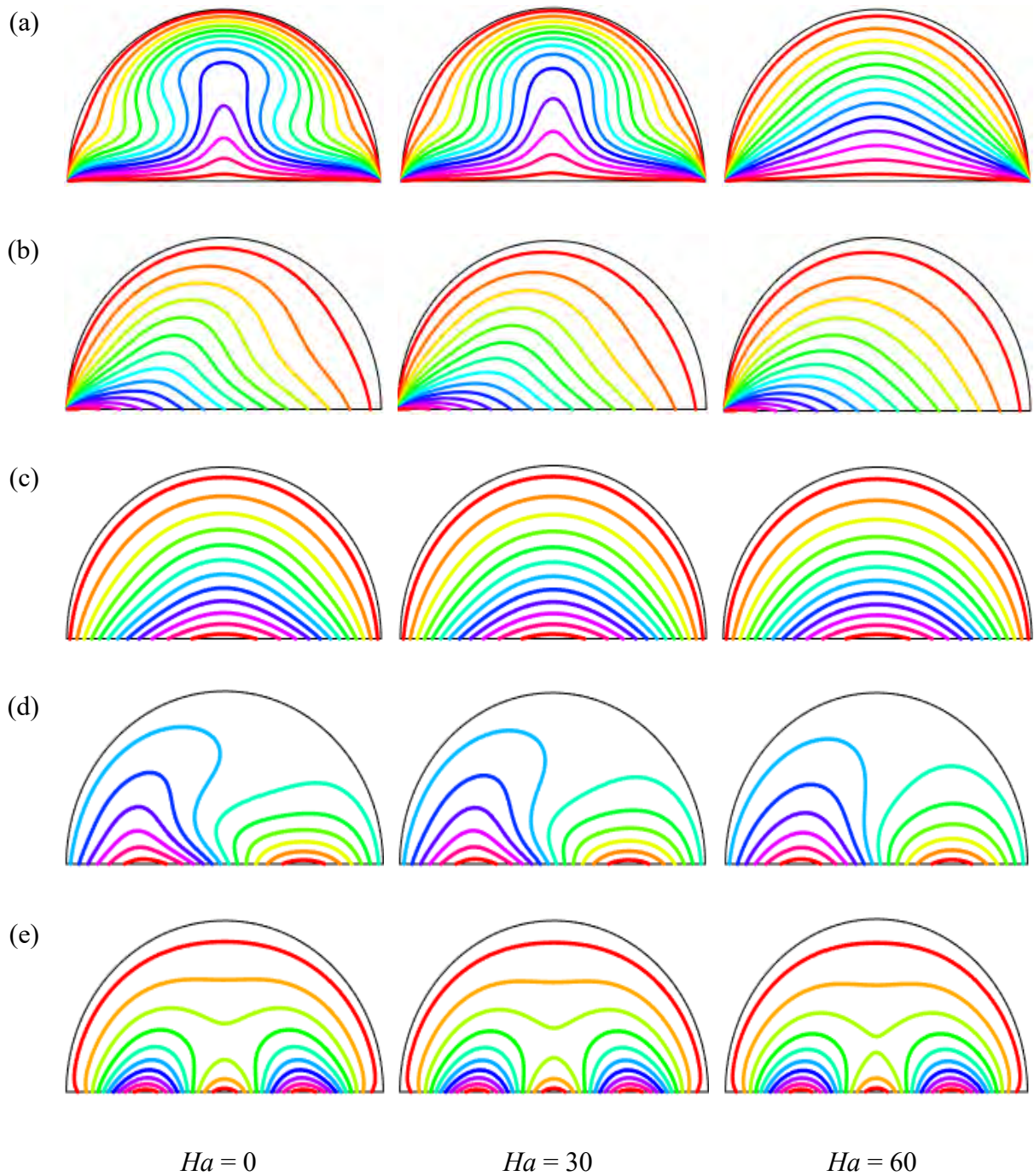
**Figure 5.20:** Variation of average Nusselt number ( $Nu_{av}$ ) along bottom heated diameter with uniform thermal boundary conditions (case I) for different volume fraction of nanoparticles ( $\phi$ ) and Rayleigh number ( $Ra$ ) for Cu-H<sub>2</sub>O nanofluid when  $Pr = 6.8377$ ,  $Ha = 20$ ,  $d = 10\text{nm}$ ,  $n = 3$ , and  $\tau = 1$ .

(case I). These figures show that the pattern of the isothermal lines is almost similar to the uniform magnetic field and low period of the non-uniform magnetic field ( $\tau = 0.1$ , and  $\lambda = 0.25$ ). These figures also show that isothermal lines are distorted near the heated wall for the absence of the Hartmann number. But, for a higher magnetic field ( $Ha = 60$ ), the isothermal lines become almost parallel to the hot bottom wall, which indicates the dominance of conduction near the hot wall. This pattern of streamlines also indicates Hartmann number ( $Ha$ ) doesn't influence the flow field greatly but also retards the thermal field within the cavity. The same results is seen for both  $\tau = 0.1$  and  $\tau = 1$ . In addition, the upper Hartmann number ( $Ha$ ) is acting against convection within the enclosure. Moreover, the period of the magnetic field has a significant impact on fluid flow. The pattern of the isothermal lines changes with the changes of the period of the magnetic field.

The magnetic field can create an encountered physical environment that can affect many processes such as biomedical and physical and chemical processes. The utilization of magnetic fields is useful in various applications such as heat exchangers, nuclear fusion, and material processes and

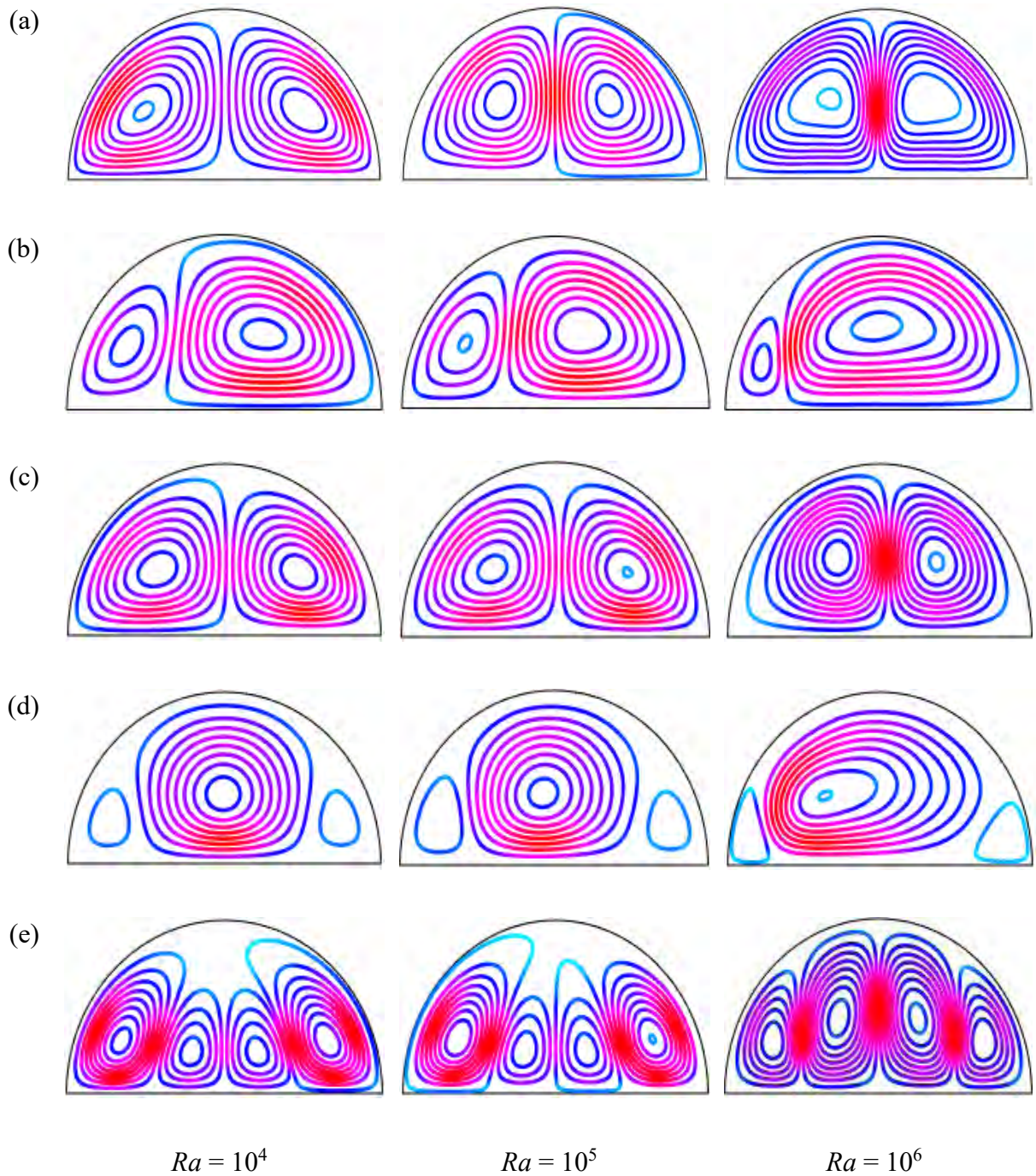


**Figure 5.21:** Streamlines of Hartmann number ( $Ha$ ) for different thermal boundary conditions (a)  $\theta = 1$  (case I), (b)  $\theta = 1 - X$  (case II), (c)  $\theta = X(1 - X)$  (case III), (d)  $\theta = A \sin(2\pi X)$  (case IV) and (e)  $\theta = A \sin^2(2\pi X)$  (case V) for Cu-H<sub>2</sub>O nanofluid when  $Ra = 10^5$ ,  $\phi = 0.04$ ,  $d = 10\text{nm}$ ,  $\lambda = 0.5$ ,  $n = 3$ , and  $\tau = 1$ .

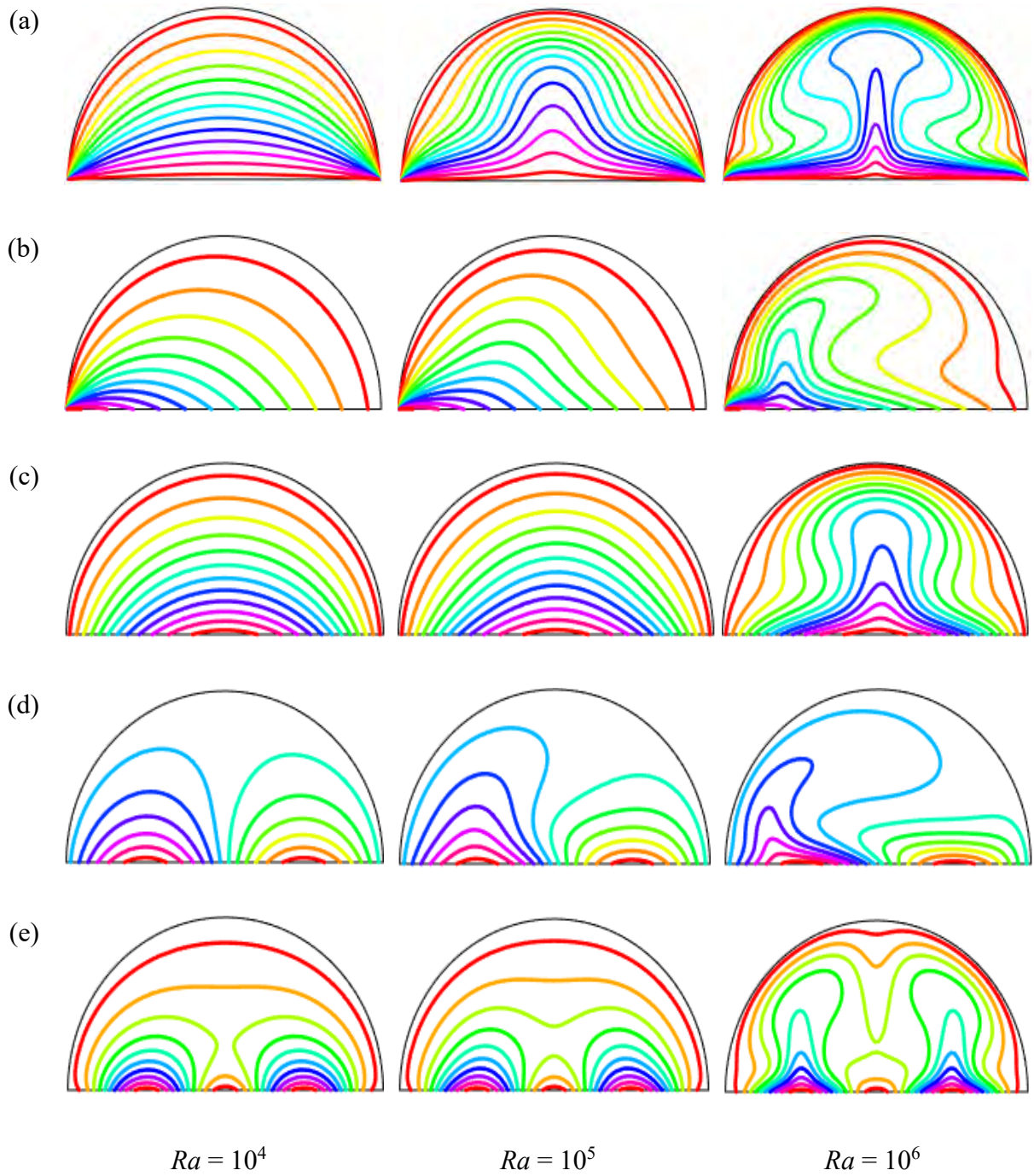


**Figure 5.22:** Isotherms of Hartmann number ( $Ha$ ) for different thermal boundary conditions (a)  $\theta = 1$  (case I), (b)  $\theta = 1 - X$  (case II), (c)  $\theta = X(1 - X)$  (case III), (d)  $\theta = A \sin(2\pi X)$  (case IV) and (e)  $\theta = A \sin^2(2\pi X)$  (case V) for Cu-H<sub>2</sub>O nanofluid when  $Ra = 10^5$ ,  $\phi = 0.04$ ,  $d = 10\text{nm}$ ,  $\lambda = 0.5$ ,  $n = 3$ , and  $\tau = 1$ .



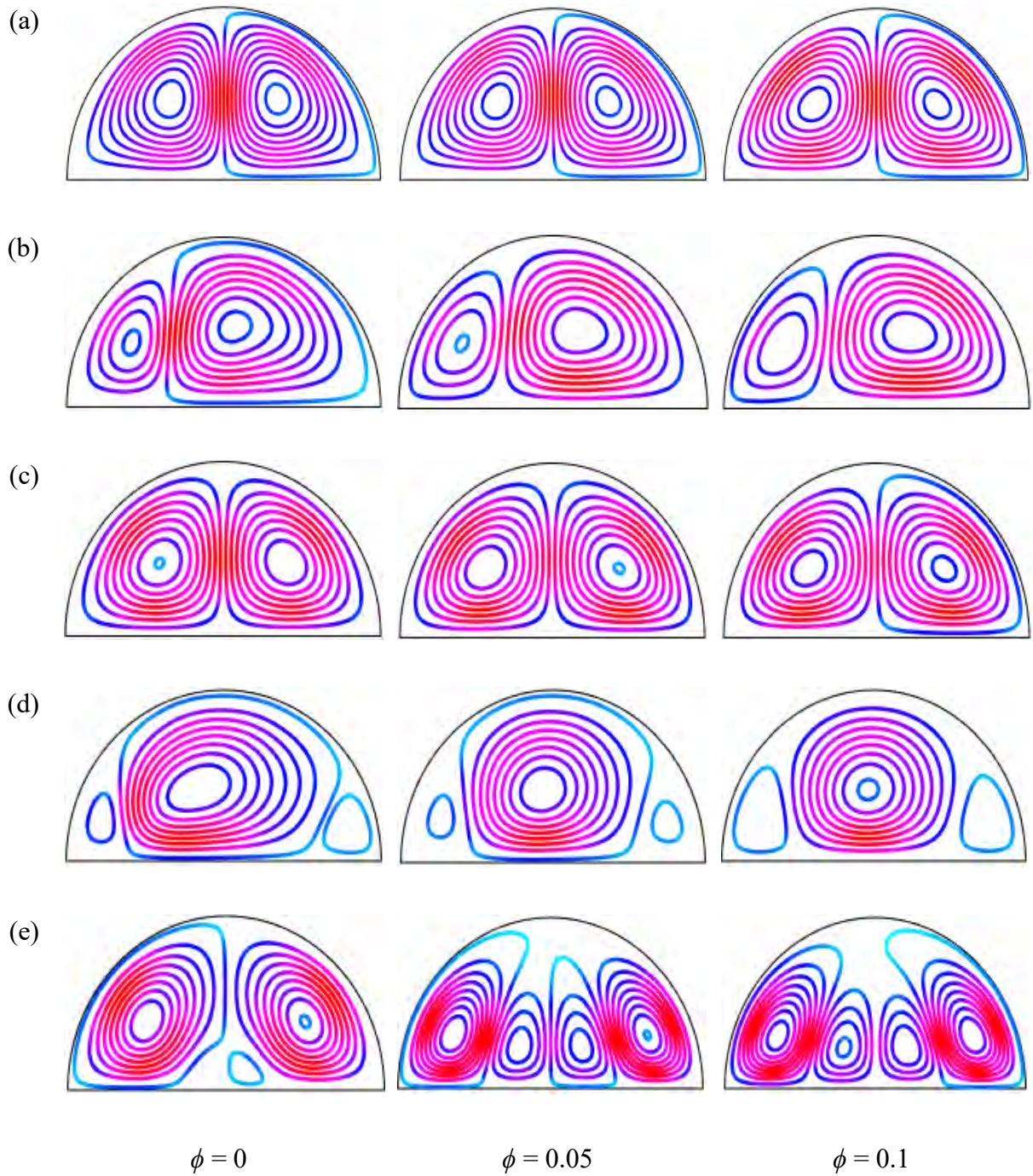


**Figure 5.23:** Streamlines of Rayleigh number ( $Ra$ ) for different thermal boundary conditions (a)  $\theta = 1$  (case I), (b)  $\theta = 1 - X$  (case II), (c)  $\theta = X(1 - X)$  (case III), (d)  $\theta = A \sin(2\pi X)$  (case IV) and (e)  $\theta = A \sin^2(2\pi X)$  (case V) for Cu-H<sub>2</sub>O nanofluid when  $Ha = 20$ ,  $\phi = 0.04$ ,  $d = 10\text{nm}$ ,  $\lambda = 0.5$ ,  $n = 3$ , and  $\tau = 1$ .

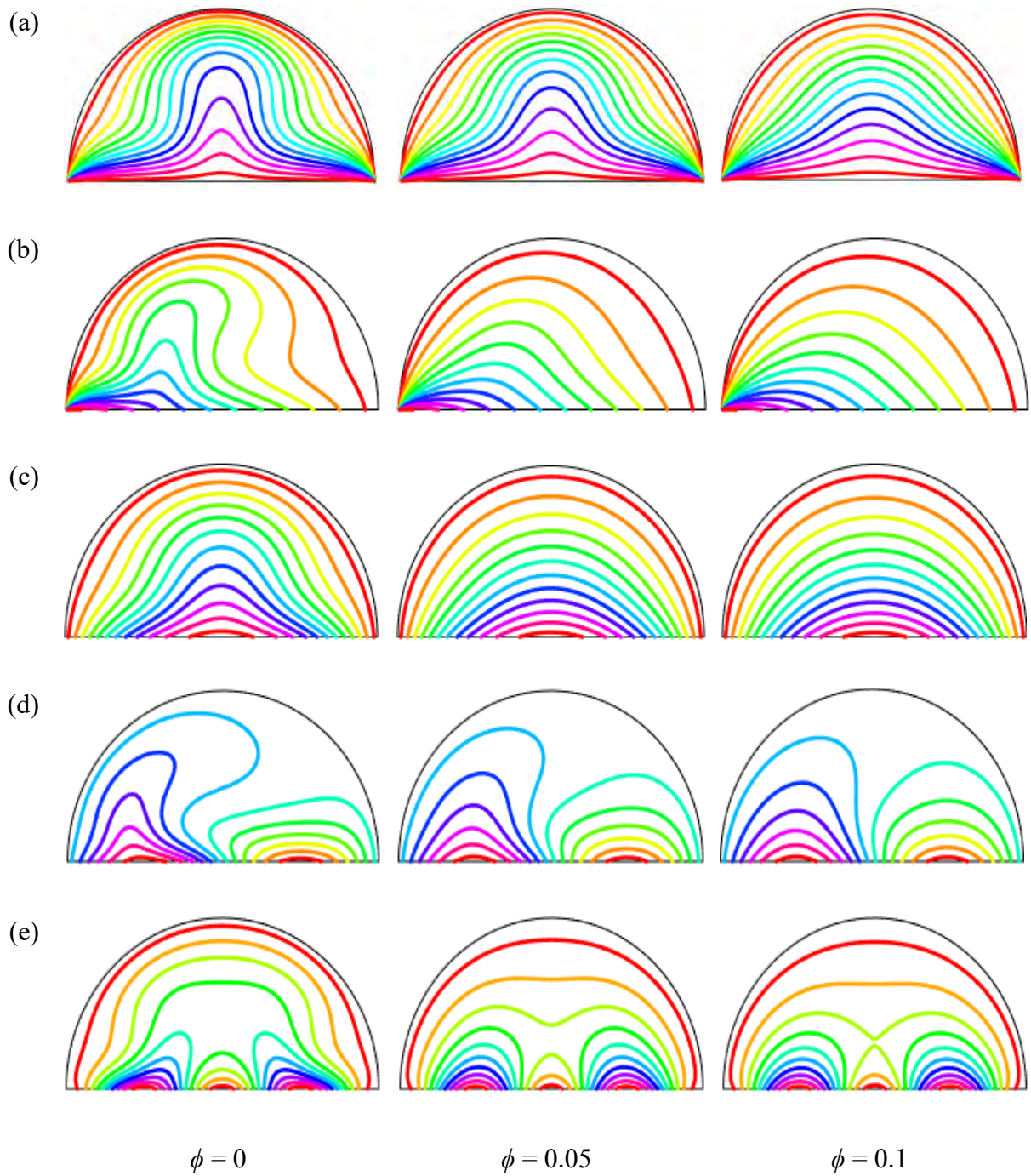


**Figure 5.24:** Isothermal lines of Rayleigh number ( $Ra$ ) for different thermal boundary conditions (a)  $\theta = 1$  (case I), (b)  $\theta = 1 - X$  (case II), (c)  $\theta = X(1 - X)$  (case III), (d)  $\theta = A \sin(2\pi X)$  (case IV) and (e)  $\theta = A \sin^2(2\pi X)$  (case V) for Cu-H<sub>2</sub>O nanofluid when  $Ha = 20$ ,  $\phi = 0.04$ ,  $d = 10\text{nm}$ ,  $\lambda = 0.5$ ,  $n = 3$ , and  $\tau = 1$ .





**Figure 5.25:** Streamlines of volume fraction of nanoparticles ( $\phi$ ) for different thermal boundary conditions (a)  $\theta = 1$  (case I), (b)  $\theta = 1 - X$  (case II), (c)  $\theta = X(1 - X)$  (case III), (d)  $\theta = A \sin(2\pi X)$  (case IV) and (e)  $\theta = A \sin^2(2\pi X)$  (case V) for Cu-H<sub>2</sub>O nanofluid when  $Ha = 20$ ,  $Ra = 10^5$ ,  $d = 10\text{nm}$ ,  $\lambda = 0.5$ ,  $n = 3$ , and  $\tau = 1$ .



**Figure 5.26:** Isothermal lines of nanoparticles volume fraction ( $\phi$ ) for different thermal boundary conditions (a)  $\theta = 1$  (case I), (b)  $\theta = 1 - X$  (case II), (c)  $\theta = X(1 - X)$  (case III), (d)  $\theta = A \sin(2\pi X)$  (case IV), and (e)  $\theta = A \sin^2(2\pi X)$  (case V) for Cu-H<sub>2</sub>O nanofluid when  $Ha = 20$ ,  $Ra = 10^5$ ,  $d = 10\text{nm}$ ,  $\lambda = 0.5$ ,  $n = 3$ , and  $\tau = 1$ .

**Table 5.1:** Variation of average Nusselt number ( $Nu_{av}$ ) along the bottom heated wall for Cu-H<sub>2</sub>O nanofluid for different Hartmann number ( $Ha$ ), nanoparticles diameter ( $d$ ), Rayleigh number ( $Ra$ ) and various thermal boundary conditions (TBC) when  $Pr = 6.8377$ ,  $n = 3$ ,  $\phi = 0.04$ ,  $\lambda = 0.5$ ,  $\tau = 1$ .

$d$ (nm)	$Ra$	TBC	$Nu_{av}$		
			$Ha = 0$	$Ha = 20$	$Ha = 80$
1	$10^4$	Case I	26.735620	26.533969	26.321813
		Case II	26.316998	26.038055	25.995851
		Case III	12.445351	12.444106	12.442448
		Case IV	26.458461	26.450799	26.444934
		Case V	24.843669	24.844373	24.848833
	$10^5$	Case I	27.569811	27.031434	26.602989
		Case II	27.497849	26.820867	25.195980
		Case III	12.500378	12.475436	12.449568
		Case IV	27.573583	27.015809	26.480938
		Case V	24.805832	24.797458	24.810186
	$10^6$	Case I	41.341946	39.948276	31.461278
		Case II	40.948269	39.542278	30.864262
		Case III	13.558934	13.196353	12.560202
		Case IV	36.963122	35.545491	29.342248
		Case V	28.444317	28.246075	26.078284
100	$10^4$	Case I	8.9956430	8.9896616	8.9829505
		Case II	8.4080995	8.1927510	8.0746080
		Case III	4.1899856	4.1884376	4.1865657
		Case IV	8.9374947	8.9153160	8.8979401
		Case V	8.3525719	8.3530166	8.3568939
	$10^5$	Case I	11.227772	10.687181	8.9432328
		Case II	10.481393	10.034730	8.1978385
		Case III	4.2769227	4.2364848	4.1946683
		Case IV	10.455805	9.9613924	9.0028997
		Case V	8.6897666	8.4827650	8.3329648
	$10^6$	Case I	16.841502	16.332445	13.281637
		Case II	14.620243	13.930468	12.680369
		Case III	5.0697260	4.9168818	4.3567629
		Case IV	14.810344	14.423448	12.270400
		Case V	11.803568	11.649541	10.549503

scientific research in various disciplines. The period of the magnetic field is essential in protein crystallization, silver deposition and water evaporation, and so on. A periodic force field can be generated by the periodic magnetic field that is available in the above applications (see Liu *et al.* [56]). Therefore the present study has a real-life application and great importance in industrial and engineering processes. Figure 5.10 shows the average Nusselt number for uniform magnetic field (umf), different periods of the magnetic field ( $\lambda$ ), and different Hartmann numbers ( $Ha$ ) for

**Table 5.2:** Variation of average Nusselt number ( $Nu_{av}$ ) along bottom heated wall with uniform thermal boundary condition (case I) for different types of nanofluids and various nanoparticles volume fractions ( $\phi$ ) when  $Ra = 10^5$ ,  $Ha = 20$ ,  $d = 10\text{nm}$ ,  $n = 3$ ,  $Pr = 6.8377$ ,  $\lambda = 0.5$ , and  $\tau = 1$ .

Nanofluids	$\phi$						
	I	II	$\left(\frac{\text{II-I}}{\text{I}}\right)_{\times}$	III	$\left(\frac{\text{III-I}}{\text{I}}\right)_{\times}$	IV	$\left(\frac{\text{IV-I}}{\text{I}}\right)_{\times}$
	0	0.01	100	0.05	100	0.1	100
<b>Cu-water</b>	8.402384	10.263187	22.15	16.069668	91.25	23.050162	174.33
<b>Co-water</b>	8.402384	10.400057	23.78	17.094337	103.45	24.412083	190.54
<b>Fe<sub>3</sub>O<sub>4</sub>-water</b>	8.402384	10.344816	23.12	17.119632	103.75	34.305417	308.28
<b>Ag-water</b>	8.402384	9.7957100	16.58	14.577452	73.49	19.514939	132.25
<b>Zn-water</b>	8.402384	9.9306699	18.19	15.129334	80.06	20.611965	145.31
<b>CuO-water</b>	8.402384	10.203048	21.43	16.902929	89.27	22.816969	171.55
<b>Al<sub>2</sub>O<sub>3</sub>-water</b>	8.402384	10.021290	19.27	15.403518	83.32	21.326972	153.82
<b>TiO<sub>2</sub>-water</b>	8.402384	9.9392978	18.29	15.051253	79.13	20.571352	144.84
<b>Cu-kerosene</b>	8.455359	13.770578	62.86	32.387029	283.04	54.620733	545.99
<b>Co-kerosene</b>	8.455359	14.192830	67.86	34.469768	307.67	58.615475	593.23
<b>Fe<sub>3</sub>O<sub>4</sub>-kerosene</b>	8.455359	13.807837	63.30	32.608736	285.66	55.038774	550.93
<b>Ag-kerosene</b>	8.455359	12.351421	46.08	25.610078	202.89	41.365016	389.22
<b>Zn-kerosene</b>	8.455359	12.779320	51.14	27.656223	227.07	45.529568	438.47
<b>CuO-kerosene</b>	8.455359	13.626599	61.16	31.766445	275.69	53.518254	532.95
<b>Al<sub>2</sub>O<sub>3</sub>-kerosene</b>	8.455359	13.135148	55.35	29.443429	248.22	49.161689	481.43
<b>TiO<sub>2</sub>-kerosene</b>	8.455359	12.958484	53.26	28.575965	237.96	47.463114	461.34
<b>Cu-EO</b>	8.4066401	8.8606325	5.400	10.548415	25.48	12.404102	47.55
<b>Co-EO</b>	8.4066401	8.8837036	5.680	10.654252	26.74	12.593793	49.81
<b>Fe<sub>3</sub>O<sub>4</sub>-EO</b>	8.4066401	8.8692171	5.500	10.628576	26.43	12.649463	50.46
<b>Ag-EO</b>	8.4066401	8.7905904	4.570	10.221352	21.59	11.811605	40.50
<b>Zn-EO</b>	8.4066401	8.7963227	4.640	10.255262	21.99	11.879283	41.31
<b>CuO-EO</b>	8.4066401	8.8385385	5.140	10.447394	24.28	12.221756	45.38
<b>Al<sub>2</sub>O<sub>3</sub>-EO</b>	8.4066401	8.7954644	4.630	10.238918	21.79	11.826526	40.68
<b>TiO<sub>2</sub>-EO</b>	8.4066401	8.7798311	4.440	10.164708	20.93	11.683716	38.98
<b>Cu-EG</b>	8.5305867	11.677559	36.89	21.899593	156.72	33.637918	294.32
<b>Co-EG</b>	8.5305867	11.924073	39.78	22.946893	168.99	35.758524	319.18
<b>Fe<sub>3</sub>O<sub>4</sub>-EG</b>	8.5305867	11.717981	37.36	22.146809	159.62	33.962013	298.12
<b>Ag-EG</b>	8.5305867	10.846328	27.15	18.446205	116.24	26.642682	212.32
<b>Zn-EG</b>	8.5305867	11.099846	30.12	19.469056	128.23	28.792146	237.52
<b>CuO-EG</b>	8.5305867	11.596755	35.94	21.531137	152.40	33.019156	287.07
<b>Al<sub>2</sub>O<sub>3</sub>-EG</b>	8.5305867	11.309295	32.57	20.278709	137.72	30.630816	259.07
<b>TiO<sub>2</sub>-EG</b>	8.5305867	11.197402	31.26	19.807656	132.20	29.640146	247.46

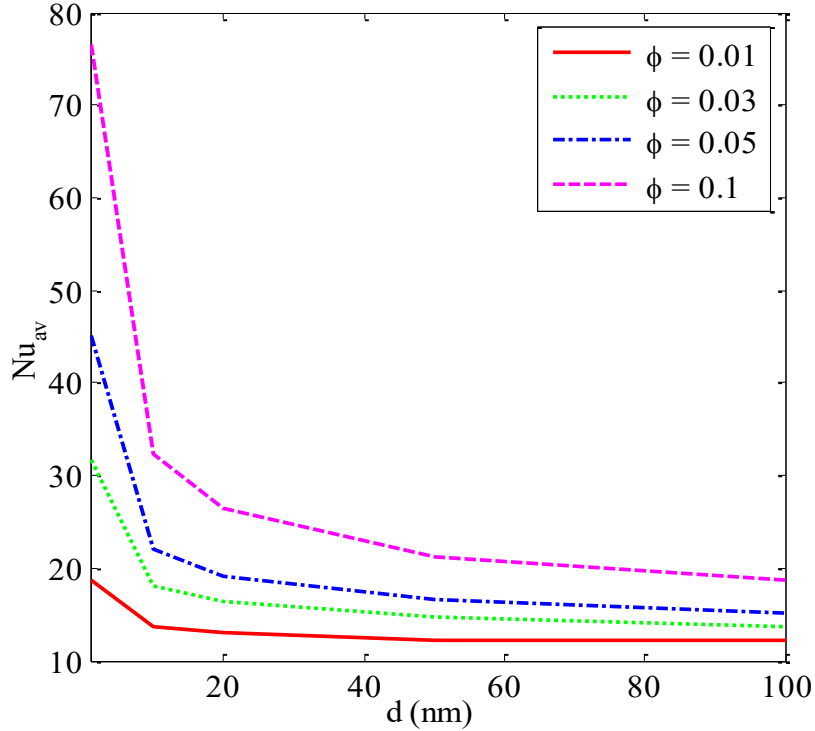
**Table 5.3:** Variation of average Nusselt number ( $Nu_{av}$ ) along heated bottom wall with uniform thermal boundary condition (case I) for different types of nanofluids and different Rayleigh numbers ( $Ra$ ) when  $\phi = 0.04$ ,  $Ha = 20$ ,  $d = 10\text{nm}$ ,  $n = 3$ ,  $\lambda = 0.5$ ,  $Pr = 6.8377$ , and  $\tau = 1$ .

Nanofluids	$Ra$		
	$10^4$	$10^5$	$10^6$
<b>Cu-water</b>	14.9104135	16.5296085	25.8359240
<b>Co-water</b>	15.5645575	17.0943371	26.7371876
<b>Fe<sub>3</sub>O<sub>4</sub>-water</b>	14.9596750	17.1196325	26.7535232
<b>Ag-water</b>	12.6912367	14.5774518	22.6628323
<b>Zn-water</b>	13.3825949	15.1293339	23.6313926
<b>CuO-water</b>	14.7154622	16.2329297	25.4391526
<b>Al<sub>2</sub>O<sub>3</sub>-water</b>	13.9693041	15.4035365	24.2005334
<b>TiO<sub>2</sub>-water</b>	13.5598410	15.0512530	23.6256620
<b>Cu-kerosene</b>	31.7154622	32.2329297	50.4391526
<b>Co-kerosene</b>	33.1183157	34.4697680	54.3365800
<b>Fe<sub>3</sub>O<sub>4</sub>-kerosene</b>	32.1914530	32.6087360	51.7909820
<b>Ag-kerosene</b>	24.8273820	25.6100781	39.4423434
<b>Zn-kerosene</b>	27.0892509	27.6562239	42.2730677
<b>CuO-kerosene</b>	31.3935577	31.7664459	47.7013210
<b>Al<sub>2</sub>O<sub>3</sub>-kerosene</b>	29.0665476	29.4434294	44.5025943
<b>TiO<sub>2</sub>-kerosene</b>	28.1593782	28.5759653	43.3677162
<b>Cu-EO</b>	8.34670334	10.5484155	16.2250263
<b>Co-EO</b>	8.44053160	10.6542520	16.3909001
<b>Fe<sub>3</sub>O<sub>4</sub>-EO</b>	8.35170214	10.6285765	16.3889366
<b>Ag-EO</b>	8.02434577	10.2213522	15.6870139
<b>Zn-EO</b>	8.12281991	10.2552620	15.8006460
<b>CuO-EO</b>	8.31565160	10.4473940	16.1202371
<b>Al<sub>2</sub>O<sub>3</sub>-EO</b>	8.20409472	10.2389182	15.8544392
<b>TiO<sub>2</sub>-EO</b>	8.12743570	10.1647083	15.7293393
<b>Cu-EG</b>	17.8770205	19.5295651	30.1697084
<b>Co-EG</b>	18.8159922	20.3701252	31.4754410
<b>Fe<sub>3</sub>O<sub>4</sub>-EG</b>	17.9692443	19.7281023	30.5170322
<b>Ag-EG</b>	14.7429474	16.7214212	25.7295481
<b>Zn-EG</b>	15.7325082	17.5570993	27.1005514
<b>CuO-EG</b>	17.6234431	19.2259332	29.7357075
<b>Al<sub>2</sub>O<sub>3</sub>-EG</b>	16.5933401	18.2110114	28.1901951
<b>TiO<sub>2</sub>-EG</b>	16.1631393	17.8319963	27.5900572



**Table 5.4:** Variation of average Nusselt number ( $Nu_{av}$ ) along heated bottom wall with uniform thermal boundary condition (case I) for different types of nanofluids and different Hartmann number ( $Ha$ ) when  $Ra = 10^5$ ,  $\phi = 0.04$ ,  $d = 10\text{nm}$ ,  $\lambda = 0.5$ ,  $n = 3$ ,  $Pr = 6.8377$ , and  $\tau = 1$ .

Nanofluids	<i>Ha</i>			
	0	20	50	80
<b>Cu-water</b>	17.693123	16.529600	14.936598	14.793671
<b>Co-water</b>	18.296096	17.094327	15.574041	15.443921
<b>Fe<sub>3</sub>O<sub>4</sub>-water</b>	18.455686	17.119632	15.029785	14.829507
<b>Ag-water</b>	15.536950	14.577451	12.809825	12.597344
<b>Zn-water</b>	16.248933	15.129333	13.432741	13.272168
<b>CuO-water</b>	17.476592	16.232929	14.716061	14.593912
<b>Al<sub>2</sub>O<sub>3</sub>-water</b>	16.686158	15.403518	13.955531	13.847116
<b>TiO<sub>2</sub>-water</b>	16.291406	15.051253	13.557010	13.440994
<b>Cu-kerosene</b>	33.266666	32.297697	31.769252	31.717056
<b>Co-kerosene</b>	35.351002	34.469760	34.000371	33.952072
<b>Fe<sub>3</sub>O<sub>4</sub>-kerosene</b>	33.818808	32.608730	32.063871	32.015211
<b>Ag-kerosene</b>	26.779776	25.610078	24.757675	24.681131
<b>Zn-kerosene</b>	28.862959	27.656223	26.990049	26.932365
<b>CuO-kerosene</b>	32.805350	31.766445	31.274587	31.228569
<b>Al<sub>2</sub>O<sub>3</sub>-kerosene</b>	30.627878	29.443429	28.946077	28.903089
<b>TiO<sub>2</sub>-kerosene</b>	29.794087	28.575965	28.043098	27.997792
<b>Cu-EO</b>	11.149469	10.548415	8.9776040	8.3407736
<b>Co-EO</b>	11.263561	10.654252	9.0669918	8.4326658
<b>Fe<sub>3</sub>O<sub>4</sub>-EO</b>	11.307574	10.628576	8.8213253	8.3348023
<b>Ag-EO</b>	10.766204	10.221352	8.7206203	8.0392124
<b>Zn-EO</b>	10.877029	10.255262	8.7057789	8.1064897
<b>CuO-EO</b>	11.105957	10.447394	8.8580616	8.2889464
<b>Al<sub>2</sub>O<sub>3</sub>-EO</b>	10.952889	10.238918	8.6513402	8.1601264
<b>TiO<sub>2</sub>-EO</b>	10.862812	10.164708	8.5930784	8.0870213
<b>Cu-EG</b>	20.598116	19.529565	17.948428	17.742257
<b>Co-EG</b>	21.471119	20.370101	18.863343	18.676018
<b>Fe<sub>3</sub>O<sub>4</sub>-EG</b>	20.924648	19.728076	18.026468	17.820832
<b>Ag-EG</b>	17.606820	16.721421	14.951914	14.637620
<b>Zn-EG</b>	18.572573	17.557078	15.849179	15.606386
<b>CuO-EG</b>	20.350352	19.225908	17.670533	17.483153
<b>Al<sub>2</sub>O<sub>3</sub>-EG</b>	19.353733	18.210990	16.635867	16.452624
<b>TiO<sub>2</sub>-EG</b>	18.944988	17.831975	16.220664	16.025650



**Figure 5.27:** Variation of average Nusselt number ( $Nu_{av}$ ) along bottom heated diameter for different nanoparticles volume fraction ( $\phi$ ) and different nanoparticles diameter ( $d$ ) for Cu-H<sub>2</sub>O nanofluid and uniform thermal boundary condition (case I) when  $Pr = 6.8377$ ,  $Ra = 10^5$ ,  $Ha = 20$ ,  $n = 3$ ,  $\lambda = 0.5$  and  $\tau = 1$ .

Cu-H<sub>2</sub>O nanofluid when  $Pr = 6.8377$ ,  $Ra = 10^5$ , and  $d = 10$  nm of uniform thermal boundary condition (case I). This figure shows average Nusselt number decreases with the increase of Hartmann ( $Ha$ ). This is because the Lorentz forces are increased by the higher Hartmann number ( $Ha = 60$ ), which produces a stronger resistance against the movement of the fluid. This reduces the thermal efficiency of the nanofluid on fluid flow and heat transfer rate. In addition, the period of the magnetic field plays a significant role in heat transport. It is noticed that a higher average rate of heat transfer is observed for the non-uniform magnetic effect when  $\lambda = 0.75$ . Moreover, it is interesting to observe that a higherrate of heat transfer is noticed for non-uniform magnetic than uniform magnetic effect. It also observed that non-uniform magnetic field conform better heat transfer rate.

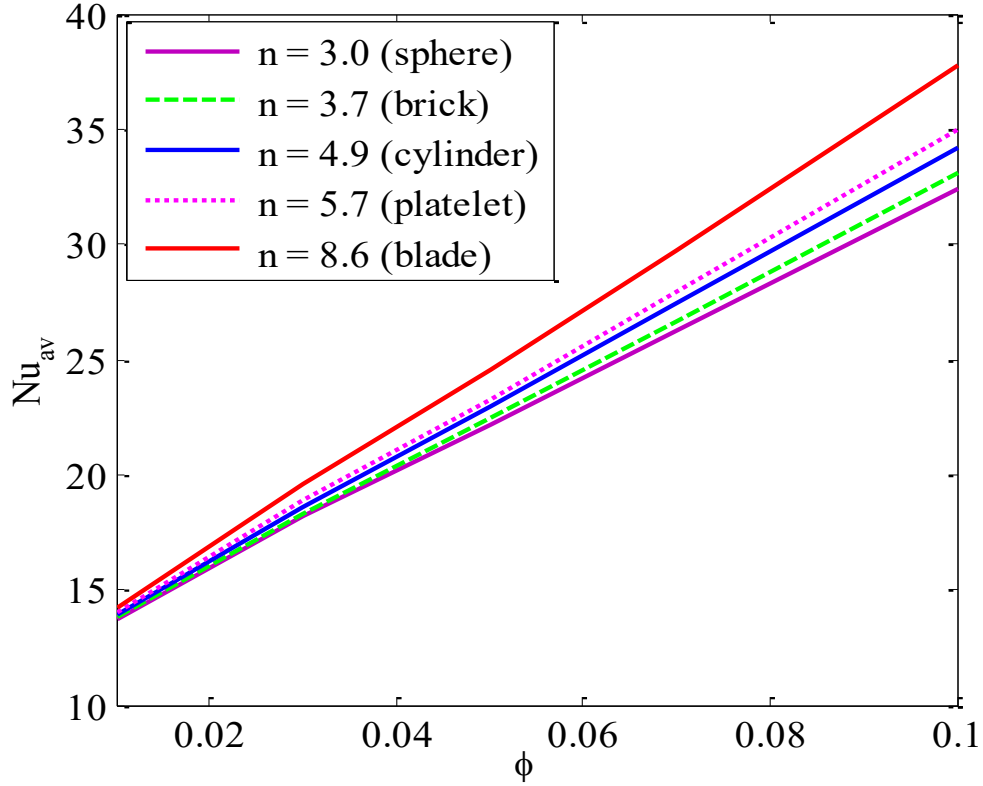
### 5.3 Effects of Rayleigh number

Figures 5.11-5.12 represent the effects of Rayleigh number ( $10^4 \leq Ra \leq 10^6$ ) on stramline contours

**Table 5.5:** Variation of average Nusselt number ( $Nu_{av}$ ) along bottom heated diameter for uniform thermal boundary condition (case I) for different types of nanofluids and different diameter of the nanoparticles ( $d$ ) when  $Ra = 10^5$ ,  $Ha = 20$ ,  $\phi = 0.04$ ,  $n = 3$ ,  $\lambda = 0.5$ , and  $\tau = 1$ .

Nanofluids	$d$						
	I	II	$\left(\frac{II-I}{I}\right)_{\times}$	III	$\left(\frac{III-I}{I}\right)_{\times}$	IV	$\left(\frac{IV-I}{I}\right)_{\times}$
	100 nm	50 nm	100	10 nm	100	1 nm	100
<b>Cu-water</b>	11.374081	12.293785	8.09	16.067946	41.27	31.700810	178.71
<b>Co-water</b>	11.892822	12.923205	8.66	17.094337	43.74	33.913170	185.16
<b>Fe<sub>3</sub>O<sub>4</sub>-water</b>	12.124072	13.120787	8.22	17.119632	41.20	32.340930	166.75
<b>Ag-water</b>	11.064490	11.759104	6.28	14.577451	31.75	25.226838	127.99
<b>Zn-water</b>	11.219880	11.993539	6.89	15.129333	34.84	27.247795	142.85
<b>CuO-water</b>	11.555746	12.480817	8.01	16.232929	40.47	31.269894	170.60
<b>Al<sub>2</sub>O<sub>3</sub>-water</b>	11.192075	12.022886	7.42	15.403518	37.63	28.957446	158.73
<b>TiO<sub>2</sub>-water</b>	10.987155	11.789976	7.31	15.051233	36.99	28.003602	154.87
<b>Cu-kerosene</b>	16.829764	19.698041	17.04	32.297697	91.91	85.138798	405.88
<b>Co-kerosene</b>	17.482286	20.608585	17.88	34.469768	97.17	92.213498	427.47
<b>Fe<sub>3</sub>O<sub>4</sub>-kerosene</b>	16.959534	19.860681	17.11	32.608736	92.27	86.126672	407.84
<b>Ag-kerosene</b>	14.783386	16.863877	14.07	25.610078	73.24	62.899239	325.47
<b>Zn-kerosene</b>	15.139935	17.671560	16.72	27.656223	82.67	70.021696	362.50
<b>CuO-kerosene</b>	16.561243	19.369649	16.95	31.766445	91.81	83.626453	404.95
<b>Al<sub>2</sub>O<sub>3</sub>-kerosene</b>	15.744905	18.279662	16.09	29.443429	87.00	76.261717	384.36
<b>TiO<sub>2</sub>-kerosene</b>	15.470431	17.906611	15.74	28.575965	84.71	73.482936	374.99
<b>Cu-EO</b>	9.771048	9.9213682	1.54	10.548415	7.96	12.903850	32.06
<b>Co-EO</b>	9.809805	9.9732187	1.67	10.654252	8.61	13.205494	34.61
<b>Fe<sub>3</sub>O<sub>4</sub>-EO</b>	9.839912	9.9924364	1.55	10.628576	8.015	13.016555	32.28
<b>Ag-EO</b>	9.664331	9.7717662	1.11	10.221352	5.76	11.926964	23.41
<b>Zn-EO</b>	9.633943	9.7538855	1.24	10.255262	6.45	12.151068	26.13
<b>CuO-EO</b>	9.694547	9.8401058	1.50	10.447394	7.77	12.730484	31.32
<b>Al<sub>2</sub>O<sub>3</sub>-EO</b>	9.565905	9.6959265	1.36	10.238918	7.04	12.287067	28.45
<b>TiO<sub>2</sub>-EO</b>	9.516902	9.6420182	1.31	10.164708	6.81	12.138114	27.54
<b>Cu-EG</b>	12.734776	14.092028	10.65	19.529565	53.36	41.595134	226.63
<b>Co-EG</b>	13.023973	14.489321	11.25	20.370101	56.40	44.526973	241.88
<b>Fe<sub>3</sub>O<sub>4</sub>-EG</b>	12.846311	14.224145	10.73	19.728076	53.57	41.923369	226.35
<b>Ag-EG</b>	11.755328	12.746742	8.43	16.721406	42.25	31.969885	171.96
<b>Zn-EG</b>	12.028086	13.132563	9.18	17.557078	45.97	34.960677	190.66
<b>CuO-EG</b>	12.600263	13.922171	10.49	19.225908	52.58	40.797270	223.78
<b>Al<sub>2</sub>O<sub>3</sub>-EG</b>	12.211485	13.407593	9.79	18.210990	49.13	37.587770	207.81
<b>TiO<sub>2</sub>-EG</b>	12.048968	13.202729	9.58	17.831975	47.99	36.363911	201.80





**Figure 5.28:** Variation of average Nusselt number ( $Nu_{av}$ ) along bottom heated diameter for uniform thermal boundary condition (case I) for different shape of nanoparticles ( $n$ ) and different volume fraction of nanoparticles ( $\phi$ ) for Cu-H<sub>2</sub>O nanofluid when  $Pr = 6.8377$ ,  $Ra = 10^5$ ,  $Ha = 20$ ,  $d = 10$  nm,  $n = 3$ ,  $\lambda = 0.5$ , and  $\tau = 1$ .

for (a) uniform magnetic field, (b)  $\lambda = 0.1$ , (c)  $\lambda = 0.25$ , (d)  $\lambda = 0.5$ , and (e)  $\lambda = 1$  for Cu-H<sub>2</sub>O nanofluid for uniform thermal boundary condition (case I) for both unsteady state ( $\tau = 0.1$ ) and steady-state ( $\tau = 1$ ), respectively when  $\phi = 0.04$ ,  $Pr = 6.8377$ ,  $Ha = 20$ ,  $d = 10$  nm, and  $n = 3$ . This result indicate that for all Rayleigh number ( $Ra$ ), the buoyancy driven rotating flows in the cavity are evident. At non-dimensional time  $\tau = 0.1$ , for almost all values of  $Ra$ , there are two symmetrical rotating cells are observed within the enclosure. The thermal boundary condition (case I) is the result of this particular pattern. The physical meaning of that the fluid adjacent to the bottom heated diameter tries to upward due to the influence of the buoyancy force after getting heated by the bottom heated wall while relatively cold water near circular wall goes towards bottom wall. Consequently, a pattern of symmetric type flow is created. For small Rayleigh numbers,  $Ra = 10^4$ , two symmetrical circulation cells of low strength are seen inside the cavity for dominant characteristics of the flow field. As the Rayleigh number increases ( $Ra > 10^4$ ), the streamlines pattern changes, and streamlines intensify, which indicates a higher velocity gradient and strength

**Table 5.6:** Variation of average Nusselt number ( $Nu_{av}$ ) along bottom heated wall with uniform thermal boundary condition (case I) for different types of nanofluids and the different shape of the nanoparticles ( $n$ ) when  $Ra = 10^5$ ,  $Ha = 20$ ,  $d = 10$  nm,  $\phi = 0.04$ ,  $\lambda = 0.5$ , and  $\tau = 1$ .

Nanofluids	$n$	$Nu_{av}$	Nanofluids	$n$	$Nu_{av}$	Nanofluids	$n$	$Nu_{av}$
Cu-water	3.0	15.6587679	Fe <sub>3</sub> O <sub>4</sub> - kerosene	3.0	32.6087368	Zn-EO	3.0	10.2552624
	3.7	15.8626473		3.7	32.8274118		3.7	10.4828489
	4.9	16.2123474		4.9	33.2013429		4.9	10.8686052
	5.7	16.4456403		5.7	33.4499621		5.7	11.1228225
	8.6	17.2925376		8.6	34.3466335		8.6	12.0260305
Co-water	3.0	17.0943371	Ag-kerosene	3.0	25.6100781	CuO-EO	3.0	10.4473942
	3.7	17.2897478		3.7	25.8227712		3.7	10.6725311
	4.9	17.6205761		4.9	26.1879836		4.9	11.0537461
	5.7	17.8383168		5.7	26.4318673		5.7	11.3047028
	8.6	18.6099691		8.6	27.3185554		8.6	12.1946035
Fe <sub>3</sub> O <sub>4</sub> -water	3.0	17.1196325	Zn- kerosene	3.0	27.6562239	Al <sub>2</sub> O <sub>3</sub> -EO	3.0	10.2389188
	3.7	17.3165693		3.7	27.8718440		3.7	10.4591691
	4.9	17.6482358		4.9	28.2412268		4.9	10.8308573
	5.7	17.8653298		5.7	28.4872900		5.7	11.0746934
	8.6	18.6270471		8.6	29.3778019		8.6	11.9340212
Ag-water	3.0	14.5774518	CuO- kerosene	3.0	31.7664459	TiO <sub>2</sub> -EO	3.0	10.1647086
	3.7	14.7841775		3.7	31.9807668		3.7	10.3671364
	4.9	15.1362467		4.9	32.3448739		4.9	10.7010030
	5.7	15.3694240		5.7	32.5853157		5.7	10.9148970
	8.6	16.2054526		8.6	33.4417648		8.6	11.6378645
Zn-water	3.0	15.1293339	Al <sub>2</sub> O <sub>3</sub> - kerosene	3.0	29.4434294	Cu-EG	3.0	19.5295651
	3.7	15.3280606		3.7	29.6591921		3.7	19.6905431
	4.9	15.6643412		4.9	30.0268301		4.9	19.9661242
	5.7	15.8855703		5.7	30.2703506		5.7	20.1496048
	8.6	16.6690970		8.6	31.1425999		8.6	20.8134273
CuO-water	3.0	16.2329297	TiO <sub>2</sub> - kerosene	3.0	28.5759653	Co-EG	3.0	20.3701017
	3.7	16.4257718		3.7	28.7723486		3.7	20.5290171
	4.9	16.7509750		4.9	29.0989551		4.9	20.8002102
	5.7	16.9641468		5.7	29.3099257		5.7	20.9801680
	8.6	17.7141652		8.6	30.0325270		8.6	21.6272073
Al <sub>2</sub> O <sub>3</sub> -water	3.0	15.4035182	Cu-EO	3.0	10.5484155	Fe <sub>3</sub> O <sub>4</sub> -EG	3.0	19.7280763
	3.7	15.5866186		3.7	10.7780180		3.7	19.8862791
	4.9	15.8912363		4.9	11.1679505		4.9	20.1557298
	5.7	16.0881365		5.7	11.4254386		5.7	20.3341689
	8.6	16.7639699		8.6	12.3435653		8.6	20.9734100
TiO <sub>2</sub> -water	3.0	15.0512339	Co-EO	3.0	10.6542525	Ag-EG	3.0	16.7214068
	3.7	15.1800793		3.7	10.8817923		3.7	16.8850889
	4.9	15.3772423		4.9	11.2674530		4.9	17.1647271
	5.7	15.4944854		5.7	11.5215887		5.7	17.3505151
	8.6	15.8461468		8.6	12.4243068		8.6	18.0201508
Cu-kerosene	3.0	32.3870295	Fe <sub>3</sub> O <sub>4</sub> -EO	3.0	10.6285765	Zn-EG	3.0	17.5570786
	3.7	32.6081395		3.7	10.8570452		3.7	17.7173019
	4.9	32.9873480		4.9	11.2439600		4.9	17.9904341
	5.7	33.2402567		5.7	11.4987002		5.7	18.1714839
	8.6	34.1576150		8.6	12.4021104		8.6	18.8212840
Co-kerosene	3.0	34.4697680	Ag-EO	3.0	10.2213522	Al <sub>2</sub> O <sub>3</sub> -EG	3.0	18.2109904
	3.7	34.6906080		3.7	10.4533527		3.7	18.3657367
	4.9	35.0684144		4.9	10.8472467		4.9	18.6277210
	5.7	35.3197336		5.7	11.1072737		5.7	18.8001321
	8.6	36.2269896		8.6	12.0339458		8.6	19.4108226

**Table 5.7:** Average Nusselt number ( $Nu_{av}$ ) along heated bottom diameter with uniform thermal boundary condition (case I) for different values of nanoparticles volume fraction ( $\phi$ ) and various Rayleigh number ( $Ra$ ) for “without Brownian motion” and “with Brownian motion” effects for Cu-H<sub>2</sub>O nanofluid when  $Ha = 20$ ,  $d = 10\text{nm}$ ,  $Pr = 6.8377$ ,  $n = 3$ ,  $\lambda = 0.5$ , and  $\tau = 1$ .

<b>Ra</b>	<b>Brownian motion</b>	$\phi$	$Nu_{av}$	<b>Increases ( % )</b>
$10^4$	with Brownian effect	0.0	6.24446694	-
		0.01	8.04799441	28.88
		0.02	9.81717724	21.98
		0.03	11.55077724	17.66
		0.04	13.24851224	14.70
		0.05	14.91041358	12.54
		0.1	22.68984437	52.17
	without Brownian effect	0.0	6.244466939	-
		0.01	6.432585544	3.01
		0.02	6.624485635	2.98
		0.03	6.820315721	2.96
		0.04	7.020220648	2.93
		0.05	7.224343783	2.91
		0.1	8.313354169	15.07
$10^5$	with Brownian effect	0.0	8.402384526	-
		0.01	10.26318709	22.17
		0.02	11.98018405	16.73
		0.03	13.58141107	13.37
		0.04	15.09063038	11.11
		0.05	16.52960849	9.54
		0.1	23.28572849	40.87
	without Brownian effect	0.0	8.40238452	-
		0.01	8.58660888	2.19
		0.02	8.76915197	2.13
		0.03	8.95033200	2.07
		0.04	9.13038558	2.01
		0.05	9.30949129	1.96
		0.1	10.1949592	9.51
$10^6$	with Brownian effect	0.0	12.82182771	-
		0.01	15.77739612	23.05
		0.02	18.53156787	17.46
		0.03	21.11366101	13.93
		0.04	23.54348518	11.51
		0.05	25.83592437	9.74
		0.1	35.59362548	37.77
	without Brownian effect	0.0	12.82182770	-
		0.01	13.09967538	2.17
		0.02	13.37793643	2.12
		0.03	13.65669173	2.08
		0.04	13.93598379	2.05
		0.05	14.21583432	2.01
		0.1	15.62411402	9.91

in the natural convection. The isothermal lines condense near the heated bottom wall and circular cooled wall representing a higher temperature gradient. At a higher Rayleigh number ( $Ra = 10^6$ ), the streamlines circulation is more pronounced. At higher Rayleigh number,  $Ra = 10^6$ , and  $\lambda = 0.5$ , more vortices are observed inside the enclosure which indicates more heat transport. Furthermore, the streamlines pattern changes with the changes of the period of the non-uniform magnetic field. The pattern of the flow remains almost the same for both  $\tau = 0.1$ , and  $\tau = 1$ , which indicates the nanofluid within the enclosure stabilizes rapidly and reaches the steady state within a shorter time.

Figures 5.13-5.14 represent the effects of Rayleigh number ( $10^4 \leq Ra \leq 10^6$ ) on isothermal lines for (a) uniform magnetic field, (b)  $\lambda = 0.1$ , (c)  $\lambda = 0.25$ , (d)  $\lambda = 0.5$ , and (e)  $\lambda = 1$  for Cu-H<sub>2</sub>O nanofluid with uniform thermal boundary condition (case I) for both unsteady state ( $\tau = 0.1$ ) and steady state ( $\tau = 1$ ), respectively when  $Pr = 6.8377$ ,  $Ha = 20$ ,  $\phi = 0.04$ ,  $d = 10\text{nm}$ , and  $n = 3$ . At the low Rayleigh number ( $Ra = 10^4$ ), the pattern of the isothermal lines is almost parallel to each other to the heat source wall due to the weaker convection inside the cavity. The isothermal lines form a cavity-like arc near the top circular cold wall, and isotherms are almost parallel to each other neighbor warmed diameter. Therefore, conduction is the significant mood of heat transfer for the lower buoyancy-driven parameter. The strength of the fluid currents enhances with the increases of Rayleigh number ( $Ra$ ) due to the influence of buoyant forces, which increase the convective force. For the increases of the buoyancy driven parameter named Rayleigh number ( $Ra$ ), the isothermal lines are more and more distorted at the middle of the heated wall, indicating convection is beginning to take over and become a dominant mode of heat transport within the enclosure. At the higher Rayleigh number ( $Ra = 10^6$ ), the streamlines form a particular pattern like a mushroom. This particular pattern of the streamlines indicates that the heat energy flows into the nanofluid within the enclosure from the heated bottom wall. For the case  $\tau = 1$ , the isothermal lines are more dispersed within the enclosure than  $\tau = 0.1$ , which represents the diffusion of heat is slower compared to matter within nanofluid.

Figure 5.15 illustrates the average Nusselt number along warmed bottom diameter with uniform thermal boundary condition (case I) for the different volume fractions of nanoparticles ( $\phi$ ) and Rayleigh number ( $Ra$ ) for Cu-H<sub>2</sub>O nanofluid when  $Pr = 6.8377$ ,  $Ha = 20$ ,  $d = 10\text{ nm}$ ,  $n = 3$ , and  $\tau = 1$ . This figure depicts that average Nusselt number is significantly higher for a higher value of nanoparticles volume fraction and upper value of Rayleigh number ( $Ra$ ). The heat transfer rate

increases monotonically with the increase of nanoparticle volume fraction. The heat transfer rate is more pronounced and increases rapidly for a higher Rayleigh number. In addition, the augmentation heat transport rate is more significant with additional amount of nanoparticles than base fluid. This is due to the fact that additional nanoparticles enhances thermal conductivity of nanofluid.

#### 5.4 Effects of nanoparticles volume fraction

Figures 5.16-5.17 represent the impact of streamlines for different nanoparticles volume fraction for Cu-H<sub>2</sub>O nanofluid for uniform thermal boundary condition (case I) when  $Pr = 6.8377$ ,  $Ha = 20$ ,  $d = 10$  nm,  $Ra = 10^5$ , and  $n = 3$  for both non-dimensional time  $\tau = 0.1$  and  $\tau = 1$ , respectively. At the non-dimensional time,  $\tau = 0.1$ , it is observed that there are two opposite circulation cells within the cavity for both uniform magnetic field and non-uniform magnetic field with different periods. Thermal boundary heating condition is the causes for the pattern of this streamlines. The nanofluids near the bottom wall become warmed by the heated bottom wall and move upwards while the bottom relatively cold nanofluid near-circular wall approaches the bottom wall, which helps to create a symmetrical flow pattern. This pattern remains the same for the categorical of nanoparticles volume fraction ( $\phi$ ). For base fluid ( $\phi = 0$ ), it is observed from the figure (left column of 5.16 and 5.17) that two rotating cells are not stronger enough except period  $\lambda = 0.5$  because streamline contours are not greatly influenced with water molecules inside the enclosure.

An interesting observation is that the addition of nanoparticles into the base fluid decreases the value of stream function for a particular period of the magnetic field. The cause behind this phenomenon is that the addition of nanoparticles enhances the total mass of the fluid within the cavity, which increases the inertia force of the fluid. The flow of the fluid becomes to slow down slightly for this higher inertia. Another point is that additional nanoparticles increase viscosity and particle-particle interactions are not significant in this solution inside the enclosure. Moreover, the streamlines pattern changes a little bit by the increases in the volume of nanoparticles. The pattern of streamlines is almost similar for both uniform magnetic fields (case (a)) and low periods ( $\lambda = 0.1$ ) of the magnetic field (case (b)). The flow pattern changes with the increases of the magnetic field period, while an interesting pattern of the streamlines is seen for the period of the magnetic field,  $\lambda = 0.5$ . At  $\lambda = 0.5$  (row (d) of figures 5.16 and 5.17), the small vortices are expanded and

become stronger within the cavity with the increase of the volume of nanoparticles. The flow becomes stabilized very soon and reaches a steady state quickly because the flow pattern remains almost the same for both  $\tau = 0.1$  and  $\tau = 1$ . In addition, an expanded and slightly stable distribution of streamlines are observed near the cold circular wall with the increases of nanoparticles volume.

The effects of isothermal lines for different volume fraction of the nanoparticles ( $\phi$ ) is presented in figures 5.18-5.19, respectively with  $\tau = 0.1$ , and  $\tau = 1$  for Cu-H<sub>2</sub>O nanofluid for uniform thermal boundary condition (case I) when  $Pr = 6.8377$ ,  $Ha = 20$ ,  $d = 10$  nm,  $Ra = 10^5$ ,  $\lambda = 0.5$  and  $n = 3$ . This figure shows that the isothermal lines are more compressed near the near the end corner of the bottom warmed diameter. The closely packing of the isotherms indicate that conduction is the major type of heat transport. The density of the isothermal lines is lower in the middle of the bottom warmed diameter, which indicates a higher heat transport region. The fluid particles adjacent to the middle of the heated wall move upward after getting warmed indicating convective heat transport in that region. The isothermal lines pattern changes and is more noticeable at the middle of the enclosure with the addition of the nanoparticles. In addition, the addition of nanoparticles into the base fluid has a stimulating effect on heat diffusion. The pattern of the isothermal lines changes with the changes of the period of the magnetic field. An interesting pattern of the isothermal lines is observed with the period of the magnetic field with the period,  $\lambda = 0.5$ .

Figure 5.20 shows average Nusselt number for different volume fraction of nanoparticles ( $\phi$ ) and Rayleigh number ( $Ra$ ) for Cu-H<sub>2</sub>O nanofluid for uniform thermal boundary condition (case I) when  $Pr = 6.8377$ ,  $Ha = 20$ ,  $d = 10$  nm,  $\lambda = 0.5$ ,  $n = 3$ , and  $\tau = 1$ . This figure shows that the average Nusselt number decreases with the increase of nanoparticle volume fractions and the Rayleigh number. The physical meaning of that as nanoparticles volume fraction increases, the thermal conductivity of the nanofluid increases. This figure also depicts that the rate of heat transfer is strongly affected by the addition of nanoparticles. Table 5.2 shows that the rate of heat transport increases for all types of mentioned nanofluids. The rate of heat transport increases by almost 22.15% for Cu-H<sub>2</sub>O nanofluid, 16.58% for Ag-water nanofluid with 1% volume of nanoparticles, whereas it increases only 5.4% for Cu-engine oil nanofluid for uniform thermal boundary condition (case I). Therefore, it can be declared that convection is dominant for higher nanoparticles volume fraction and Rayleigh number.



## 5.5 Effects of different thermal boundary conditions

Figures 5.21-5.26 show the numerical outcomes of natural convective temperature transport inside the semi-circular shaped enclosure with various thermal boundary conditions (case I:  $\theta = 1$  (uniformly heated), case II:  $\theta = 1 - X$  (linearly heated), case III:  $\theta = X(1 - X)$  (parabolically heated), case IV:  $\theta = A \sin(2\pi X)$  (sinusoidally heated), and case V:  $\theta = A \sin^2(2\pi X)$  (sinusoidally heated)). The characteristics of controlling parameters such as Rayleigh number ( $Ra$ ), Hartmann number ( $Ha$ ), and nanoparticles volume fraction ( $\phi$ ), and nanoparticles diameter ( $d$ ) are investigated on the physical phenomenon of the flow field and heat transport. For numerical simulation regarding streamlines and isothermal lines, Cu-H<sub>2</sub>O nanofluid is considered as default nanofluid and different nanoparticles, and base fluid are also engaged to investigate heat transport performance. Figure 5.21-5.22 displays the effects of streamlines and isothermal lines respectively for different Hartmann numbers ( $Ha$ ) for Cu-H<sub>2</sub>O nanofluid with  $Ra = 10^5$ ,  $\phi = 0.04$ ,  $d = 10\text{nm}$ ,  $\lambda = 0.5$ ,  $n = 3$ , and  $\tau = 1$  when the bottom diameter is heated uniformly (case I), linearly (case II) and non-uniformly (case III, IV, V). The fluid near the bottom diameter is hotter compared to the circular wall. So, the fluid near the bottom wall has a lower density compared to the fluid near-circular wall. Consequently, the fluid near the middle of the bottom wall moves upward while relatively heavy fluid near the circular wall moves downward along the circular wall. As a result, the fluid loss energy moves downward and eventually forces the separation of the thermal boundary layer along the circular wall.

In Figure 5.21, for uniformly thermal boundary condition (case I), two counter-clockwise central circulation cells are observed within the enclosure. The eye of rotations is situated near the center of each half of the cross-section of the enclosure. But for non-uniform thermal boundary conditions (case V), four counter-clockwise rotating vortices are observed. Also, two symmetrical rotating circulation cells are also observed for the absence of magnetic force ( $Ha = 0$ ). But, for applying magnetic force introduced by Hartmann number ( $Ha = 60$ ), it is seen that the movement of the fluid become slower within the enclosure compared to the case of Hartmann number ( $Ha = 0$ ) because the magnetic field has a trend to make slowdown the motion of the fluid. The symmetry also changes for the increase of Hartmann number for case III and case V because the magnetic field suppresses the circulation of the flow within the enclosure. A large rotating cell is seen for a higher magnetic field in case II and case IV.

The isothermal contours of Hartmann number ( $Ha$ ) for various thermal boundary conditions are presented in Fig. 5.22 for Cu-H<sub>2</sub>O nanofluid when  $Ra = 10^5$ ,  $\phi = 0.04$ ,  $d = 10\text{nm}$ ,  $\lambda = 0.5$ ,  $n = 3$ , and  $\tau = 1$ . These figures show that the isothermal lines are clustered with the heated bottom diameter, indicating the existence of a temperature gradient along the vertical direction of this region. It is also observed that the temperature gradient is weak at the center of the cavity. At higher Hartmann numbers ( $Ha = 60$ ), the isothermal lines are almost parallel to each other in case I, case IV, and case V. The isothermal lines are densely distributed at the left corner inside the cavity in case II. In contrast, isotherms are densely distributed at both the bottom corner of the enclosure for case I and case III. In case I, the isothermal lines are formed a mushroom shape at the middle of the cavity for low Hartmann Number. For the consideration of Lorentz forces, i.e., an increase of Hartmann number, the isothermal lines start to move away from the hot bottom wall, indicating temperature gradient decreases within the enclosure.

Figures 5.23-5.24 represent the impact of streamlines and isothermal lines, respectively for different Rayleigh number ( $Ra$ ) with various thermal boundary conditions for Cu-H<sub>2</sub>O nanofluid when  $Ha = 20$ ,  $\phi = 0.04$ ,  $d = 10\text{nm}$ ,  $\lambda = 0.5$ ,  $n = 3$ , and  $\tau = 1$ . For uniform thermal boundary conditions (case I) and non-uniform thermal boundary conditions (case III), two counter symmetrical circulation cells are observed inside the cavity, and the eye of the rotation is located near the center of each cross-section of the cavity. But the symmetry is distorted with the increase of Rayleigh number. As the Rayleigh number increases ( $Ra = 10^6$ ), the convection is more pronounced than conduction. A large central circulation cell with two small tubes at the corner of the bottom wall is observed at the center of the cavity for the sinusoidal thermal boundary condition (case IV). The density of the streamlines enhances within the enclosure with the increase of Rayleigh number ( $Ra$ ) due to the convection mode of heat transfer dominates in those regions. There are four symmetric circulating cells for non-uniform thermal boundary conditions (case V). Two larger cells at the middle of the enclosure are observed for a higher Rayleigh number ( $Ra = 10^6$ ) in case V. Besides these two primary cells, two secondary cells are formed at the corner of the heated bottom wall.

To detect the effectiveness of temperature transfer, isothermal lines are useful. The isothermal lines also help us to detect the mode of temperature transport, whether it is conduction or convection. Figure 5.24 shows that isothermal lines are more compressed near the heated bottom

diameter. These compressed isothermal lines tell us that the principal mode of heat transport is conduction at those regions. At the middle of the cavity, the density of the isothermal lines is less, which represents relatively weaker convective heat transfer. Figure 5.24(a) represents uniform heating at the bottom wall causes a finite discontinuity in Dirichlet type of boundary conditions for the distribution of the temperature at both edges of the bottom wall. For non-uniform heating (case IV and case V), the singularity is removed at the edges of the bottom wall. The isothermal lines are quite dispersed throughout the cavity for a relatively higher Rayleigh number. For sinusoidal thermal boundary conditions, the dispersion of isothermal lines increases within the enclosure. Figure 5.24(a) shows that isothermal lines are distributed uniformly, representing conduction as the principal mode of heat transport. For the higher Rayleigh number ( $Ra$ ), the isothermal lines are more distorted due to the more substantial effects of convection. At  $Ra = 10^6$ , case I and case III, the isothermal lines form like a mushroom shape at the middle of the cavity, indicating convection is dominant at that region. Therefore, a higher value of Rayleigh number ( $Ra$ ) improves the convection heat transfer characteristics.

Figures 5.25-5.26 depict the impact of streamline contours and isotherms, respectively for different nanoparticles volume fraction ( $\phi$ ) with various thermal boundary conditions for Cu-H<sub>2</sub>O nanofluid when  $Ha = 20$ ,  $Ra = 10^5$ ,  $d = 10\text{nm}$ ,  $\lambda = 0.5$ ,  $n = 3$ , and  $\tau = 1$ . These figures show that both of the streamline contours and isothermal lines are affected significantly with the increases of nanoparticles volume fraction in all thermal boundary conditions (case I, II, III, IV and V). The pattern of the streamline contours is almost similar for the thermal system cases I and III. A central large rotating vortex with two small eddies is observed for sinusoidal thermal boundary conditions (case IV). The streamline contours are expanded, and the little eddies become stronger within the cavity with the increase of the volume of nanoparticles. This figure shows that three symmetrical parallel distributions of the family of curves of isothermal lines from bottom diameter for the entire range of nanoparticles volume in case V. The thickness of the isothermal lines increases with the increment of nanoparticles volume fraction.

To determine the rate of heat transfer along the bottom heated wall, the average Nusselt number is calculated varying diameter of nanoparticles ( $d$ ), Rayleigh number ( $Ra$ ), and Hartmann number ( $Ha$ ) regarding uniform thermal boundary condition (case I), linear thermal boundary condition (case II), non-uniform thermal boundary condition (case III, IV, and V). Table 5.1 represents the

average Nusselt number on the heated bottom wall with various thermal boundary conditions (case I, II, III, IV, and V) for Cu-H<sub>2</sub>O nanofluid when  $Pr = 6.8377$ ,  $n = 3$ ,  $\phi = 0.04$ , and  $\tau = 1$ . This table shows that the average Nusselt number decreases with the increase of the Hartmann number ( $Ha$ ). It is seen that heat transport rate decreases 23.90% for uniform thermal boundary conditions when  $Ha$  varies 0 to 80 with  $Ra = 10^6$ ,  $\phi = 0.04$ ,  $n = 3$ ,  $d = 1\text{nm}$  in steady state case. Therefore, the rate of heat transfer is reduced by the stronger magnetic field. It is also seen that heat transport rate increase 54.63% without magnetic effect when  $Ra$  varies  $10^4$  to  $10^6$  whereas it increases 19.53% with magnetic effect ( $Ha = 80$ ) for uniform thermal condition (case I). This Table also shows that the heat transport is intensified for copper-water nanofluid by decreasing the size of nanoparticles. The rate of heat transport decreases 23.90% with  $d = 1\text{nm}$ , whereas it decreases 21.14% with  $d = 100\text{nm}$  when  $Ha$  varies 0 to 80 for uniform thermal boundary condition (case I) and Cu-H<sub>2</sub>O nanofluid. Another important point is that the heat transport is more pronounced in higher buoyancy driven parameter Rayleigh number ( $Ra$ ). This table shows that heat transport rate decrease 1.55% with  $Ra = 10^4$ , whereas it decreases 21.14% with  $Ra = 10^6$  when  $Ha$  varies 0 to 80 with  $d = 1\text{nm}$  and uniform thermal system (case I). In addition, it is interesting to observe that height heat transmission is achieved when the bottom wall is heated uniformly. The temperature transport rate increases 19.53% for case I, 18.73% for case II, 0.95% for case III, 10.56% for case IV and 4.95% for case V when  $Ra$  varies  $10^4$  to  $10^6$  when  $Ha = 80$ , and  $d = 1\text{nm}$ .

## 5.6 Average heat transfer rate for different nanofluids

The current study has been investigated the effects of governing physical parameters like as diameter of the nanoparticles ( $d$ ), the volume fraction of nanoparticles ( $\phi$ ), Hartmann number ( $Ha$ ), the different shape factor of nanoparticles ( $n$ ), Brownian motion of the nanoparticles, and Rayleigh number ( $Ra$ ) of different nanofluids on the temperature transport rate regarding Nusselt number along the heated bottom wall of the cavity. This goal is satisfied by Table 5.2-5.4. The results of the present problem are discussed for copper-water nanofluid. Also, various types of nanoparticles such as Cu, Co, Fe<sub>3</sub>O<sub>4</sub>, Al<sub>2</sub>O<sub>3</sub>, TiO<sub>2</sub>, Ag, Zn, and CuO and base fluid such as water (H<sub>2</sub>O), kerosene, ethylene glycol (EG), and engine oil (EO) are considered in this investigation to observe how the temperature transport rate and fluid flow depend on parameters as mentioned earlier.

Table 5.2 illustrates the average Nusselt number at the heated wall of the cavity for different types of nanofluids and various nanoparticles volume fractions for uniform thermal boundary condition

(case I) for steady state case ( $\tau = 1$ ) when  $Ra = 10^5$ ,  $Ha = 20$ ,  $\lambda = 0.5$ ,  $d = 10\text{nm}$ . It is seen that the temperature changes are significant despite nanoparticles providing 1% into the base fluid. The heat transfer rate increase 5.4% for engine oil-based nanofluid and 36.89% for ethylene glycol-based nanofluid with the increases of 1% nanoparticles volume fraction. For all thirty-two different types of nanofluids, the average Nusselt number increases with the increase of nanoparticle volume fraction. This is due to the higher thermal conductivity of nanoparticles. This is also a cause of the considering the effect of Brownian motion in the thermal conductivity equation. The table shows that highest heat transfer for kerosene-based nanofluids compared to water-based, ethylene-based, and engine oil-based nanofluids. It is observed that Co-kerosene and  $\text{Fe}_3\text{O}_4$ -kerosene nanofluids show a higher rate of heat transfer, although copper (Cu) nanoparticles have higher thermal conductivity compare to cobalt (Co) nanoparticles and magnetite ( $\text{Fe}_3\text{O}_4$ ) nanoparticles. This is due to the Brownian motion effect of the nano-sized particles of nanofluids that is considered in the thermal conductivity equation. The temperature transport rate increases 67.86% for Cobalt-kerosene nanofluid and 63.30% for magnetite-kerosene nanofluid, whereas it increases 62.86% for Copper-kerosene nanofluid. On the other hand, the lowest heat transfer is observed for engine oil-based nanofluids due to the lower thermal conductivity and higher dynamical viscosity of the based fluid. In addition, copper oxide nanoparticles based nanofluids show the most insufficient heat transfer than copper nanoparticles based nanofluids. The heat transfer rate increases 22.15% for Cu- $\text{H}_2\text{O}$  nanofluid whereas it increases 21.43% for  $\text{CuO-H}_2\text{O}$  nanofluid for 1% nanoparticles volume.

Table 5.3 depicts the heat transport rate regarding mean Nusselt number along the heated bottom diameter of the enclosure for different types of nanofluids and different Rayleigh numbers for uniform thermal boundary condition (case I) when  $Pr = 6.8377$ ,  $Ha = 20$ ,  $d = 10\text{ nm}$ ,  $Ra = 10^5$ ,  $\lambda = 0.5$ ,  $n = 3$ , and  $\tau = 1$ . This table shows that the average Nusselt number increases significantly with the increase of buoyancy-driven parameter Rayleigh number for all types of nanofluids. The rate of temperature transport increases 10.86% and 73.27% when the Rayleigh number increases  $10^4$  to  $10^5$  and  $10^4$  to  $10^6$ , respectively, for copper-water nanofluids. The Kerosene-based nanofluid shows a more significant impact on the augmentation of heat transfer rate. The rate of heat transport increases 59.04% for copper-kerosene nanofluids, 64.07% for cobalt-kerosene nanofluids, 60.88% for magnetite-kerosene nanofluids, 58.87% for Ag-kerosene nanofluids,

51.94% for CuO-kerosene nanofluids, and 54.01% for TiO<sub>2</sub>-kerosene nanofluids when Rayleigh number ( $Ra$ ) varies  $10^4$  to  $10^6$ .

Table 5.4 illustrates the average Nusselt number along the heated bottom diameter of the enclosure for different types of nanofluids and different values of Hartmann number for uniform thermal boundary conditions (case I) when  $Pr = 6.8377$ ,  $Ha = 20$ ,  $d = 10$  nm,  $Ra = 10^5$ ,  $\lambda = 0.5$ ,  $n = 3$  and  $\tau = 1$ . In a steady-state case ( $\tau = 1.0$ ), the average Nusselt number decreases with the increase of the Hartmann number. This is because the magnetic field suppresses the convective flows with increases in the magnetic field's intensity that slow down the heat transfer rate. The heat transfer rate decreases 16.38% for Cu-water nanofluid, 4.66% for Cu-kerosene nanofluid, 25.19% for Cu-engine oil nanofluid, and 13.86% for Cu-ethylene glycol nanofluid when Hartmann number varies 0 to 80. In addition, this table shows that the heat flux is higher at the heated bottom diameter when no magnetic field affects the flow. Therefore, the applied magnetic field can be used in controlling the flow as well as heat transfer.

## 5.7 Effects of nanoparticles diameter

Figure 5.27 shows the average Nusselt number for different nanoparticles volume fractions ( $\phi$ ) and different diameters of nanoparticles ( $d$ ) for Cu-H<sub>2</sub>O nanofluid with uniform thermal system (case I) when  $Pr = 6.8377$ ,  $Ra = 10^5$ ,  $\lambda = 0.5$ ,  $Ha = 20$ , and  $\tau = 1$ . This figure shows that the average Nusselt number is decreased with the increase in the diameter of the nanoparticles. The significant changes of the average Nusselt number happen for about 1-50nm size of nanoparticles. After that, it remains almost the same for 51-100nm size of nanoparticles within the solution. In addition, the average Nusselt number is significantly higher for the 1-10nm size of nanoparticles. It is noticed that the average Nusselt number is more pronounced and intensified for a higher volume fraction of nanoparticles. Moreover, an increasing trend of temperature transport rate is seen for the increases of the nanoparticles volume. Furthermore, the nanoparticles move the cold upper wall because of the temperature gradient between heated and cooled walls. These outcomes indicate that as the temperature gradient enhances, the diffusion of the nanoparticles also increases, which increases the heat transfer rate.

Table 5.5 depicts the average Nusselt number on the heated bottom wall of the enclosure for different types of nanofluids and different diameters of nanoparticles for uniform thermal



boundary condition (case I) for four different types of base fluids such as water (H<sub>2</sub>O), kerosene, ethylene glycol (EG) and engine oil (EO) with eight different types of nanoparticles such as Cu, Co, Fe<sub>3</sub>O<sub>4</sub>, Al<sub>2</sub>O<sub>3</sub>, TiO<sub>2</sub>, Ag, Zn, and CuO when  $Ra = 10^5$ ,  $Ha = 20$ ,  $d = 10$  nm,  $\lambda = 0.5$  and  $\tau = 1$ . This Table shows that the average rate of heat transfer decreases with the increase of the diameter of nanoparticles. Kerosene-based nanoparticles show significant augmentation in heat transfer rate. Engine oil-based nanofluids show a lower rate of heat transfer. This is because engine oil has higher dynamical viscosity, which suppresses the nanoparticle's Brownian motion. Therefore, kerosene-based nanofluids show a higher heat transfer rate compared to water-based nanofluids. In addition, by decreasing nanoparticles diameter, the specific area increases, which helps to enhance nanofluid thermal conductivity and consequently increases the average Nusselt number. This Table shows that the rate of heat transfer rate increases 97.17% in a kerosene-cobalt nanofluid when the nanoparticles diameter decreases from 100nm to 10nm. In contrast, it increases 8.61% for engine oil-based cobalt nanoparticles when the nanoparticles diameter decreases from 100nm to 10nm.

## 5.8 Effects of nanoparticles shape factor

The shape of the nanoparticles has an effective influence on temperature transport. It has been mentioned before that the different values of  $n$  indicate different shapes of the nanoparticles. The numerical values of  $n = 8.6, 5.7, 4.9, 3.7,$  and  $3.0$  represent the blade, platelet, cylinder, brick and sphere shape of nanoparticles. The spherical shape of nanoparticles is considered for the numerical outcomes of the present problem. Different shape of nanoparticles are also used in the current investigation for analyzing the shape effects on the heat transfer of nanofluid. Figure 5.28 represents the impact of average Nusselt number for different nanoparticle volume fractions and different shapes of nanoparticles such as spherical, brick, cylinder, platelet, and blade shape for copper-water nanofluid with uniform thermal boundary condition (case I). This figure depicts that the rate of heat transfer is significantly higher for the blade shape of nanoparticles than all other shapes of nanoparticles. This is because of the less sphericity of the blade shape of nanoparticles. The physical meaning of the higher total surface area of the blade-shaped solid-liquid crossing point is associated with the whole external area of the other-shaped nanoparticle-liquid edge for the same amount of volume of nanoparticles. In addition, the average Nusselt number is more apparent for the higher value of nanoparticle volume fraction. It is also mentioned that temperature

transport is more significant for the addition of nanoparticles in the base fluid.

Moreover, the average Nusselt number is higher for the blade shape of nanoparticles compared to all other shapes of nanoparticles such as spherical, brick, cylinder, and platelet. It is also clear from this figure that a classification of the performance of heat transport from higher performance to lesser performance with respect to the shape of nanoparticles is the blade, platelet, cylinder, brick, and spherical shape, respectively. Table 5.6 shows the impact of the shape of the nanoparticles for different types of nanofluid for uniform thermal boundary conditions (case I). For all types of nanofluids, the blade shape of nanoparticles shows a higher heat transfer rate than other shapes of nanoparticles. The cause of that blade shape of nanoparticles has higher surface factor 3.29 (1/nm) than bricks (0.19 (1/nm)), cylinders (0.58 (1/nm)), and platelets (2.22 (1/nm)) (see Timofeeva et al. [55]). The highest surface factor indicates the highest area of the surface that can be defined as the ratio of the surface and volume of the particle of a certain size and shape. It is further mentioned that the highest heat transfer rate can be obtained for the blade shape of nanoparticles irrespective of the materials of nanoparticles and base fluids. The rate of heat transport increases 10.43% blade shape of nanoparticles instead of the spherical shape of nanoparticles for Cu-H<sub>2</sub>O nanofluid with uniform thermal boundary conditions.

## 5.9 Effects of Brownian motion

The random movement of nano-sized particles in the fluid significantly influences nanofluid flow and heat transport. The effect of Brownian motion of nanoparticles has been considered in the thermal conductivity equation (3.15) for calculating all results concerning streamlines, isothermal lines and average heat transport rate. To examine the influence of Brownian motion on the temperature transport rate, the average Nusselt number along the heated bottom diameter is calculated for both including Brownian effects and neglecting Brownian effects of nanoparticles with various Rayleigh numbers ( $10^4 \leq Ra \leq 10^6$ ), and nanoparticles volume fraction ( $0 \leq \phi \leq 0.1$ ). A comparison study of the increment of the average Nusselt number is presented in Table 5.7 for different nanoparticles and Rayleigh numbers when Hartmann number,  $Ha = 20$ , the diameter of nanoparticles  $d = 10\text{nm}$ , and  $\tau = 1$  for the copper-water nanofluids. The outcome indicates Brownian effects of nanoparticles play an influential role in the augmentation of temperature transport rate. Due to the random movement of the nano-sized particles into the base fluid, the Brownian motion nanoparticles contribute to the transfer of more heat in the nanofluids, and it

enhances the micro-convection of the fluid around individual particles. The result shows that at low Rayleigh number, the impact of nanoparticles volume fraction on average Nusselt number is more effective for both cases without and with Brownian motion of the nanoparticles. In addition, for higher nanoparticles volume fraction ( $\phi = 0.01$ ), the average Nusselt number at the heated wall is increased by 28.88% 1% nanoparticles volume at low Rayleigh number ( $Ra = 10^4$ ) when Brownian motion of the nanoparticles is considered into account and by 3.01% when Brownian motion of the nanoparticles is neglected. It is also mentioned that the Brownian motion of nanoparticles is more effective in enhancing temperature transport rate (heat transport rate increases 28.88% with 1% nanoparticles volume for  $Ra = 10^4$  and 23.05% for  $Ra = 10^6$ ) in lower Rayleigh number compared to higher Rayleigh number. .

# CHAPTER SIX

## Conclusions and Recommendations

### 6.1 Summary of the Major Outcomes

In this thesis, the primary purpose of the numerical investigation is to perform the influence of non-uniform vertically periodic magnetic field on time-dependent, two-dimensional, laminar, viscous, incompressible convection flow and heat transport enhancement considering nanoparticles Brownian motion for various nanofluids inside a semi-circular cavity. Natural convection has been considered due to the difference of the density resulting from the difference of temperature between the heated bottom diameter and cold circular wall. The upper circular wall has been cooled at low temperature, while the horizontal diameter is heated at high temperature. The function of the non-uniform magnetic fields has been considered as the sine function of  $x$ . However, both uniform magnetic fields and non-uniform magnetic fields have also been considered for comparison in this thesis work. The average Nusselt number along horizontal heated diameter is calculated for various types of nanofluids. Different types of thermal boundary conditions have also been examined to investigate the natural convection heat transport mechanism. The nonlinear governing partial differential equations have been transformed into the non-dimensional form using a set of similarity variables.

The robust partial differential equations solver computer software COMSOL Multiphysics that employs the finite element technique of Galerkin weighted residual form has been employed to simulate the dimensionless governing equations for the present problem. An excellent agreement has been found with the numerical and experimental data presented in the literature review. The flow pattern and the structure of temperature transfer mechanisms have been shown in terms of streamline contours and isothermal lines, respectively. The outcomes for different physical model parameters such as Hartmann number ( $Ha$ ), Rayleigh number ( $Ra$ ) diameter of nanoparticles ( $d$ ), the volume fraction of nanoparticles ( $\phi$ ), period of the magnetic field ( $\lambda$ ), and Brownian motion of the nanoparticles have been displayed using streamlines, isotherms as well as the average rate of heat transfer. A comprehensive discussion of these physical parameters has been done from the physical point of view. The enhancement of temperature transport of thirty-two different

nanofluids has also been obtained and examined for the above-mentioned different model physical parameters. The important findings are listed as follows:

- The flow is needed time to reaches the study state, which can be controlled by various model parameters such as Hartmann number ( $Ha$ ), Rayleigh number ( $Ra$ ), the diameter of nanoparticles ( $d$ ), nanoparticles volume fraction ( $\phi$ ), and size and shape of the nanoparticles.
- The heat transfer mechanisms of the solution for Cu-H<sub>2</sub>O nanofluid reach a steady state from the unsteady state within a very short time for uniform thermal boundary conditions. It has been calculated after  $\tau = 0.65$ .
- The non-uniform magnetic field has a significant impact in controlling the flow and heat transport of nanofluid. It shows a higher heat transfer rate along the heated wall than the uniform magnetic field. The intensity of flow as well as heat transfer change with different periods of the magnetic field. The period  $\lambda = 0.75$  shows the highest heat transport rate along the heated bottom wall.
- The strength of the flow enhances significantly, and the pattern of the flow vortices changes with a higher Rayleigh number. Lower Rayleigh number shows heat transfer through conduction which is observed from isotherms. In contrast, the higher value of the Rayleigh number conform better temperature transport through convection, and natural convection heat transport is intensified for higher Rayleigh number. Heat transfer rate increases 56.30% when  $Ra$  varies from  $10^5$  to  $10^6$ .
- The thermal fields vary, and heat transport changes significantly with the increment of Hartmann number. Higher Hartmann number diminishes heat transport rate. A stronger magnetic field can decrease natural convection compared to the lower Rayleigh number.
- For the addition of nanoparticles, the flow and the thermal fields are modified slightly. However, the rate of heat transport enhances remarkably. The amounts of nanoparticles significantly improve heat transport rate (approximately 22.14% for Cu-H<sub>2</sub>O nanofluid) even the addition is 1% of the volume fraction of nanoparticles.
- As the nanoparticles diameter decreases, the thermal field changes remarkably. The small size of nanoparticles enhances more heat transfer rate. The heat transport rate enhances

quickly due to the increases in the specific surface area of the nanoparticles. The rate of heat transfer increases 30.70% when the diameter of the nanoparticles decreases from 50nm to 10nm.

- The size of the nanoparticles have significant effects for making the solution of the nanofluid stable. The small size of nanoparticles assists in augmenting the thermal conductivity of nanofluids. The rate of heat transport increases 41.27% when the size of particles decreases 100nm to 10nm for copper-water nanofluid, and it increases 91.91% for Cu-kerosene nanofluid and 53.36% for Cu-ethylene glycol nanofluid.
- The nanoparticle's Brownian motion performs a vital role in enhancing heat transport rate due to the random movement of the nanoparticles. Therefore, the principal mechanism in the thermal conductivity equation is the addition of the random movements of nanoparticles to enhance nanofluid's thermal conductivity. The heat transfer increase about 22.17% with the Brownian effect, whereas it enhances about 2.19% without the Brownian effect for 4% nanoparticles volume fraction when  $Ha = 20$  and  $Ra = 10^5$ .
- The heat transport rate remarkably enhances kerosene-based nanofluid compared to water or ethylene glycol or engine oil-based nanofluid. The heat transport rate is observed at 67.86% for Cobalt (Co)-kerosene based nanofluids, whereas 23.78% for Co-water, 5.67% for Co-engine oil, and 39.78% for Co-ethylene glycol-based nanofluid with the increase of 1% nanoparticles volume.
- The shape of the nanoparticles has a significant impact on heat transport. The blade shape of nanoparticles shows the highest temperature transport rate than other shapes of nanoparticles. The heat transfer rate increases about 5.10% for the blade shape of particles instead of the spherical shape for Co-kerosene nanofluid.
- The thermal boundary conditions have an effective role in fluid flow and temperature transport. The uniform thermal condition (case I) provides highest the heat transport rate than other thermal conditions (case II, III, IV, V) for the copper-water nanofluid steady-state case. The rate of heat transport increases 47.78% for case I, 47.43% for case II, 5.77% for case III, 31.57% for case IV, and 13.90% for case V when Rayleigh number varies  $10^5$  to  $10^6$  with  $d = 1\text{nm}$ ,  $\phi = 0.04$ ,  $Ha = 20$ ,  $n = 3$ ,  $\lambda = 0.5$ .



## 6.2 Further works

In the future, there are a lot of scopes for research in this area. For request and wide occurrence of nanofluids in a diverse range of application both in nature and in technology. Many more mathematical models are available for representing such nanofluids. Therefore, there are many possibilities to extend this investigation in many directions. The following recommendations can be put forward for the further work on the present study.

- The study can be extended by including the effect of heat generation/absorption parameters.
- Investigation can be performed by using lid-driven mixed convection heat transport.
- Investigation can be performed using the porous media at the cavity's walls.
- This study can be extended using a partial heater at the cavity wall and changing the geometry, boundary conditions, and nanofluid.

## References

- [1] Wong, K.V., and Leon, O.D.. “Applications of nanofluids: current and future- A review article,” *Advances in Mechanical Engineering*, vol. 2010, Article ID 519659 (2010).
- [2] Choi, S.U.S., and Eastman, J.A.. “Enhancing thermal conductivity of fluids with nanoparticles,” *Int. Mech. Eng. Cong. and Expo.*, ASME, San Francisco, USA (1995).
- [3] Das, S.K., Choi, S.U., Yu, W., and Pradeep, T.. “Nanofluids: science and technology,” *John Wiley and Sons*, (2017).
- [4] Ma, H.B., Wilson, C., Borgmeyer, B.. “Effect of nanofluid on the heat transport capability in an oscillating heat pipe” *Applied Physics Letters*, Vol. 88, Article ID 143116 (2006a).
- [5] Buongiorno, J.. “Convective transports in nanofluids,” *ASME: Journal Heat Transfer*, Vol. 128, pp. 240-250 (2006).
- [6] Murshed, S.M.S., Leong, K.C., and Yang, C.. “Enhanced thermal conductivity of TiO<sub>2</sub>-water based nanofluids,” *International Journal Thermal Science*, Vol. 44, pp. 367-373 (2005).
- [7] Ece, M.C. and Buyuk, E.. “Natural convection flow under a magnetic field in an inclined rectangular enclosure heated and cooled on adjacent wall,” *Fluid Dynamics Res.*, Vol. 38, pp. 564–590 (2005).
- [8] Hwang, K., Lee, J., and Jang, J.. “Buoyancy-driven heat transfer of water-based Al<sub>2</sub>O<sub>3</sub> nanofluids in a rectangular cavity,” *Int. J. Heat Mass Transf.*, Vol. 50, pp. 4003–4010 (2007).
- [9] Jou, R., and Tzeng, S.. “Numerical research of nature convective heat transfer enhancement filled with nanofluids in rectangular enclosures,” *International Commun. Heat Mass Transfer*, Vol. 33(6), pp. 727–736 (2006).
- [10] Oztop, H., and Abu-Nada E.. “Numerical study of natural convection in partially heated rectangular enclosures filled with nanofluids,” *Int. J. Heat Fluid Flow*, Vol. 29, pp. 1326–1336 (2008).
- [11] Ghasemi, B., and Aminossadati, S.M.. “Natural convection heat transfer in an inclined enclosure filled with a water-Cuo nanofluid,” *Numerical Heat Transfer Analysis*, Vol. 55, pp. 807–823 (2009).
- [12] Aminossadati, S.M., and Ghasemi, B.. “Enhanced natural convection in an isosceles triangular enclosure filled with a nanofluids,” *Computational Math. Appli.*, vol. 61, pp. 1739-1753 (2011).
- [13] Saleh, H., Rosel R., and Hashim, I.. “Natural convection heat transfer in a nanofluid-filled trapezoidal enclosure,” *Int. J. of Heat and Mass transfer*, Vol. 54, pp. 194-201 (2011).
- [14] Rashmi, W., Ismail, A.F., and Khalid, M.. “CFD studies on natural convection heat transfer of Al<sub>2</sub>O<sub>3</sub>-water nanofluids,” *Heat Mass Transfer*, Vol. 47, pp. 1301–1310 (2011).

- [15] Sheikhzadeh, G.A., Arefmanesh, A., and Mahmoodi, M.. “Numerical study of natural convection in a differentially-heated rectangular cavity filled with TiO<sub>2</sub>-water nanofluid,” *Journal of Nano Research*, Vol. 13, pp. 75–80 (2011).
- [16] Arani, A., Mahmoodi, M., and Amini, M.. “Free convection in a nanofluid filled square cavity with horizontal heated plate,” *Defect and Diffusion Forum*, Vol. 312–315, pp. 433–438 (2011).
- [17] Solemani, S., Sheikholeslami, M., Ganji, D.D., and Gorji-Bandpay, M.. “Natural convection heat transfer in a nanofluid filled semi-annulus enclosure,” *Int. Commun. Heat Mass Transfer*, Vol. 39, pp. 565–574 (2012).
- [18] Nasrin, R., and Parvin, S.. “Investigation of buoyancy-driven flow and heat transfer in a trapezoidal cavity filled with water-Cu nanofluid,” *International Communication in Heat and Mass Transfer*, Vol. 39, pp. 270-274 (2012).
- [19] Sheikholeslami, M., Gorji-Bandpy, M., Ganji D.D., and Soleimani, S.. “Effect of a magnetic field on natural convection in an inclined half annulus enclosure filled with Cu-water nanofluid using CVFEM,” *Adv. Powder Technology*, Vol. 24, pp. 980–991 (2013).
- [20] Nasrin, R. and Alim, M.A.. “Free convective flow of nanofluid having two nanoparticles inside a complicated cavity,” *International Journal of Heat and Mass Transfer*, Vol. 63, pp. 191-198 (2013).
- [21] Hussain, S.H., and Hussain, A.K.. “Natural convection heat transfer enhancement in a differentially heated parallelogrammic enclosure filled with Cu-water nanofluid,” *ASME J. Heat Transfer*, Vol. 136, pp. 82502–82508 (2014).
- [22] Malvandi, A., Moshizi, S.A., and Ganji, D.D.. “Effect of magnetic fields on heat convection inside a concentric annulus filled with Al<sub>2</sub>O<sub>2</sub>-water nanofluid,” *Advanced Powder Technology*, Vol. 25(6), pp. 1817-1824 (2014).
- [23] Rahman, M.M. and Al-Hatmi, M.M.. “Hydromagnetic boundary layer flow and heat transfer characteristics of a nanofluid over an inclined stretching surface in the presence of convective surface: a comprehensive study,” *SQU J. Sci.*, Vol. 19(2), pp. 53–76 (2014).
- [24] Koopae, M.K. and Jelodari, I.. “Numerical investigation of magnetic field inclination angle on transient natural convection in an enclosure filled with nanofluid,” *Engineering Computations*, Vol. 31, pp. 1342-1360 (2014).
- [25] Mejri, I., Mahmoudi, A., Abbassi, M.A., Omri, A.. “Magnetic field effect on entropy generation in a nanofluid-filled enclosure with sinusoidal heating on both side walls,” *Powder Technology*, Vol. 266, pp. 340-353 (2014).
- [26] Sheikholeslami, M., Bandpy, M.G., Ellahi, R., and Zeeshan, A.. “Simulation of MHD CuO-water nanofluid flow and convective heat transfer considering Lorentz forces,” *J. Magn. Mater.* Vol. 369, pp. 69-80 (2014).

- [27] Rahman, M.M., Mojumder, S., Saha S., Joarder A.H., Saidur, R., and Naim, A.G.. “Numerical and statistical analysis on unsteady magnetohydrodynamic convection in a semi-circular enclosure filled with ferrofluid,” *Int. J. Heat Mass Transf.*, Vol. 89, pp. 1316-1330 (2015).
- [28] Rahman, M.M., Öztop, H.F., Steele, M., Naim, A.G., Al-Salem, K., and Ibrahim, T.A.. “Unsteady natural convection and statistical analysis in a CNT-water filled cavity with non-isothermal heating,” *Int. Commun. Heat Mass Transf.*, Vol. 64, pp. 50-60 (2015).
- [29] Alsabery, A.I., Chamkha, A.J., Saleh, H., and Hashim, I.. “Heatline visualization of conjugate natural convection in a square cavity filled with nanofluid with sinusoidal temperature variations on both horizontal walls,” *Int. J. Heat Mass Transfer.*, Vol. 100, pp. 835–850 (2016).
- [30] Ouyahia, S., Benkahla, Y.K., and Labsi, N.. “Numerical study of the hydrodynamic and thermal proprieties of titanium dioxide nanofluids trapped in a triangular geometry,” *Arab. J. Sci. Eng.*, Vol. 41, pp. 1995–2009 (2016).
- [31] Mojumder, S., Rabbi, K.M., Saha S., Hasan, M.N. and Saha, S.C.. “Magnetic field effect on natural convection and entropy generation in a half-moon shaped cavity with semi-circular bottom heater having different ferrofluid inside,” *Journal of Magnetism and Magnetic Materials*, Vol. 407, pp. 412-444 (2016).
- [32] Kalbani, A.K.S., Alam, M.S., and Rahman, M.M.. “Finite element analysis of unsteady natural convective heat transfer and fluid flow of nanofluids inside a tilted square enclosure in the presence of oriented magnetic field,” *Am. J. Heat Mass Transf.*, Vol. 3, pp. 186–224 (2016).
- [33] Uddin, M.J., Kalbani, A.K.S., Rahman, M.M., Alam, M.S., Al-Salti, N., and Eltayeb, I.. “Fundamentals of nanofluids: evolution, applications and new theory. International Journal of Biomathematics and Systems Biology,” *International Journal of Biomathematics and Systems Biology*, Vol. 2(1), pp. 1-32 (2016).
- [34] Parvin S., Chowdhury, R., Khan, M.A.H., and Alim, M.A.. “Performance of nanofluid in free convective heat transfer inside a cavity with non-isothermal boundary conditions,” *Mechanical Engineering Research Journal*, Vol. 10, pp. 01-06 (2016).
- [35] Rahman, M.M., Öztop, H.F., Joarder, A.H., Saidur, R., Hamzah, N., Al-Salem, K. and Ibrahim, T.A.. “Unsteady analysis of natural convection in a carbon nanotube-water filled cavity with inclined heater,” *Numerical Heat Transfer Part A.*, Vol. 69(7), pp. 1-18 (2016).
- [36] Weheibi S.M.A., Rahman, M.M., Alam, S.S., and Vajravelu, K.. “Numerical Simulation of natural convection heat transfer in a trapezoidal enclosure filled with nanoparticles,” *Int. Journal of Mechanical Sciences*, Vol. 131-132, pp. 599-612 (2017).

- [37] Qi, C., Cui, X., Liu, Y., Yang, Z., and Huang.. “Natural convection heat transfer of liquid metal Gallium nanofluids in a rectangular enclosure,” *Journal of Heat Transfer*, Vol. 46(1), pp. 1–17 (2017).
- [38] Parvin, S., and Akter, A..“Effect of magnetic field on natural convection flow in a prism shaped cavity filled with nanofluid,” *Procedia Engineering*, Vol. 194C, pp. 421-427 (2017).
- [39] Uddin, M.J., and Rahman, M.M.. “Finite element computational procedure for convective flow of nanofluids in an annulus,” *Thermal Science and Engineering Progress*, Vol. 6, pp. 251-267 (2018).
- [40] Kalbani, A.K.S., Rahman, M.M., Alam, M.S., Al-Salti, N., and Eltayeb, I.A.. “Buoyancy induced heat transfer flow inside a tilted square enclosure filled with nanofluids in the presence of oriented magnetic field,” *Journal Heat Transfer Engineering*, Vol. 39(6), pp. 511-525 (2018).
- [41] Uddin, M.J., and Rasel, S.K.. “Numerical analysis of natural convective heat transport of copper oxide-water nanofluid flow inside a quadrilateral vessel,” *Heliyon*, Vol. 5(5), pp. 1-18 (2019).
- [42] Uddin, M.J.. “Numerical simulation on free convective heat transfer in a copper-water nanofluid filled semicircular annulus with the magnetic field,” *Italian J. of Engg. Science: Tecnica Italiana*, Vol. 62(2), pp. 119-129 (2018).
- [43] Mehryan, S.A.M., Mohsen, Izadi, Chamkha, A.J., and Sheremet, M.A..“Natural convection and entropy generation of a ferrofluid in a square enclosure under the effect of a horizontal periodic magnetic field,” *J. of Molecular Liquids*, Vol. 263, pp. 510-525 (2018).
- [44] Mahian, O., Kolsi, L., Amani, M., Estellé, P., Ahmadi, G., Kleinstreuer, C., Marshall, J.S., Siavashi, M., Taylor, R.A., Niazmand, H., Wongwises, S., Hayat, T., Kolarjijil, A., Kasaeian, A., and Pop, I.. “Recent advances in modeling and simulation of nanofluid flows- Part I: Fundamentals and theory,” *Physics Reports*, Vol. 790, pp. 1-48 (2019).
- [45] Kalbani, A.K.S., and Rahman, M.M.. “Convective heat transfer in nanofluids inside an inclined square enclosure in the presence of heat source, Brownian motion and oriented magnetic field,” *J. of Engg. Physics and Thermophysics*, Vol. 92(5), pp. 2188-2207 (2019).
- [46] Balushi, L.M.A., Uddin, M.J., and Rahman, M.M.. “Natural convective heat transfer in a square enclosure utilizing magnetic nanoparticles,” *Propulsion and Power Research*, Vol. 8(3), pp. 194-209 (2019).
- [47] Mohsen, Izadi, Sheremet, M.A., and Mehryan, S.A.M.. “Natural convection of a hybrid nanofluid affected by an inclined periodic magnetic field within a porous medium,” *Chinese Journal of Physics*, Vol. 65, pp. 447-458 (2020).

- [48] Marzougui, S., Oudina, F.M., Assia, A., Magherbi, M., Shah, Z., and Ramesh, K.. “Entropy generation on magneto-convective flow of copper–water nanofluid in a cavity with chamfers,” *Journal of Thermal Analysis and Calorimetry*, Vol. 143, pp. 2203-2214 (2020).
- [49] Giwa, S.O., Sharifpur, M., Ahmadi, M.H., and Meyer, J.P.. “A review of magnetic field influence on natural convection heat transfer performance of nanofluids in square cavities,” *J. of Thermal Analysis & Calorimetry*, Vol. 145, pp. 2581-2623, (2021).
- [50] Hamilton, R.L. and Crosser, O.K.. “Thermal conductivity of heterogeneous two-component systems,” *Ind. Eng. Chem. Fundam.*, Vol. 1, pp. 18-191 (1962).
- [51] Timofeeva, V., Routbort, L., and Singh. “Particle shapes effects on thermophysical properties of alumina nanofluids,” *J. Appl. Phy.*, Vol. 106, pp. 124-9, (2009).
- [52] Uddin, M.J., and Rahman, M.M.. “Numerical computation of natural convective heat transport within nanofluids filled semi-circular shaped enclosure using nonhomogeneous dynamic model,” *Thermal Science and Engineering Progress*, Vol. 1, pp. 25-38 (2017).
- [53] Zienkiewicz, O.C., and Taylor, R.L.. “The finite element method solid and structural mechanics,” *Sixth Edition, McGraw-Hill*, (2005).
- [54] Ghasemi, B., Aminossadati, S.M., and Raisi, A.. “Magnetic field effects on natural convection in a nanofluid-filled square enclosure,” *International Journal Thermal Science*, Vol. 50, pp. 1748-1756 (2011).
- [55] Akgün, N.A.. “Effect of an uniform magnetic field on unsteady natural convection of nanofluid,” *J. of Taibah University for Sci.*, Vol. 13(1), pp. 1073–1086 (2019).
- [56] Liu Y.L., Li, D.W., He, J., Xie, X.Z., Chen, D., Yan, E.K., Ye, W.J., and Yina, D.C.. “A periodic magnetic field as a special environment for scientific research created by rotating permanent magnet pairs,” *Review of Scientific Instruments*, Vol. 89, pp. 105103-9, 105103 (2018).